



**Danish Meteorological Institute**  
Ministry of Climate, Energy and Utilities



**Series title:** DMI Report 25-17  
**Title:** The ozone layer over Denmark and Greenland 1979-2024  
**Authors:** Helge Jønch-Sørensen, Nis Jepsen and Guisella Gacitúa  
**Responsible Institution:** Danish Meteorological Institute  
**Language:** English  
**Keyword:** Ozone layer over Denmark, Greenland and Antarctica.  
**Url:** <http://dmi.dk/publikationer/>  
**Digital ISBN:** 978-87-7478-763-1  
**ISSN:** 2445-9127  
**Version date:** November 2025  
**Link to website:** <http://www.dmi.dk>  
**Copyright:** Danish Meteorological Institute

# Content:

1	Introduction	7
2	Ozone Monitoring	8
2.1	Observation Sites	8
2.2	The Ozone Layer over Denmark	8
2.3	The Ozone Layer over Greenland	10
2.3.1	Kangerlussuaq	10
2.3.2	Ittoqqortoormiit	14
2.4	Ozone Depletion in the Arctic	14
2.5	Ozone Depletion and UV Radiation	22
2.6	The Ozone Hole Over Antarctica	23
<b>A</b>	<b>Daily Measurements of the Ozone Layer over Denmark</b>	<b>30</b>
<b>B</b>	<b>Daily Measurements of the Ozone Layer over Kangerlussuaq</b>	<b>39</b>
<b>C</b>	<b>Daily Measurements of the Ozone Layer over Pituffik</b>	<b>48</b>
<b>D</b>	<b>PSC area over the Northern Hemisphere</b>	<b>56</b>
<b>E</b>	<b>UV Dose measured in Copenhagen</b>	<b>63</b>
<b>F</b>	<b>The Ozone Layer</b>	<b>73</b>
<b>G</b>	<b>The Vienna Convention and the Montreal Protocol</b>	<b>88</b>
<b>H</b>	<b>International Cooperation</b>	<b>91</b>

## Abstract

The implementation of the Montreal Protocol has led to a steady decline in atmospheric concentrations of ozone-depleting substances, with recovery of the ozone layer to pre-1980 levels projected by mid-century. However, climate-related factors such as greenhouse-gas-induced stratospheric cooling, increasing levels of nitrous oxide, methane, and possibly water vapour, continue to influence Arctic ozone variability.

The Danish Meteorological Institute (DMI), in collaboration with the Danish Environmental Protection Agency, carries out ongoing monitoring of the ozone layer from one station in Copenhagen and two stations in Greenland (Kangerlussuaq and Ittoqqortoormiit). This report presents measurements and updates of ozone layer thickness over Denmark and Greenland from 1979 to 2024, combining satellite observations with long-term ground-based measurements.

Several Arctic winters since the early 1990s have exhibited significant chemical depletion of the ozone layer. The most severe event occurred in 2019/2020, when about 37% of the ozone column within the polar vortex was destroyed, with losses reaching 93% at 19 km—comparable to Antarctic conditions. During March 2020 a regular ozone hole (total ozone column values below 220 DU) were present over part of the Arctic. In 2024/2025, ozone depletion was prominent during February but ended early March. Because of the location of the polar vortex very low ozone column values were seen over Copenhagen during most of March. Overall results confirm both the effectiveness of international regulation under the Montreal Protocol and the importance of continued monitoring, as interactions between climate change and stratospheric processes remain a key uncertainty for future ozone recovery.

## Resumé

Danmarks Meteorologiske Institut (DMI), i samarbejde med Miljøstyrelsen, overvåger ozonlaget fra én station i København og to stationer i Grønland. Denne rapport præsenterer målinger af ozonlagets tykkelse over Danmark og Grønland i perioden 1979–2024, baseret på både satellitobservationer og langvarige jordbaserede målinger.

Siden begyndelsen af 1990'erne har flere arktiske vintre vist betydelig kemisk nedbrydning af ozonlaget. Den mest markante hændelse fandt sted i vinteren 2019/2020, hvor omkring 37% af ozonsøjlen inden for den polare hvirvelvind blev nedbrudt, med tab på op til 93% i 19 km højde — niveauer sammenlignelige med forholdene over Antarktis. I marts 2020 opstod der et regulært ozonhul (total ozon kolonne værdier under 220 DU) over dele af det Arktiske område. Lignende, men mindre udtalte, episoder fandt sted i foråret 2005 (over 30% tab, op til 70% ved 18 km) og foråret 2016 (ca. 27% tab). I vinteren 2024/2025 var der kraftig ozonnedbrydning i løbet af februar, men dette ophørte tidligt i marts. På grund af placeringen af den polare vortex blev der i marts 2020 observeret meget lave ozonværdier over København.

Resultaterne understreger både effektiviteten af de internationale reguleringer under Montreal-protokollen og nødvendigheden af fortsat overvågning, da samspillet mellem klimaændringer og stratosfæriske processer fortsat er en væsentlig usikkerhed for ozonlagets fremtidige udvikling.

# 1 Introduction

The ozone layer plays a crucial role in shielding the Earth's surface from harmful ultraviolet (UV) radiation. Its depletion can increase UV exposure, with potentially serious impacts on human health, ecosystems, and materials. The primary causes of ozone depletion are chlorine- and bromine-containing compounds, notably chlorofluorocarbons (CFCs) and halons, which are primarily of anthropogenic origin.

Significant chemical depletion of the ozone layer has been observed in the Arctic since the early 1990s, with the strongest depletion historically occurring over Antarctica, leading to the formation of the Antarctic ozone hole during the spring. Similar, though less extensive, Arctic ozone depletion events were observed in winter 2010/2011 [Manney et al., 2011] and again in winter 2019/2020 [Wohlmann et al., 2021]. Long-term observations indicate that colder stratospheric temperatures, which promote the formation of polar stratospheric clouds (PSCs), are closely linked to the severity of chemical ozone loss. These temperatures exhibit interannual variability, but there is a long-term trend toward colder Arctic winters and increased ozone depletion since 1960.

Following the implementation of the Montreal Protocol in 1987 and its subsequent amendments, the production and use of ozone-depleting substances have declined. Stratospheric chlorine concentrations peaked in the late 1990s and are slowly decreasing [WMO, 2022]. However, the recovery of the ozone layer is influenced by additional factors, including rising concentrations of greenhouse gases, nitrous oxide, methane, and possibly water vapor, as well as natural variability from volcanic eruptions and solar activity. Moreover, the substitute compounds for CFCs and halons, such as hydrofluorocarbons (HFCs), are potent greenhouse gases, and their use has been further limited under the Kigali amendment to the Montreal Protocol (effective 2019). Despite these efforts, unexpected releases of certain CFCs, notably CFC-11, were detected in the Northern Hemisphere after 2012 [Rigby et al., 2019]. Investigations traced a substantial portion of these emissions to unregulated production in southern China, prompting remedial actions to halt the releases. These events highlight the ongoing scientific and policy challenges in predicting the future state of the ozone layer.

Global assessments under the Montreal Protocol, including the latest WMO report [WMO, 2022], indicate that while ozone-depleting substances continue to decline, the recovery of the ozone layer is uneven. Rebuilding is occurring in the upper stratosphere, whereas the lower stratosphere has yet to show significant recovery. Current projections suggest a return to 1980 ozone levels between 60°S and 60°N by around 2040, in the Arctic by approximately 2050, and in Antarctica by around 2065.

Observations of the ozone layer have been carried out using satellite data and ground-based measurements. DMI started ozone monitoring between 1989–1993 at stations in Ittoqqortoormiit (Scoresbysund), Pittufik (Thule), Kangerlussuaq (Søndre Strømfjord) and Copenhagen. The Brewer spectrophotometers determine the ozone layer's thickness based on ozone absorption in the ultraviolet range (at five selected wavelengths). At one of these wavelengths, absorption is also influenced by the presence of sulphur dioxide (SO<sub>2</sub>) in the atmosphere. This influence can therefore be used to calculate the SO<sub>2</sub> concentration. The SAOZ (Système D'Analyse par Observations Zénithales) is a zenith sky UV-visible spectrometer which is used to retrieve mean values of total ozone and nitrogen dioxide (NO<sub>2</sub>) both at sunrise and sunset on a daily basis. Measurements also include weekly balloon-launched ozone sondes. This is an instrument carried aloft by a balloon, which uses an electrochemical cell to measure ozone concentration as a function of altitude. This provides a vertical profile of the ozone layer up to 35 km, rather than a single column value as obtained by spectrometers. DMI also operates a multiwavelength Ground-based Ultraviolet Radiometer (GUV2511) and AERONET (AERosol RObotic NETwork), which are part of the ground-based remote sensing aerosol network established by NASA and PHOTONS (PHOTométrie pour le Traitement Opérationnel de Normalisation Satellitaire; Univ. of Lille 1, CNES, and CNRS-INSU)

This report presents the annual status of the ozone layer over Denmark and Greenland, combining observational data, stratospheric conditions, and UV radiation measurements. The state of the ozone layer over these regions is strongly influenced by Arctic chemical ozone depletion during the preceding winter, which in turn affects UV radiation doses at the surface. The report also documents exceptional events such as the Arctic ozone hole in spring 2020 and provides background on historical measurements, ozone chemistry, international agreements, and DMI's role in research and monitoring under national and international programs.

The monitoring and research activities described respond to Denmark's commitments under the Vienna Convention and Montreal Protocol, contribute to Arctic climate assessments under the Arctic Monitoring and Assessment Programme (AMAP), and form part of the national strategy for space-based atmospheric observations [Regeringen 2021]. Continuous updates on DMI's ozone and UV measurements are publicly available online<sup>1</sup>

<sup>1</sup><http://psc.dmi.dk/ozone-data/>

## 2 Ozone Monitoring

### 2.1 Observation Sites

DMI measures ozone layer thickness and UV index in Denmark using a Brewer spectrophotometer and a YES pyranometer respectively. In Greenland, DMI carries out measurements at the following locations:

- In Kangerlussuaq, using 2 Brewers, a SAOZ spectrometer, and a sun photometer (AERONET)
- In Ittoqqortoormiit, using a SAOZ spectrometer, ozone sonde launches, a GUV2511 and a sun photometer
- In Narsarsuaq, a sun photometer



Figure 2.1: Ozone and UV monitoring locations in Greenland.

The Greenlandic stations (Figure 2.1) and the measurements in Copenhagen form part of a global network for detecting changes in the upper troposphere and lower stratosphere. Measurements from all stations contribute to the WMO's Global Atmosphere Watch (GAW) network. Monitoring data are reported to various databases, including NILU (ozone sondes only), the World Ozone and Ultraviolet Radiation Data Center (WOUDC), which is part of the World Meteorological Organisation (WMO), and to the Network for the Detection of Atmospheric Composition Change. Furthermore, data are uploaded to EuBrewNet (Brewer data only) and LATMOS (SAOZ data only).

### 2.2 The Ozone Layer over Denmark

From October 1978 the ozone layer thickness was measured globally using the satellite instrument TOMS (Total Ozone Mapping Spectrometer), onboard NASA's Nimbus-7 satellite. Over its 15-year operational period, the instrument provided

Table 1: Instrumentation and funding sources for DMI’s ozone and UV observation sites in Greenland.

Location	Instrumentation	Funding Sources
Kangerlussuaq	Brewer, SAOZ, AERONET sun photometer	Danish Environmental Protection Agency, EUMETSAT, NASA
Ittoqqortoormiit	Ozone sondes, GUV-2511, SAOZ, AERONET sun photometer	Danish Environmental Protection Agency, LATMOS, NASA, Tusass
Narsarsuaq	AERONET sun photometer	NASA, Tusass

global ozone data, and its measurements have shown good agreement with those from ground-based instruments. Ozone layer measurements using a Brewer spectrophotometer in Copenhagen began in June 1992.

The annual mean ozone layer thickness over Denmark is shown in Figure 2.2. Although meteorological studies often use climatic normals based on 30-year averages or longer, the 10-year period from 1979–1988 is commonly used as a reference in ozone studies. This is because very few locations worldwide have ozone measurements from before 1979. Ozone depletion had already begun during this period, meaning that deviations from this reference represent a lower bound for the extent of ozone layer thinning over Denmark and Greenland.

Daily measurements dating back to 1979 are presented in Appendix A. Due to Denmark’s relatively small geographical extent, the ozone layer thickness measured over Copenhagen can be considered representative of the country as a whole.

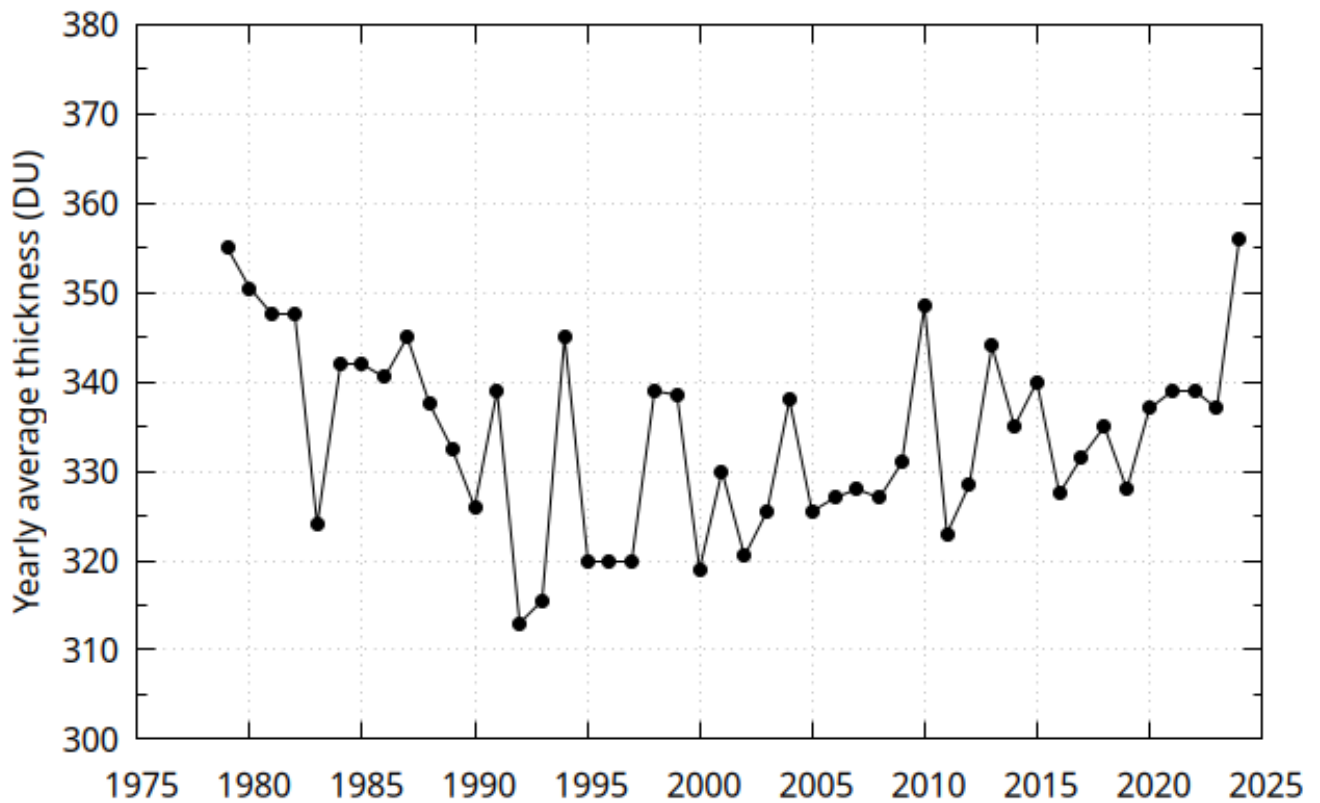


Figure 2.2: Annual mean ozone layer thickness over Denmark for the period 1979–2024. The average for the 10-year reference period 1979–1988 is 344 DU. Data prior to 1993 originate from NASA’s TOMS instrument aboard the Nimbus-7 satellite. From 1993 onwards, the data are based on DMI’s ground-based measurements in Copenhagen using a Brewer spectrophotometer.

The result for 2024 shows that the average thickness of the ozone layer was the highest measured for the last 45 years. This was partly due to a very warm stratosphere in February and March with practically no PSC formation leading to close to zero ozone depletion. Furthermore, the meteorological situation during May to August resulted in enhanced transport of ozone rich air from the tropics to our latitude. Thus the average ozone layer thickness over Denmark during the summer (June–August) was the highest ever measured (Figure 2.3), this was also traceable in the measured UV dose (see Section 2.5).

Ozone depletion in the Arctic stratosphere during late winter and early spring can influence ozone levels at mid-latitudes, including over Denmark. For instance, if significant depletion occurs in the Arctic stratosphere between January and March, the ozone layer over Denmark will remain thinner through spring and summer, typically only returning to normal by late autumn. This occurs when ozone-poor air from the polar regions mixes with ozone-rich air outside the polar vortex as it breaks down in mid to late spring. As a result, the ozone layer at mid-latitudes also becomes thinner than normal for this time of the year. In addition, chlorine and bromine can destroy some ozone even when temperatures are not low enough for stratospheric clouds to form. Years showing major negative deviations in Figure 2.2 include 1983, 1992, and 1993. These years follow large volcanic eruptions — El Chichón in Mexico (1982) and Mount Pinatubo in the Philippines (1991) — which released substantial amounts of sulphur into the atmosphere. This led to increased ozone depletion for one year (El Chichón) or two years (Mount Pinatubo) following the eruptions.

The unusually high ozone layer thickness over Denmark in 2010 (Figure 2.2) was also observed across all northern mid-latitudes. Analyses have shown that this unexpected anomaly can be attributed to a pronounced and persistent negative phase of the North Atlantic Oscillation (NAO), combined with an easterly phase of the quasi-biennial oscillation (QBO), resulting in enhanced transport of ozone from the tropics to higher latitudes [Steinbrecht et al., 2011]. Consequently, the average ozone layer thickness across much of Europe was unusually high in 2010.

Seasonal variations in the ozone layer over Denmark are shown in Figure 2.3, based on daily mean values for each season: winter (December–February), spring (March–May), summer (June–August), and autumn (September–November). Notably large negative deviations are seen during the winter seasons following volcanic eruptions (1983, 1992, and 1993), as well as the exceptionally high autumn value in 2010 due to the atmospheric conditions described above.

Globally, a decline in ozone layer thickness was observed from the mid-1970s to the mid-1990s. This trend is also evident in the measurements from Denmark (Copenhagen). Since then a small positive trend is noted, especially for the spring season, which indicates a slow recovery of the ozone layer at our latitude.

## 2.3 The Ozone Layer over Greenland

DMI began measuring ozone layer thickness in Kangerlussuaq (Søndre Strømfjord) and Pituffik (Thule Air Base) in autumn 1990. Following the closure of DMI's operations in Pituffik, the SAOZ spectrometer was relocated to Kangerlussuaq. Daily measurements are presented in Appendix B.

### 2.3.1 Kangerlussuaq

In Kangerlussuaq, the ozone layer thickness and UV radiation have been measured using a Brewer spectrophotometer from September 1991. Additionally, ozone layer thickness and total NO<sub>2</sub> are measured using a SAOZ spectrometer operating on a different principle than the Brewer: while the Brewer measures direct sunlight, the SAOZ measures zenith-scattered light at sunrise and sunset.

The SAOZ spectrometer enables measurements from early January to late December. However, the SAOZ spectrometer is not well suited for periods when the sun remains high in the sky throughout the day, which occurs in Kangerlussuaq from late May to mid-July. In contrast, the Brewer spectrophotometer can typically only operate from early February to late October, as it requires a minimum solar elevation to function properly (around 8 degrees). No measurements can be made during the three-month period around the winter solstice. Consequently, an annual average ozone layer thickness is not calculated.

Figures 2.4 and 2.5 show the overall and seasonal patterns of ozone layer thickness over Kangerlussuaq respectively. Figure 2.5 presents the seasonal mean values across three seasons, while Figure 2.4 covers the full measurement period from March to November, where substantial ozone depletion during the winter of 2019–2020 is clearly visible. The data clearly show that spring exhibits the greatest variability in ozone layer thickness. This is due to the occasional presence of the polar vortex over Kangerlussuaq when significant ozone depletion occurs within the vortex. However, the effects of volcanic eruptions are not as pronounced as they are in the data from Denmark. As noted earlier, ozone layer thinning was observed in most parts of the world from the mid-1970s to the mid-1990s. This pattern is also evident in the Kangerlussuaq data, although not during autumn. No significant trend is found in any season since 1994.

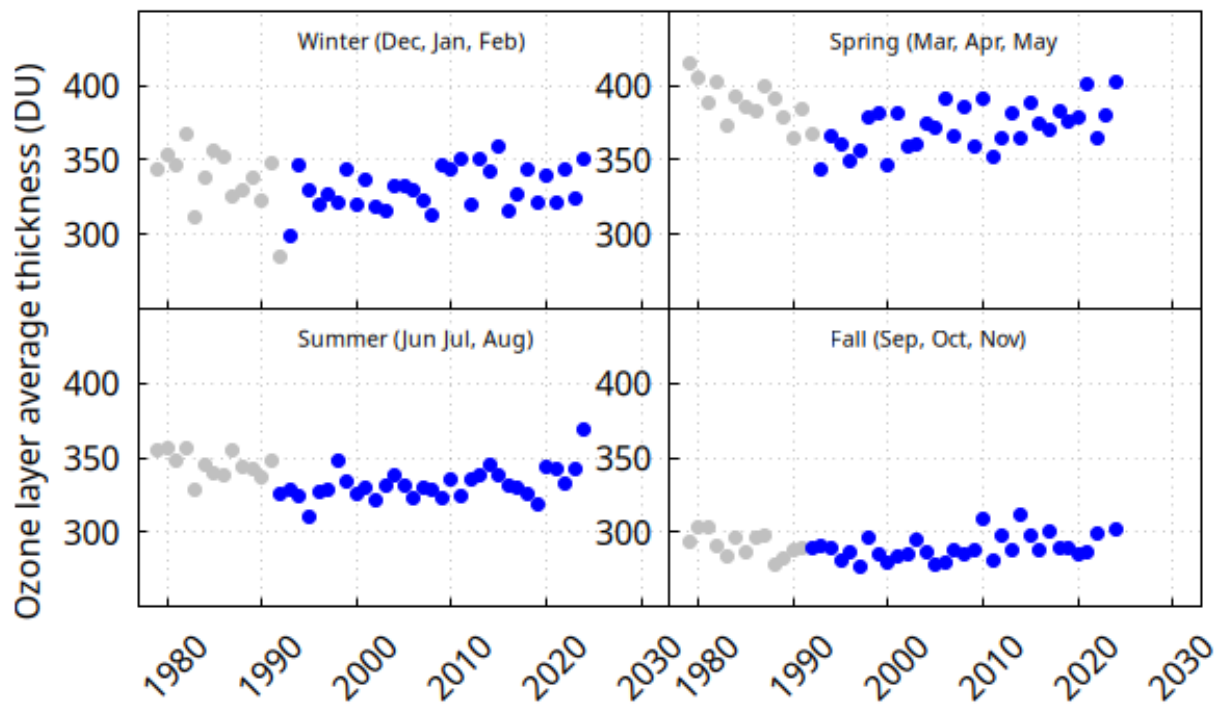


Figure 2.3: Seasonal mean ozone layer thickness over Denmark for the period 1979–2024.

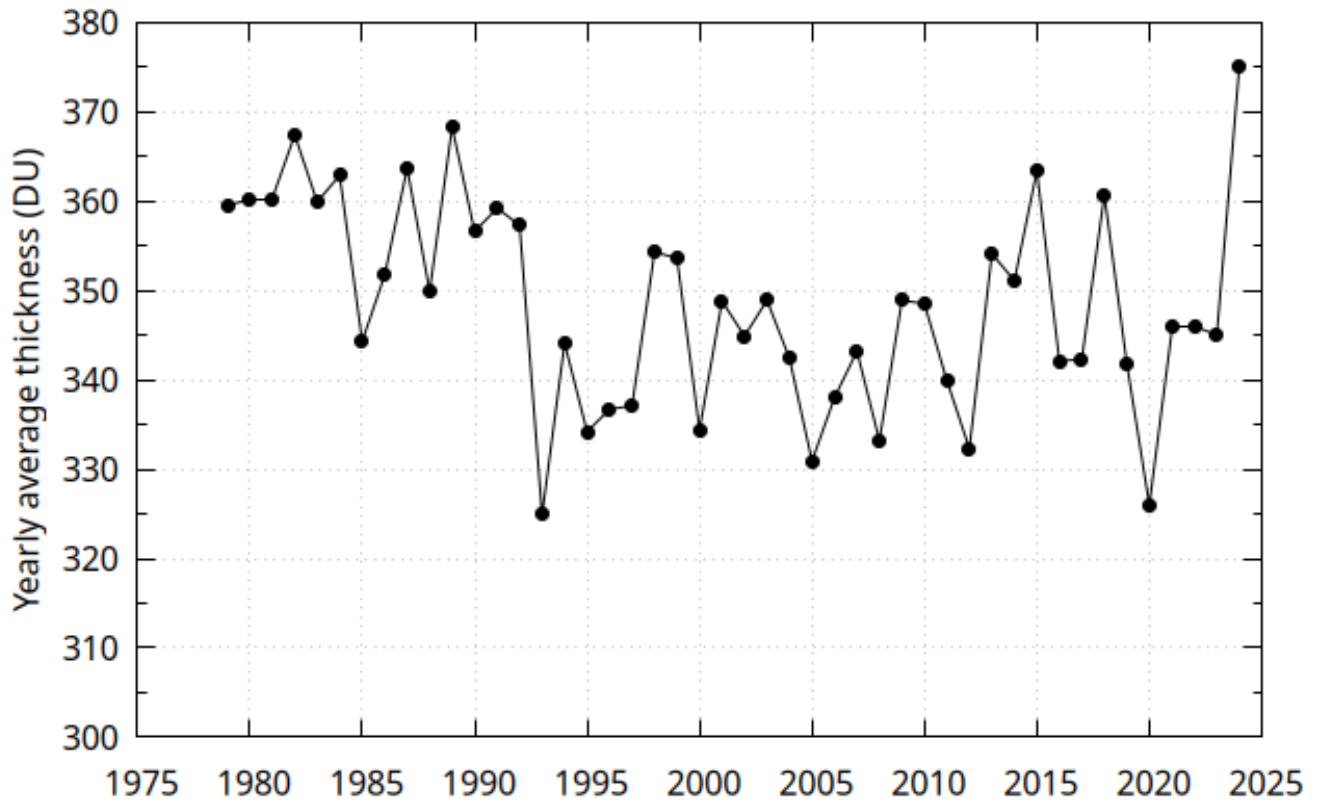


Figure 2.4: Average ozone layer thickness over Kangerlussuaq from March to November (three seasons) through to the end of 2024. Data up to and including 1991 are based on NASA's satellite measurements from the TOMS instrument onboard the Nimbus-7 satellite.

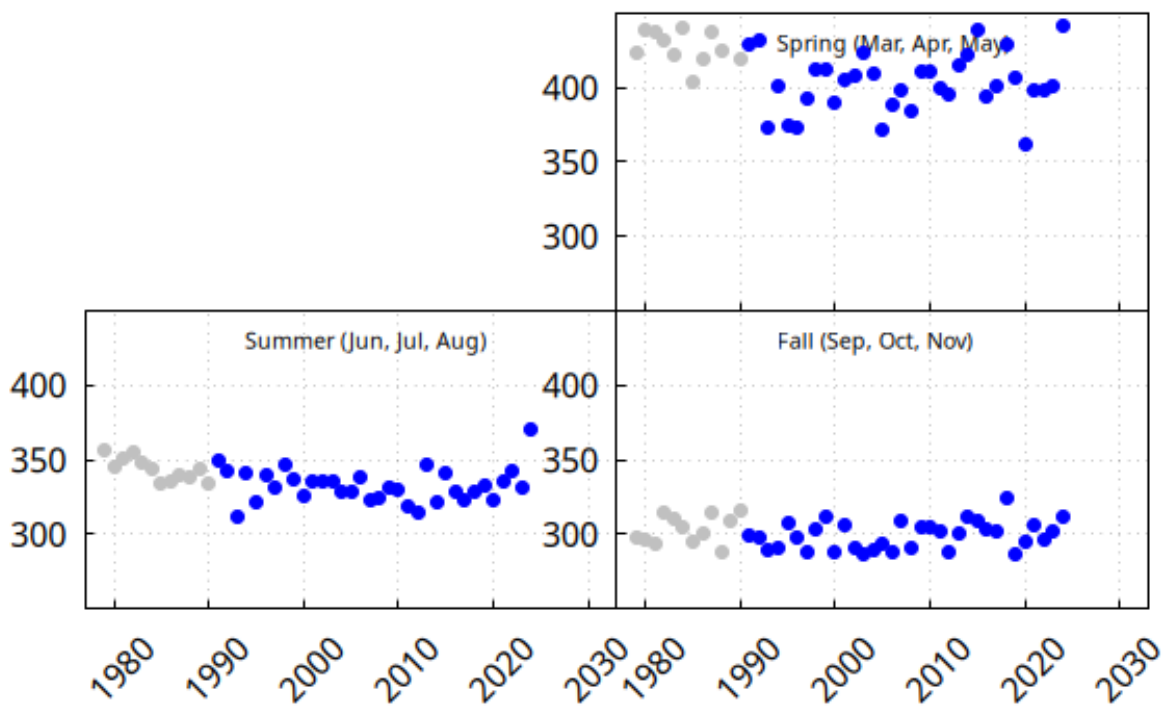


Figure 2.5: Seasonal mean ozone layer thickness over Kangerlussuaq for the period 1979–2024. No statistically significant change in atmospheric ozone levels has been observed since 1990.

### 2.3.2 Ittoqqortoormiit

Ozone soundings have been conducted in Ittoqqortoormiit since 1989. Figure 2.6 provides an overview of the ozone soundings from the site. The figure shows that ozone partial pressure was relatively high in 2006. In contrast, values were relatively low in 2011 in the 150–30 hPa range (corresponding to roughly 15–25 km altitude), similar to the levels observed in the late 1990s when ozone depletion was particularly severe.

DMI conducts weekly ozone soundings in Ittoqqortoormiit for satellite validation. In 2024, only 17 ozone soundings were conducted successfully. Additional soundings have been carried out as part of international cooperation, such as Match campaigns, which are performed using ozonesondes launched at many polar and sub-polar stations aimed at assessing Arctic ozone depletion; however, these had to be halted because currently there are too few sounding stations in the Arctic.

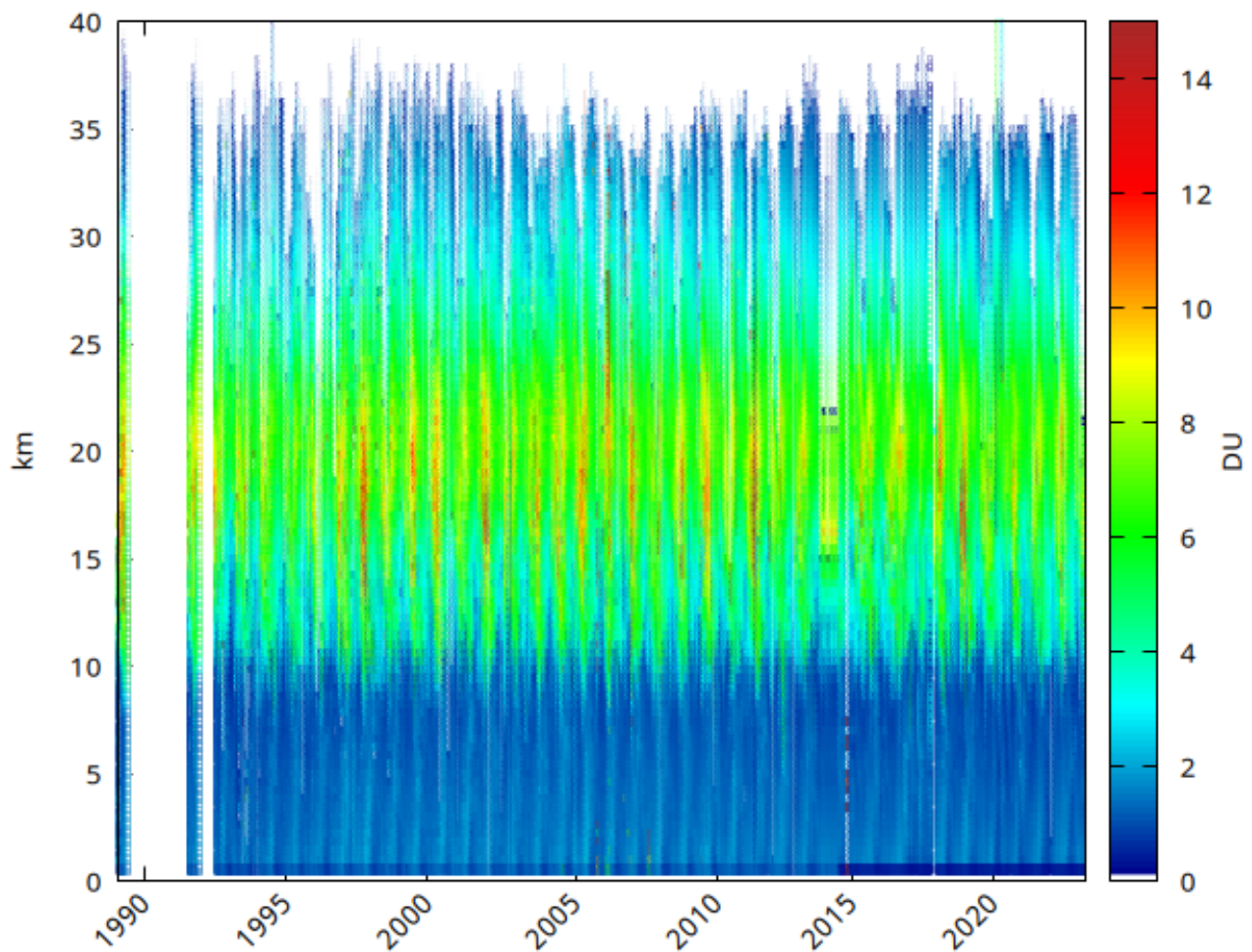


Figure 2.6: Ozone soundings in Ittoqqortoormiit, 1989–2024. The colours indicate ozone partial pressure converted to Dobson Units (DU) for a given altitude, according to the scale shown to the right of the figure.

## 2.4 Ozone Depletion in the Arctic

In general, four main conditions must be met for significant ozone depletion to occur over the polar regions:

1. Elevated concentrations of chlorine- and bromine-containing substances in the atmosphere. These concentrations have increased due to emissions of man-made CFCs and halons (e.g. Freon).
2. Low stratospheric temperatures. Chlorine compounds only become ozone-depleting when converted into chemically reactive forms (a process known as activation). This conversion occurs primarily on the surface of PSCs, which

form only at very low temperatures. At the same time, reactive nitrogen is removed from the stratosphere via sedimentation of cloud particles (denitrification), which further enhances ozone depletion.

3. Sunlight. The chemically reactive chlorine and bromine compounds only destroy ozone in the presence of sunlight, which returns to the polar regions in early spring.
4. An isolated air mass. Each winter, the polar vortex forms over the polar regions — a system of strong winds circulating at altitudes above approximately 15 km. The vortex isolates the polar air masses and prevents mixing with ozone-rich air from lower latitudes.

Radio occultation measurements from EUMETSAT/ROM SAF provide highly accurate temperature data with high vertical resolution throughout the stratosphere. These measurements are used to calculate the total volume of air cold enough for PSC formation.

The development of the Arctic polar vortex boundary during the winter of 2024/2025 is shown with red contour lines in Figure 2.7. In the figure, the vortex location is shown at a potential temperature level of 550 K, corresponding to an altitude of about 23 km. Thin blue contour lines indicate the temperature threshold for the possible formation of polar stratospheric clouds (type 1 PSCs, composed mainly of nitric acid trihydrate), while thick blue lines indicate areas where type 2 PSCs can form (composed primarily of water ice). Both types of PSCs provide surfaces for chemical reactions that convert chlorine- and bromine-containing compounds into forms that rapidly destroy ozone once sunlight returns in spring.

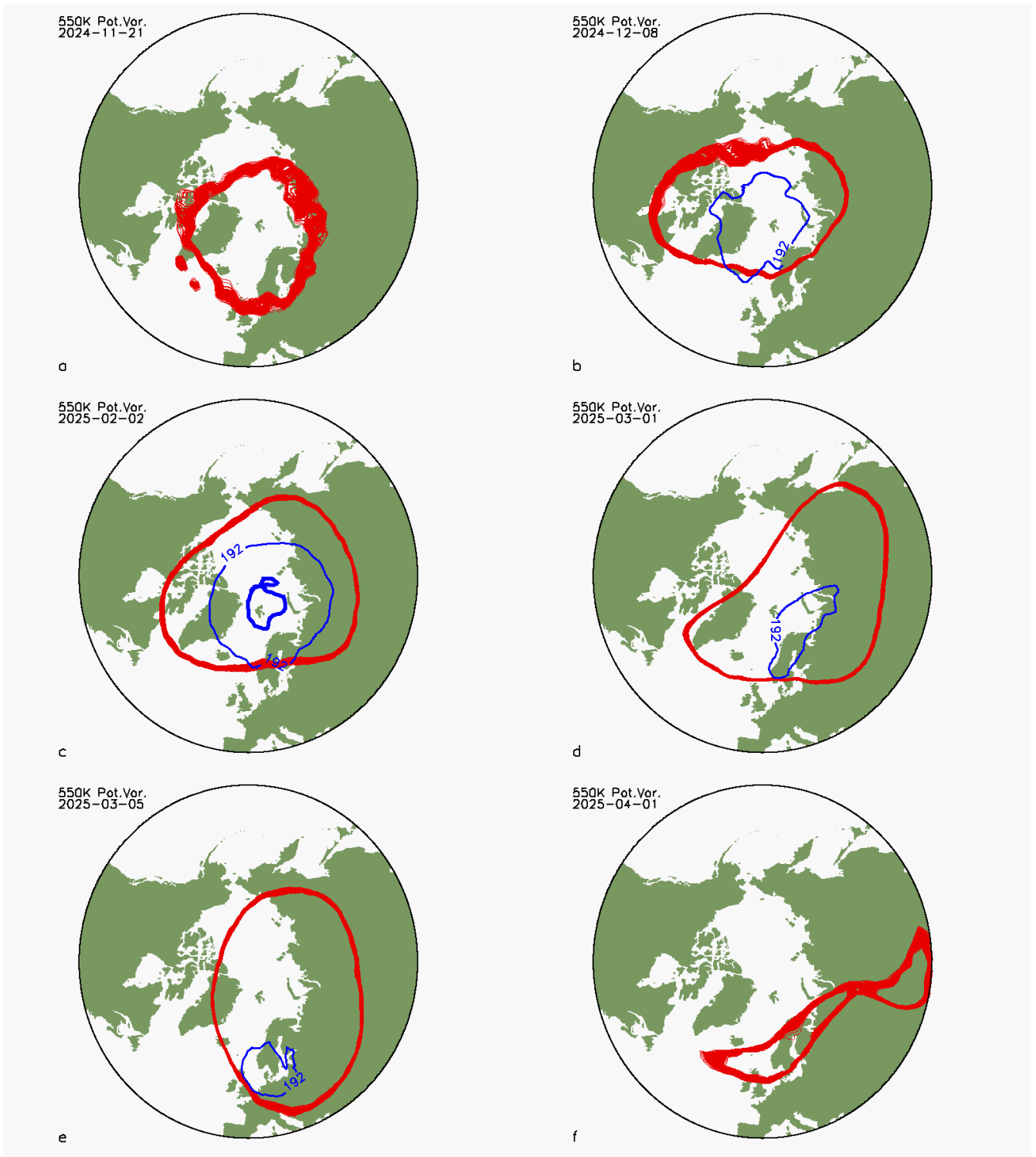


Figure 2.7: The polar vortex (red contours) from November 2024 to April 2025. Areas with conditions suitable for the formation of type 1 PSC (thin blue contours) and type 2 PSC (thick blue contour).

From late November 2024, a stable polar vortex was present at an altitude of about 23 km, and in early December the first large cold area formed, allowing for the development of type 1 PSCs (Figure 2.7a). Both the vortex and the PSC area remained stable through December and January. In early January 2025, temperatures dropped low enough for

type 2 PSCs to form (Figure 2.7c). From 29 January to 5 February, the volume of the stratosphere where PSC formation was possible was even larger than observed in the previous 24 years (Figure 2.8). By 1st March, temperatures had risen so much that the PSC area quickly shrank, and the ozone depletion development therefore stopped entirely around 10 March.

Figure 2.8 shows the evolution of mean and minimum temperatures, as well as the volume of the PSC area in the Arctic stratosphere, from January to April 2025. For most of January, the PSC volume was well above normal, and between 29 January and 5 February it reached the highest values recorded in the past 24 years. In the following week, a warming event temporarily reduced the PSC volume, but it remained above normal. The volume stayed relatively large until 5 March, when a rapid stratospheric warming caused the PSC volume to disappear and ozone depletion to cease.

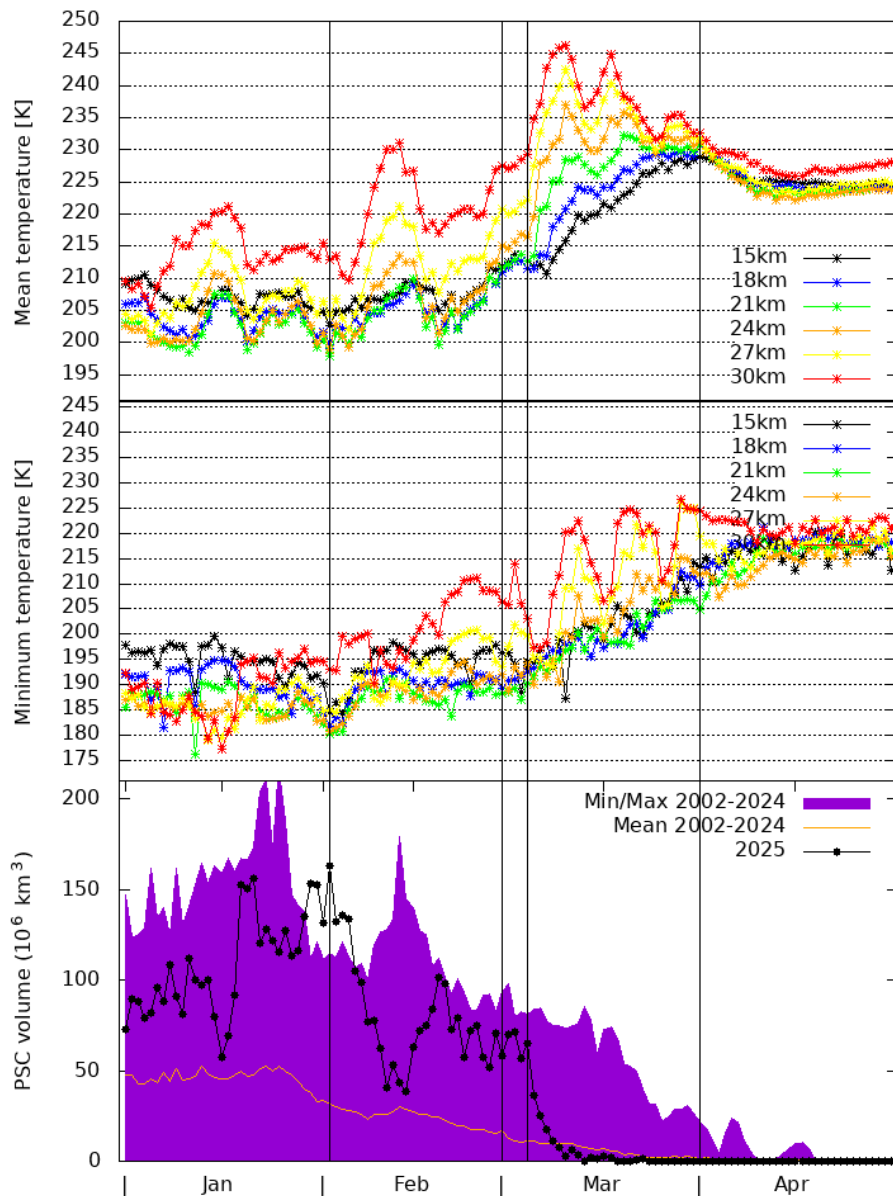


Figure 2.8: Measurements from near real-time satellite radio occultation data. Top: Mean temperature measured at six different altitudes in the Arctic stratosphere. Middle: Minimum temperature at the same altitudes. In both panels, the dates February 2, March 1, 5 and April 1 are marked with vertical lines, corresponding to features in Figure 2.7c–f. Bottom: Volume of the area with temperatures low enough for PSC formation (EUMETSAT/ROM SAF)

The area covered by PSCs throughout the winter, within the altitude range corresponding to 350–675 K potential temperature (about 14–26 km), is shown in Figure 2.9. The area increased rapidly around the turn of the year and, as described above, disappeared quickly in early March. The PSC area remained quite large throughout February, when sunlight returns to the region, so a significant amount of ozone depletion was expected.

The typical seasonal pattern, in which a warming begins in the upper layers and causes the PSC area to shift downward, is clearly visible in the figure.

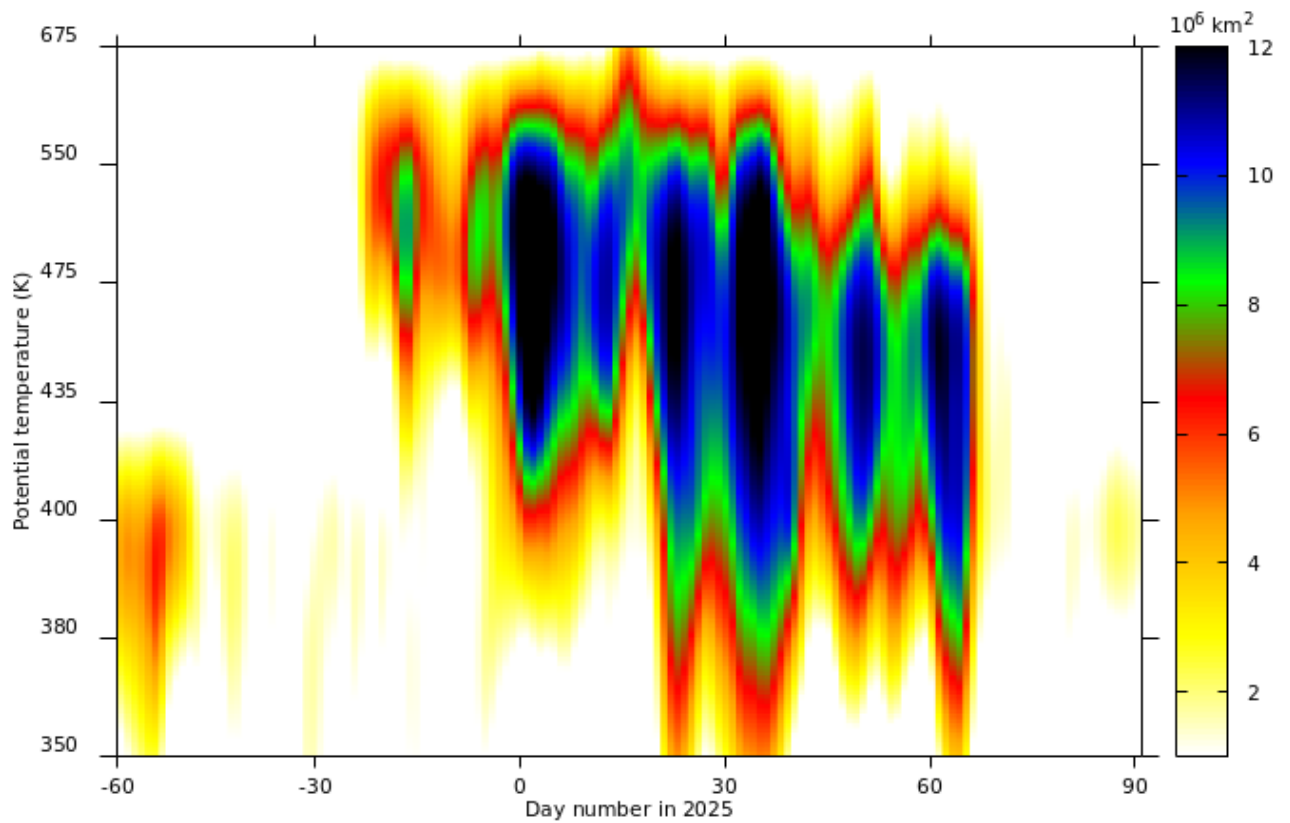


Figure 2.9: Area of the Northern Hemisphere covered by PSCs in the altitude range 350–675 K potential temperature (approximately 14–26 km) during the winter of 2024–2025 (ECMWF).

For most of January and February Ittoqqortoomiit was situated below the polar vortex and low ozone total columns were measured until mid March where the polar vortex left the area on its southward journey.

During February 2025 three radio soundings were performed and Figure 2.10 shows the three soundings compared with the average profile compiled from the previous 36 years. The profile from February 13 shows a prominent depletion of ozone in the 13-19 km altitude range. At 16 km the ozone partial pressure was only 25% of the normal. Furthermore, the three profiles from 2025 also illustrate the current problem of soundings not reaching higher than 20 km, which will be addressed during 2025.

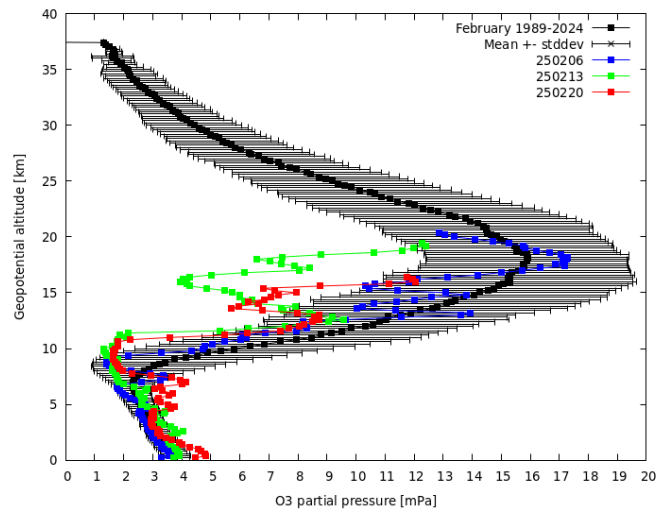


Figure 2.10: Ozone partial pressure as a function of altitude over Ittoqqortoormiit for February. Black curve is the average values for 1989-2024. Coloured curves are the profiles obtained in February 2025.

The vortex itself remained stable throughout March and shifted southward over northern Europe, bringing ozone-poor air into the region including Denmark. Measurements in Copenhagen showed that the ozone layer was about 25% thinner than normal for March (Figure 2.11), until the vortex finally broke up on 1 April.

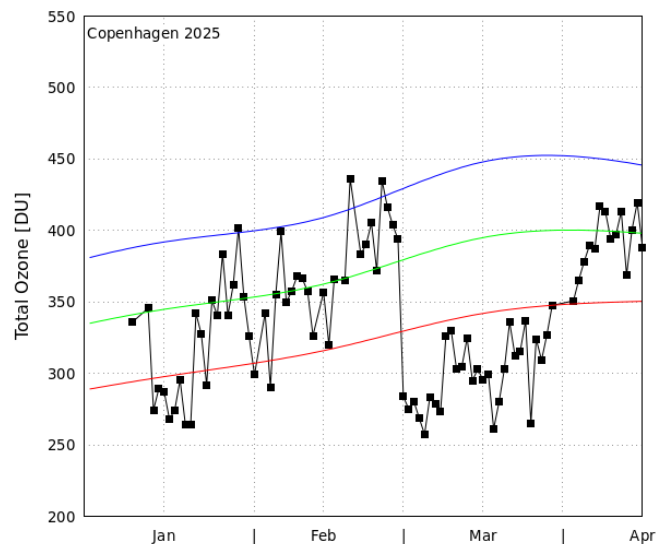


Figure 2.11: Ozone layer thickness over Copenhagen, January 1 – April 15, 2025.

Since low stratospheric temperatures promote the formation of PSC, an estimation of the cold air volume is presented here, following the method of Rex et al. [2004]. The calculation covers the period from December 15 to March 31 of the following year, with 105 days for normal years and 106 days for leap years. Figure 2.12 shows the average volume of cold air masses in million  $\text{km}^3/\text{day}$  for each winter since 1958, with the largest volumes over successive five-year periods marked with squares and used for the regression line. Data before 1992 are based on reanalysis data from ECMWF ERA-40 [Uppala et al., 2005], and after that from ECMWF operational analysis data. There is an 11-year overlap between the two datasets from 1992 to 2002, during which the correlation is 94%. The figure illustrates how much air in the atmosphere is cold enough for PSCs formation. During some winters, the intrusion of warm air from lower latitudes prevent the formation of PSC, causing annual variability. However, the coldest winters show a clear trend of increasing PSC volume, reflecting an intensification of Arctic stratospheric cold, and corresponding rise in ozone depletion. This

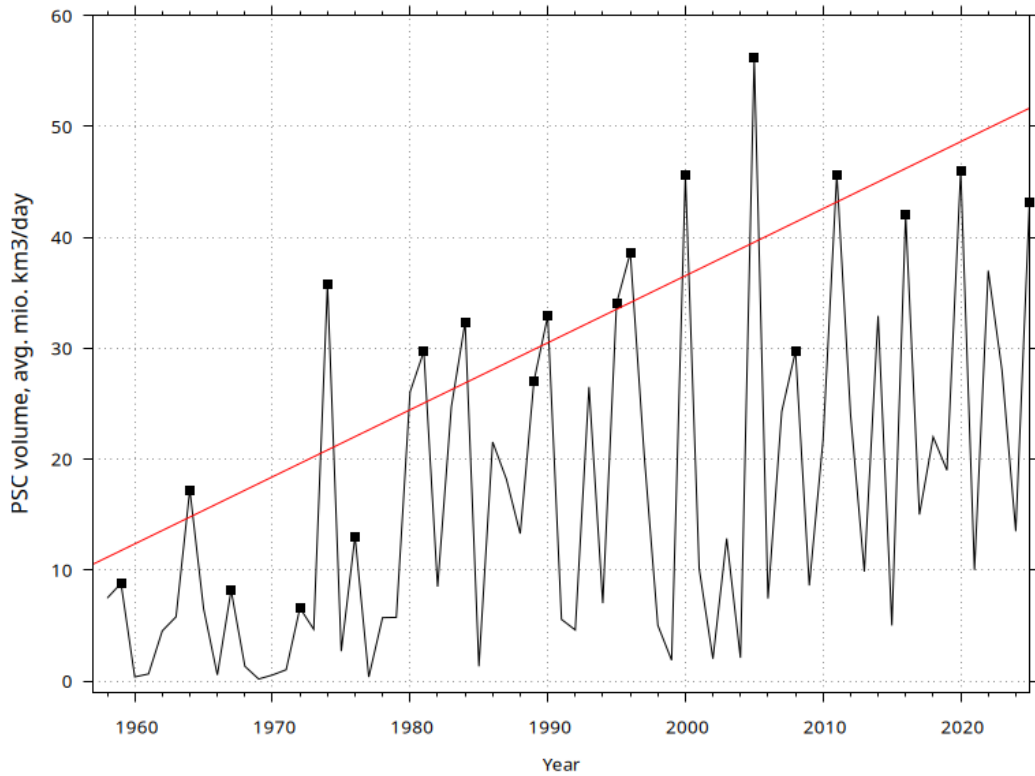


Figure 2.12: Average winter atmospheric volume suitable for PSC formation, 1958–present.

cooling is partly due to the greenhouse effect: while it warms the lower atmosphere (troposphere), it cools the ozone layer (stratosphere) because less reflected heat from Earth’s surface reaches the upper layer. As seen in Figure 2.12 this trend may have changed or weakened since 2010 but more years of data is needed to verify that.

Figure 2.13 shows the approximate maximum ozone depletion from January to March within the Arctic vortex for the years 1992–2025, plotted as a function of the winter’s average PSC volume, illustrating that ozone depletion is strongly correlated with PSC volume. Since the coldest winters have become colder over the past 52 years, it can be assumed that greater ozone depletion will also occur during the coldest winters in the future. However, the amount of ozone-depleting substances has started to decline as a result of the Montreal Protocol’s requirements for participating countries to ban their production (see Appendix G).

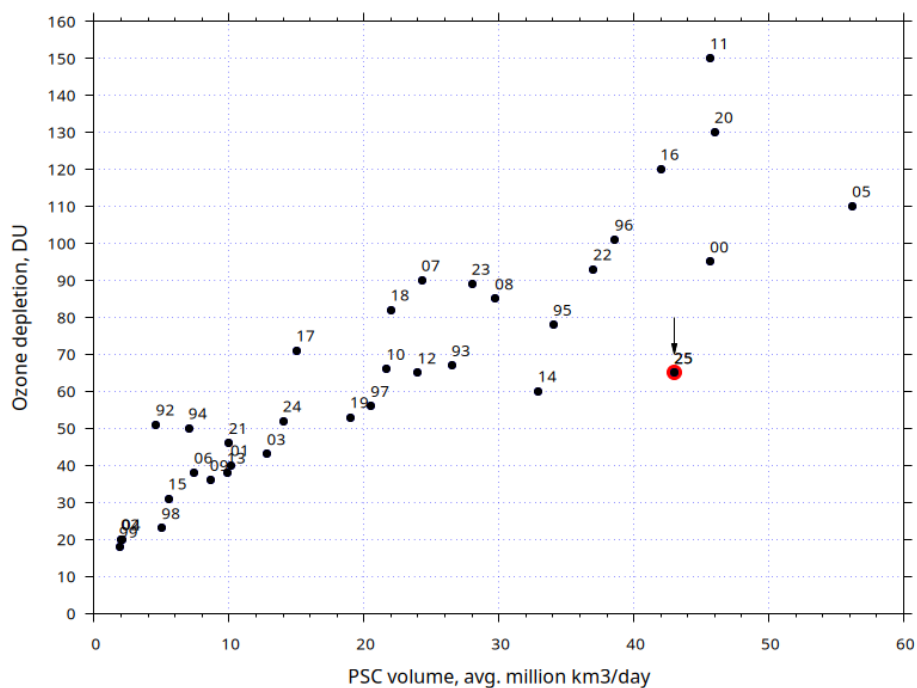


Figure 2.13: Maximum ozone depletion from January to March within the Arctic vortex from 1992 to 2025 as a function of the winter's average PSC volume. The numbers indicate the year. Winters 2011 and 2020 stand out with record-high ozone depletion. The PSC volume data are the same as in the Figure 2.12.

The Arctic ozone depletion estimates are partly based on DMI's Greenland ozone sondes conducted as part of the international Match campaigns. For winters where no MATCH campaign were carried out (because of high stratospheric temperatures or other reasons) the ozone depletion values are calculated from the SAOZ network alone (using the SLIMCAT and/or REPROBUS models).

## 2.5 Ozone Depletion and UV Radiation

The harmful UV radiation reaching the Earth's surface depends on several parameters, the most important of which are solar elevation and cloud cover and cloud type, followed by the thickness of the ozone layer, the reflectivity of the Earth's surface (albedo), and the atmosphere's aerosol content.

In summer, the intensity of harmful UV radiation at the equator is about twice as high as it can be in Denmark. This is also influenced by the fact that the ozone layer over the equator is thinner than over Denmark. Clouds noticeably affect UV radiation: on a day with an overcast sky and low, rain-heavy clouds, the intensity of harmful UV radiation is only 10-20% of what it would be without clouds. Conversely, on an overcast day with high, thin cirrus clouds, the intensity of harmful UV radiation can be up to 90% of what it would be without clouds. If, on average over many years, there are no changes in cloud type occurrence, cloud cover, albedo, and aerosols, then the thickness of the ozone layer is the decisive factor for changes in UV radiation.

Daily and monthly accumulated skin-damaging UV radiation from continuous measurements in Copenhagen are shown in Figure 2.14. A large day-to-day variation in the calculated daily accumulated dose (kJ/m<sup>2</sup>) is observed due to varying cloud cover (Figure 2.14a).

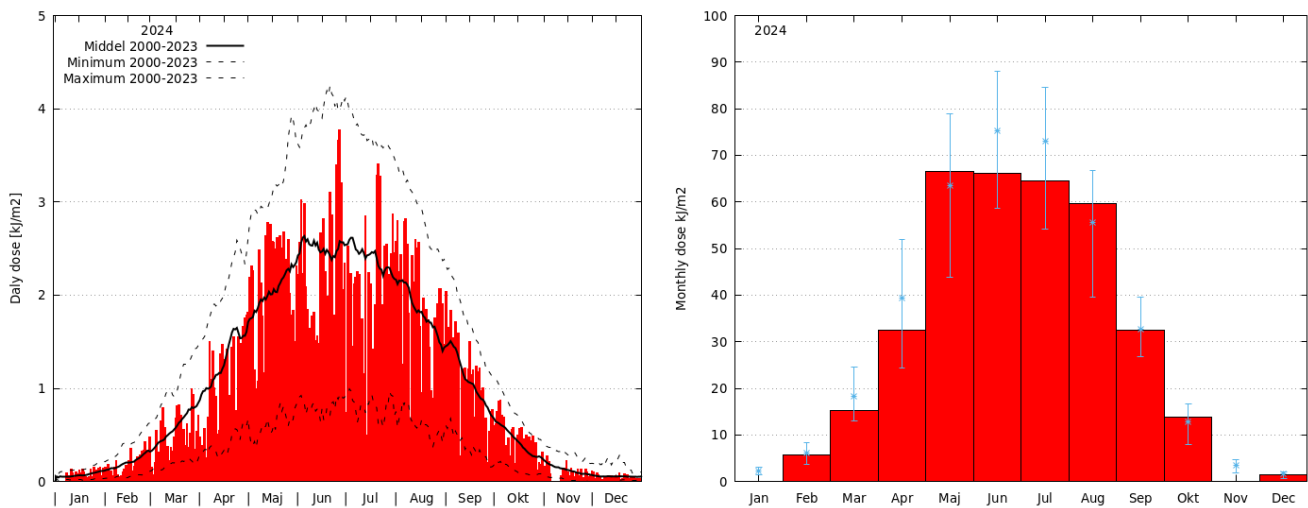


Figure 2.14: Skin-damaging UV radiation in 2024 in Copenhagen. Left: The daily measured total in  $\text{kJ}/\text{m}^2/\text{day}$ . The solid curve shows the corresponding mean dose for 2000–2024. The upper and lower dashed curves indicate the maximum and minimum, respectively, for the same period. Right: The monthly total dose in 2024, in  $\text{kJ}/\text{m}^2$ . Blue dots and bars indicate the monthly mean and the minimum and maximum values obtained in the period 2000–2023.

The total UV dose for 2024 measured in Copenhagen ended up being 6% below the average for the previous 23 years, making it the lowest recorded since 2011. The major reasons for this low UV dose was the very high ozone layer thickness during summer and a particularly overcast summer in the Copenhagen area. The monthly doses for June and July were significantly below normal; in June, the dose was 13% below the 2000–2023 average and the lowest measured since 2007. The trend since 2000 has otherwise shown a 17% increase in the annually accumulated UV dose. It should be noted, as shown in Section 2.2, that the increased UV dose since 2000 cannot be explained by a thinner ozone layer over Denmark — instead changes in cloud cover, likely influenced by climate change, are the most plausible explanation [Vitt et al., 2020].

## 2.6 The Ozone Hole Over Antarctica

Ozone depletion over Antarctica is significantly stronger than over the Arctic, and each year an ozone hole forms from August and remains until late December, where the ozone from about 14–20 km altitude is almost entirely depleted. Figure 2.15 illustrates measurements at the South Pole [WMO, 2003] and Ittoqqortoormiit for comparison.

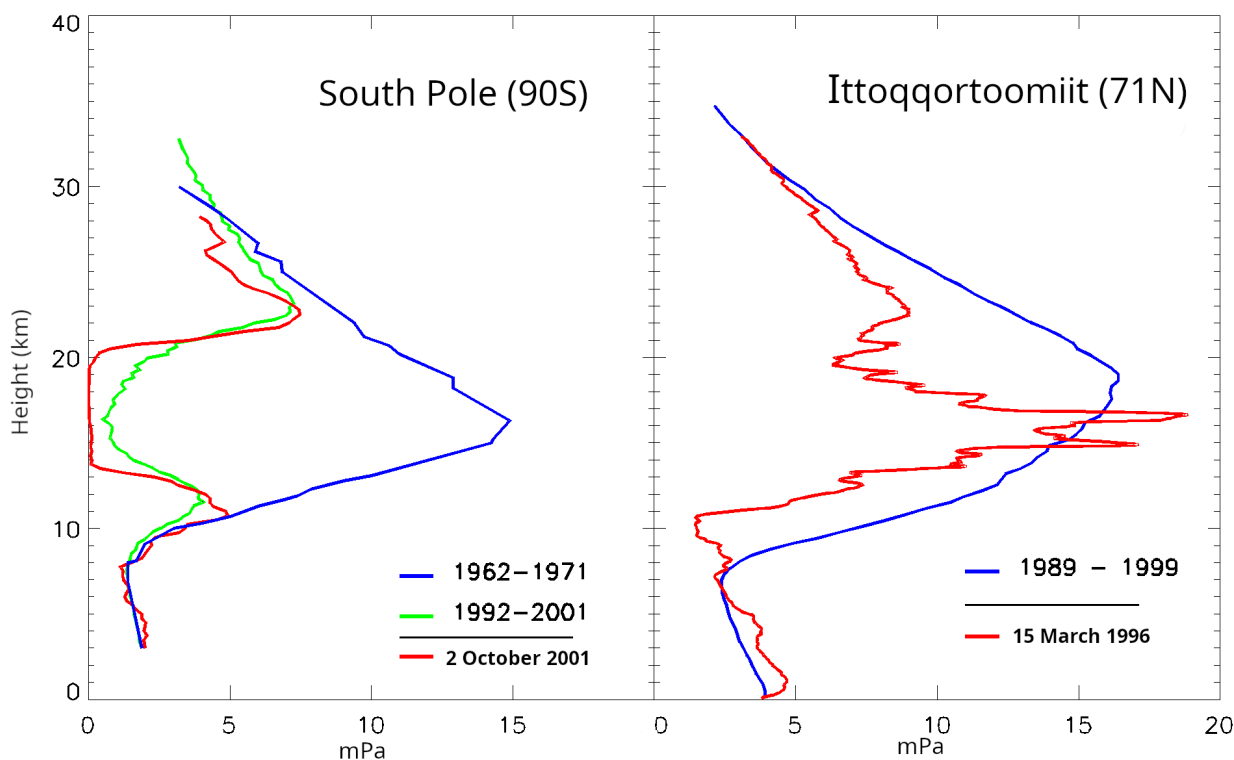


Figure 2.15: Vertical profile of ozone depletion over Antarctica (left) and the Arctic (right). Blue and green lines depict the average for the corresponding years for October in the South Hemisphere and March in the North Hemisphere. Red lines show measurements at specific dates.

The reason for the greater ozone depletion over Antarctica is that at high southern latitudes, the absence of large landmasses and significant mountain ranges allows the circumpolar westerly winds to flow more uniformly, reducing the exchange of air masses with lower latitudes. This stable circulation isolates the Antarctic stratosphere, enabling temperatures to drop much lower than in the Arctic.

Figure 2.16 shows temperatures in the Arctic and Antarctic. It can be seen that the lowest minimum temperatures in the Arctic only occasionally reach the highest minimum temperatures in the Antarctic, and average temperatures in the Arctic are about 10 degrees higher than in the Antarctic. This means that much larger amounts of PSCs form over Antarctica, leading to much stronger ozone depletion when sunlight returns after the polar night.

Measurements of ozone over Antarctica has been performed since the 1960s, in the beginning mostly by balloon soundings. In 1985 the ozone hole was discovered and analysis of older data showed that the hole had existed since 1980. The development of the area of the ozone hole over Antarctica since 1980 is shown in Figure 2.17. The ozone hole is here defined as the area where the ozone layer thickness is below 220 DU, meaning that more than half of the total ozone column is depleted. During the first 20 years the ozone hole grew in size to a maximum of 28.5 million km<sup>2</sup> in 2000, an area twice the size of the Antarctic continent.

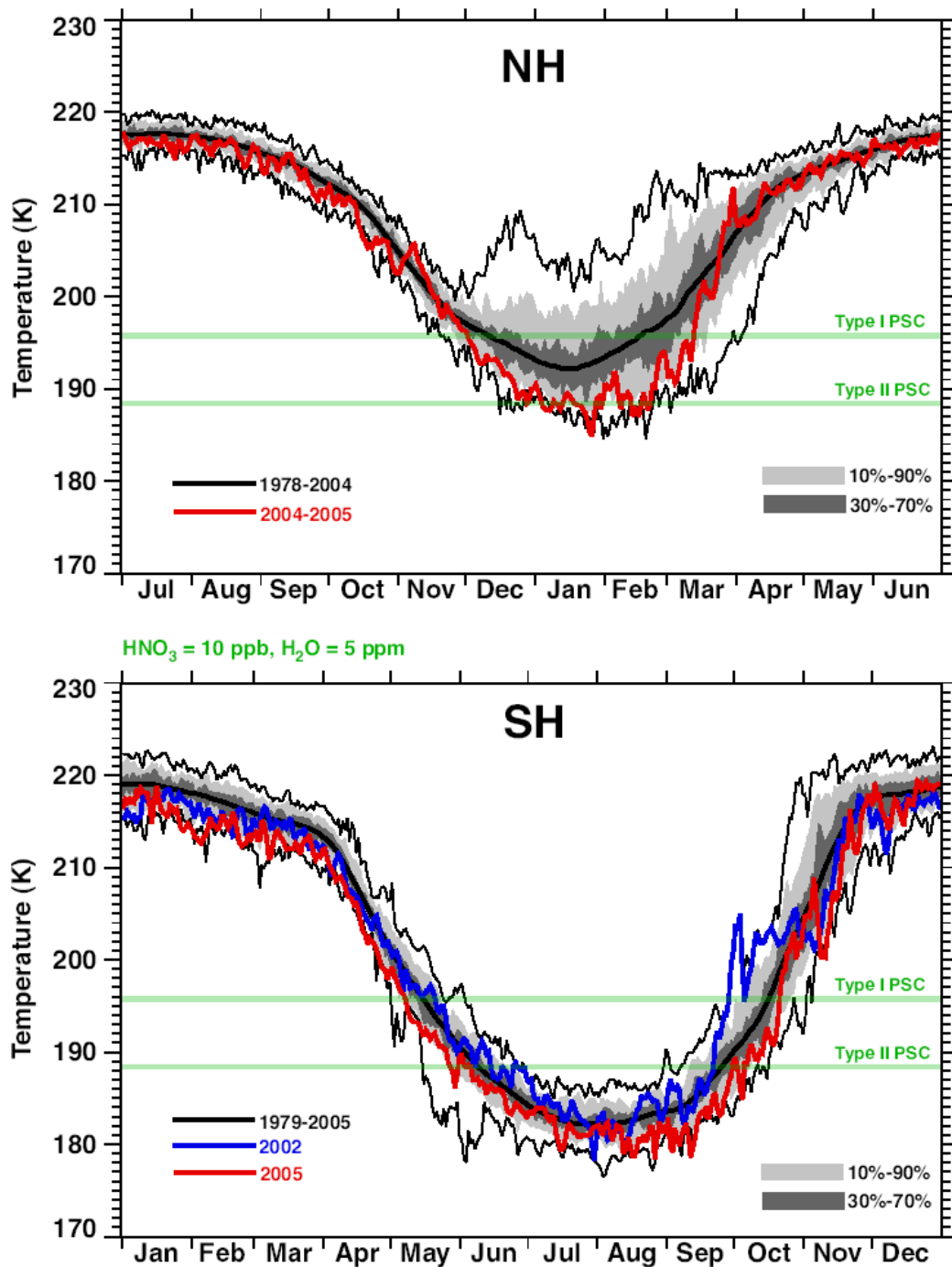


Figure 2.16: Annual stratospheric temperature cycle and variability in the Arctic (NH) and Antarctic (SH). The green lines indicate the temperature threshold below which PSCs can form. The black curve shows the mean temperature for the period 1979–2004 (NH) and 1979–2005 (SH) with record values indicated (thin black curves). The red line shows the development in the Arctic (2004/2005) and Antarctic (2005), and 2002 (blue). The grey shaded area shows the interval within which the percentage of observations falls [WMO, 2007].

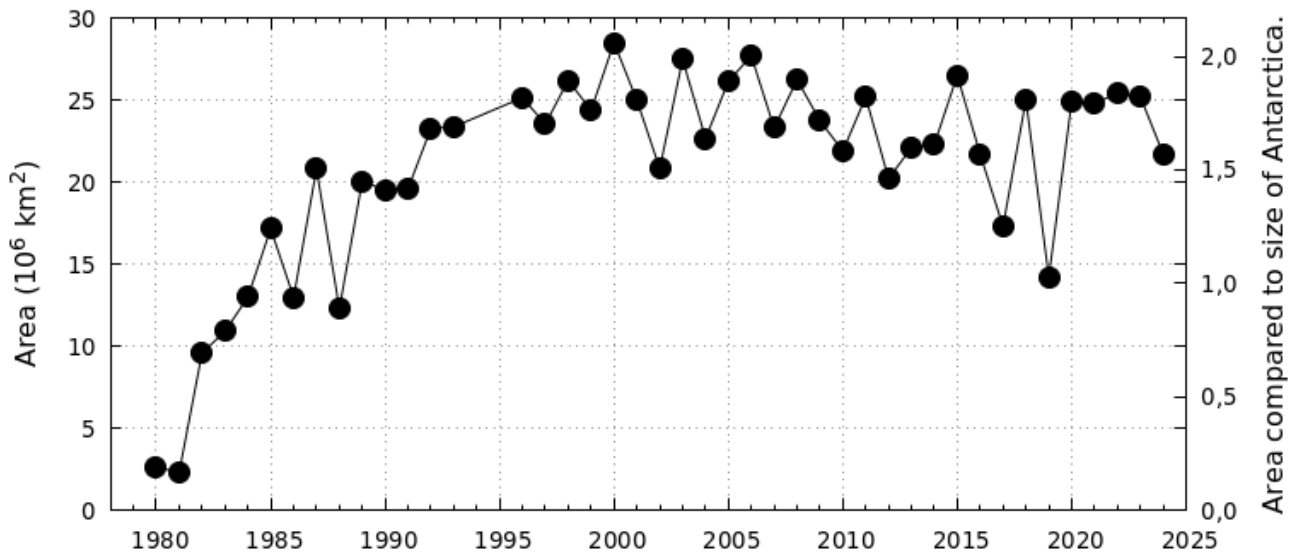


Figure 2.17: Maximum extent of the Antarctic ozone hole during the period 1979–2024, based on satellite observations from NASA, ESA, and EUMETSAT.

A general decrease in the size of the ozone hole is expected due to the declining amount of ozone-depleting substances in the stratosphere as a result of the Montreal Protocol. This trend is visible in Fig. 2.17, where the ozone hole size peaks around the year 2000, followed by a reduction with year-to-year variations caused by meteorological conditions in subsequent years. In recent years (2018 to 2023), the Antarctic ozone hole has shown relatively consistent behavior. With the exception of 2019, when a rare sudden stratospheric warming event occurred in early September, all years exhibited a stable maximum ozone hole area of approximately 25 million km<sup>2</sup>. During this period the polar stratospheric cloud (PSC) volume in August, when ozone depletion typically begins, was about 16% larger than in earlier years. The exceptional warming event in September 2019 disrupted these conditions and prevented further expansion of the ozone hole despite initial similarities to the surrounding years.

As for the past year 2024, the ozone hole appeared in late August (Fig. 2.18), slightly later than usual, and grew to its maximum size of 21.7 million km<sup>2</sup> on 28 September. The size remained very close to the normal range for 1986–2023 until early December, when the vortex broke down. The smaller ozone hole during 2024 therefore indicates that progress towards the recovery of the ozone layer over Antarctica around the year 2065 is still on track. However, a definitive conclusion requires several more years of observations.

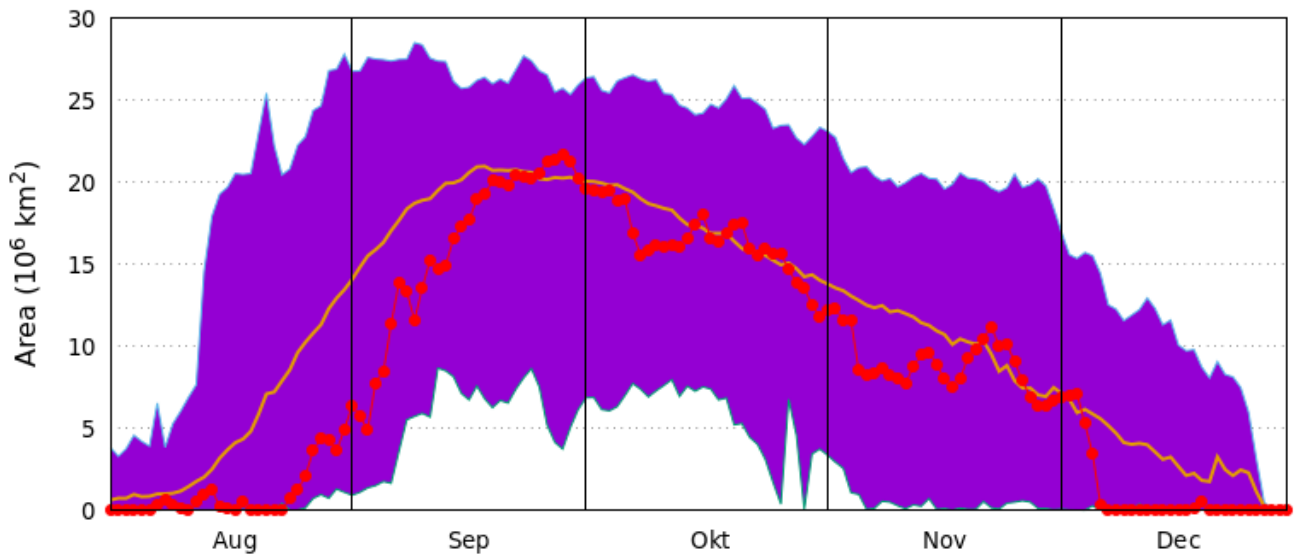


Figure 2.18: Size of the ozone hole from August to December. The orange curve shows the average size for 1986–2023, and the purple area indicates the minimum and maximum sizes during the same period. The red points represent the data for 2024 based on satellite data from NASA, ESA and EUMETSAT.

Figure 2.19 shows the extent of the ozone hole (dark blue area where the thickness is below 220 DU) at its maximum size on 28 September. The blue area is defined by the polar vortex, which isolates the region with a very thin ozone layer from mixing with ozone-rich air transported from the tropics. When the vortex eventually breaks down during the spring or summer, the two air masses mix and the ozone hole disappears.

At the time of the ozone hole's maximum extent, the solar elevation over the Antarctic region is still relatively low, and the impact of the ozone hole, manifested as increased ultraviolet (UV) radiation reaching the Earth's surface, occurs at a later stage. In 2024, the peak additional UV exposure in the region occurred around 3 December. Although the ozone hole had contracted by approximately 60% compared with its maximum size, the effect of the generally thinned ozone layer still allowed for UV Index values exceeding 13 under cloud-free conditions on the Antarctic continent (see Fig. 2.20). Such high values are otherwise only observed in equatorial regions and never at comparable latitudes in the Northern Hemisphere.

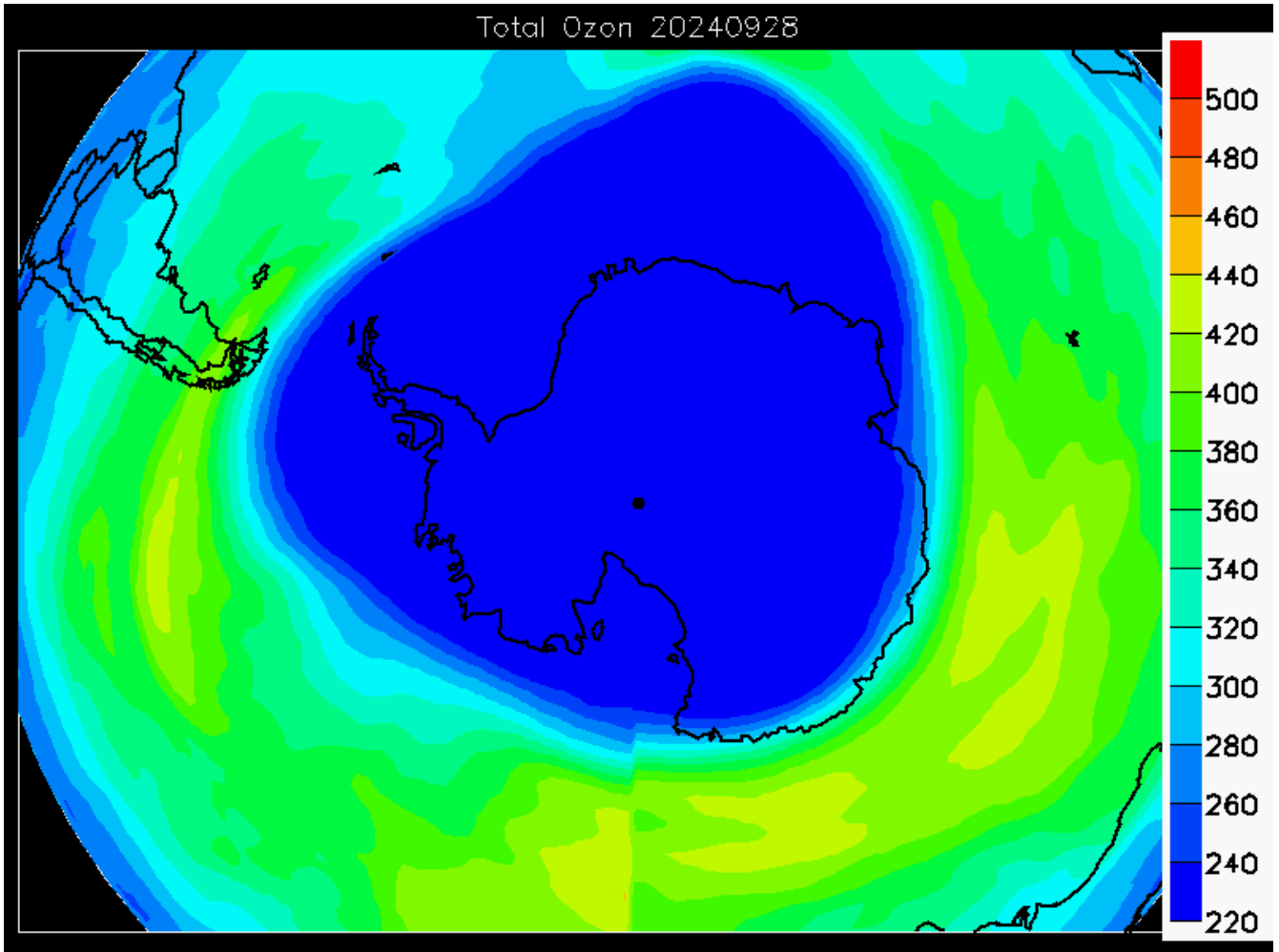


Figure 2.19: The ozone hole (dark blue area) at its maximum extent on 28 September 2024. (Data from EUMETSAT/AC SAF)

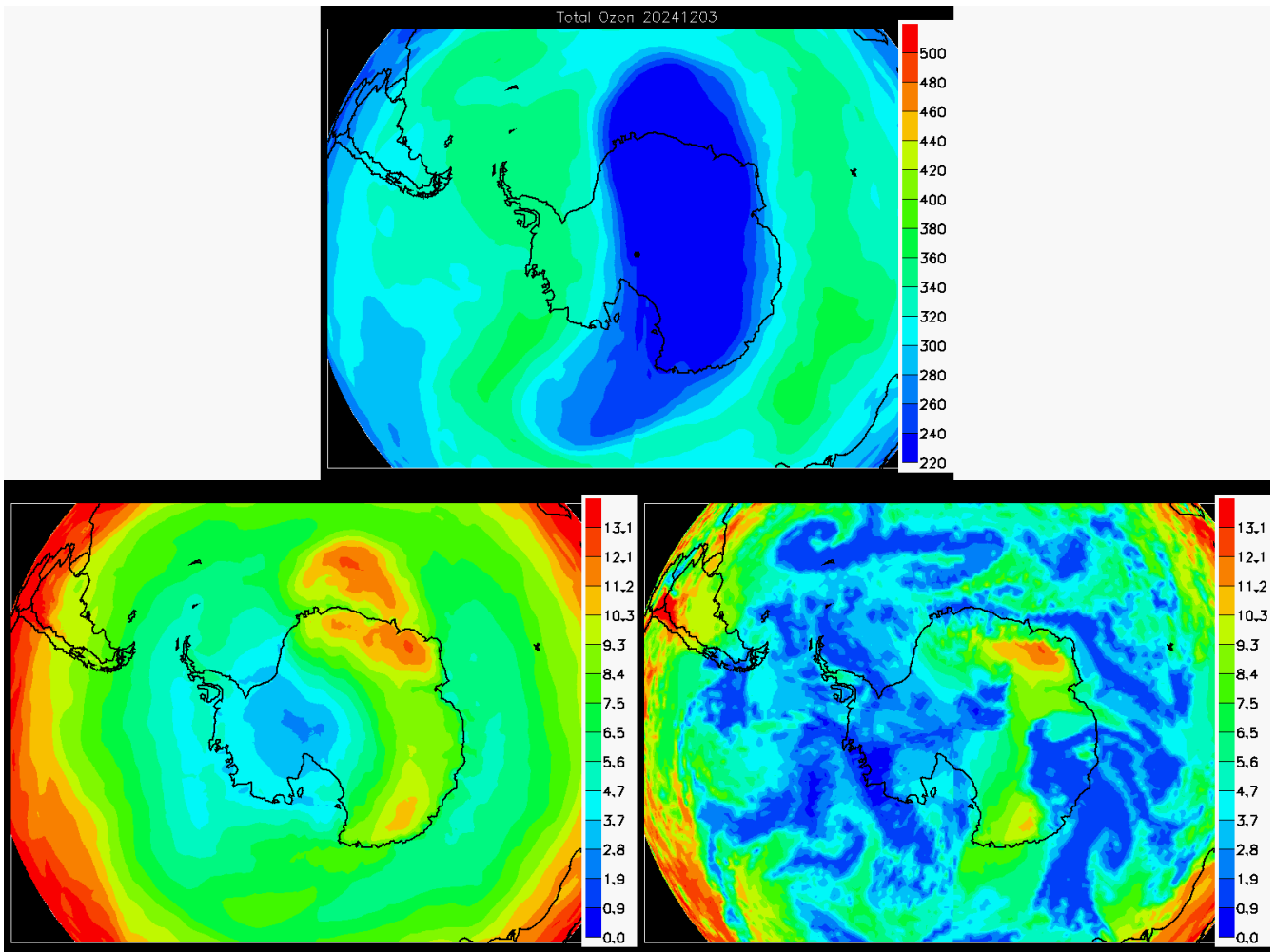


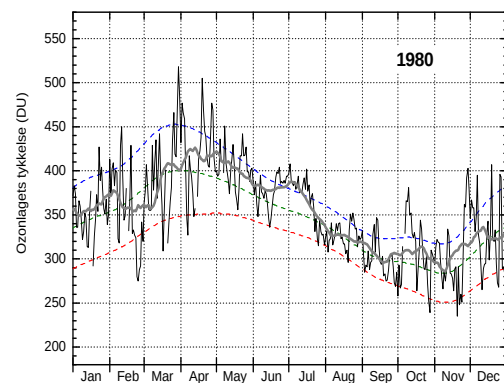
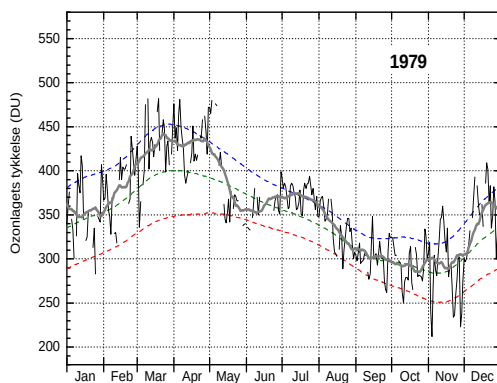
Figure 2.20: Top: Antarctic ozone hole extent on 3 December 2024. Bottom left: UV index at local noon for clear-sky conditions on the same date. Bottom right: UV index adjusted for cloud cover. (Data from EUMETSAT/AC SAF).

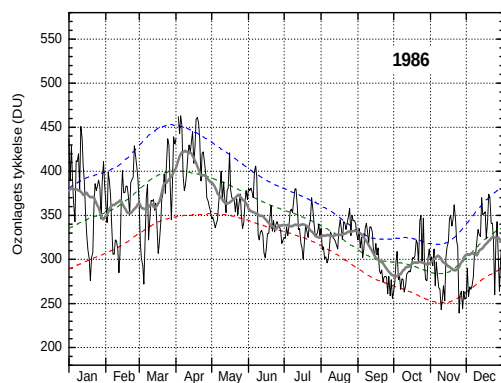
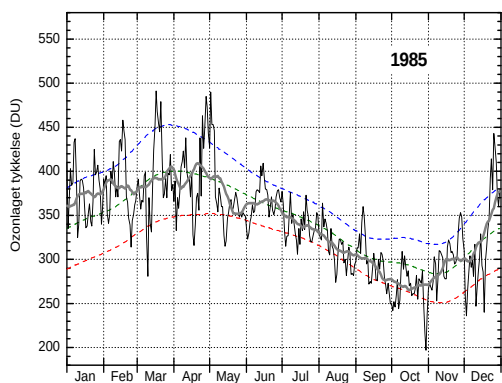
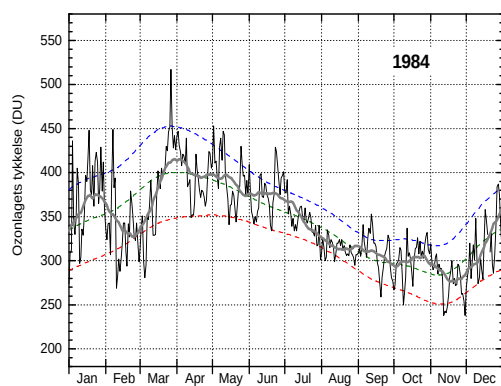
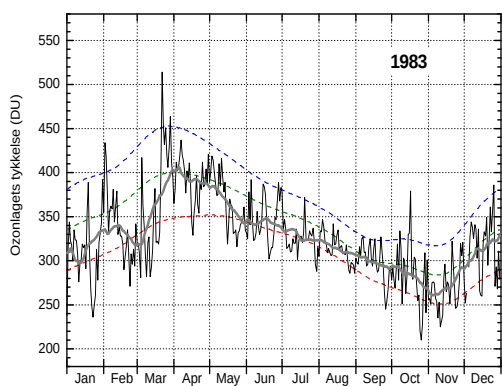
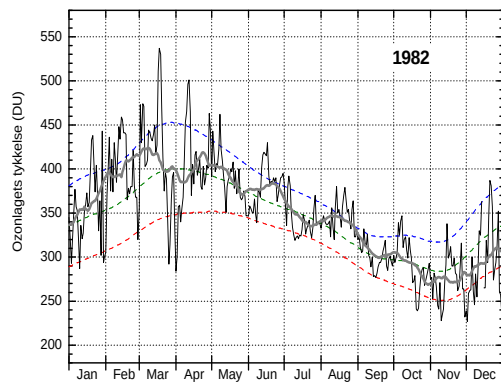
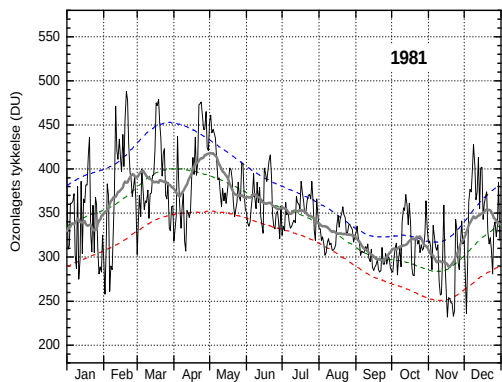
## Appendix A

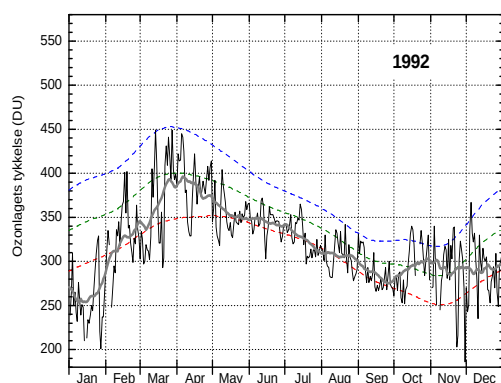
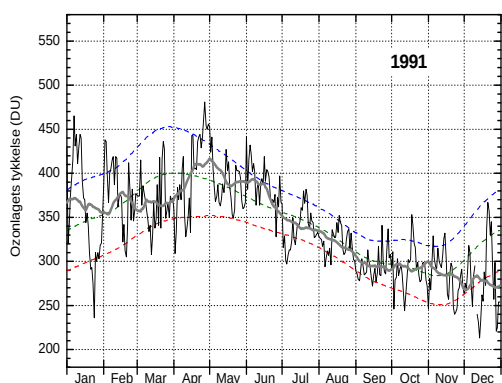
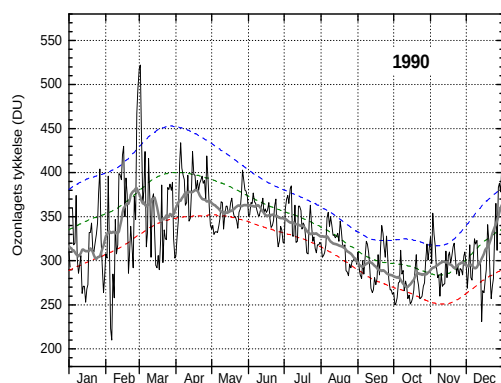
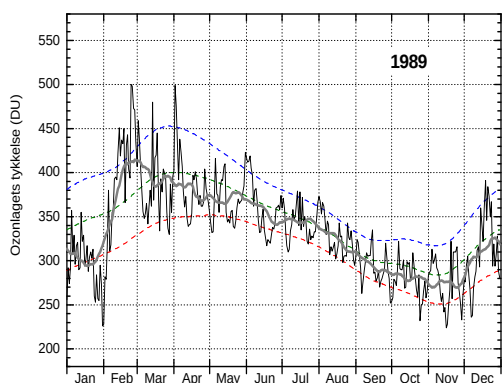
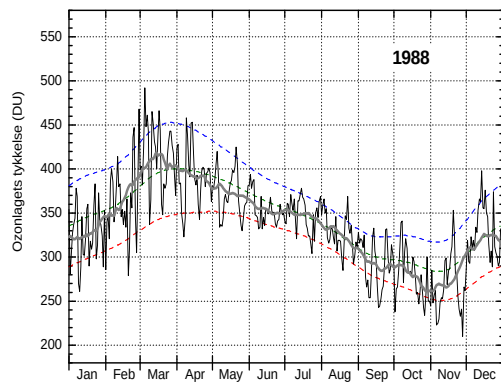
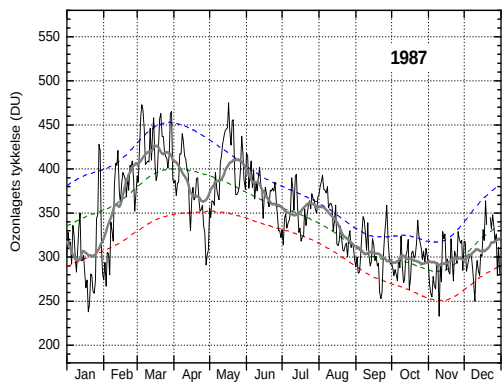
# Daily Measurements of the Ozone Layer over Denmark

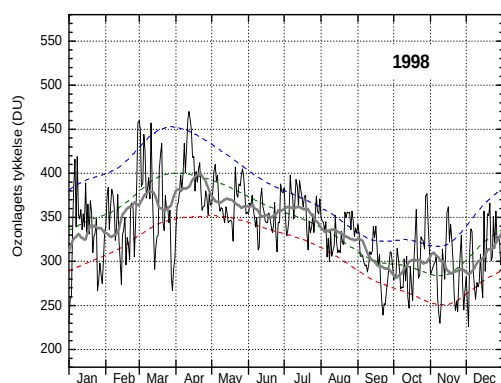
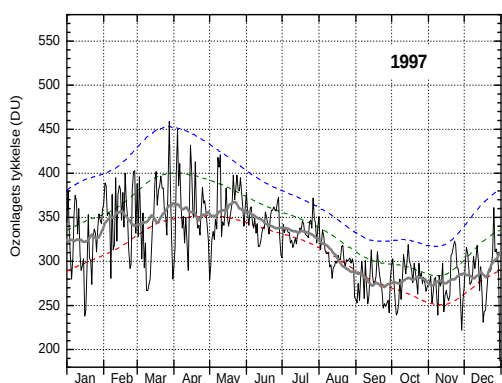
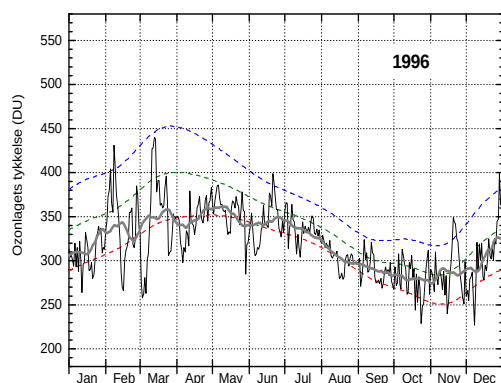
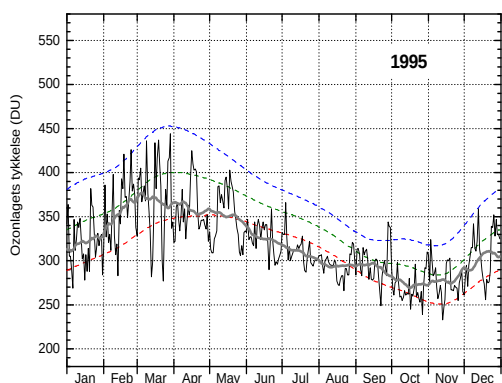
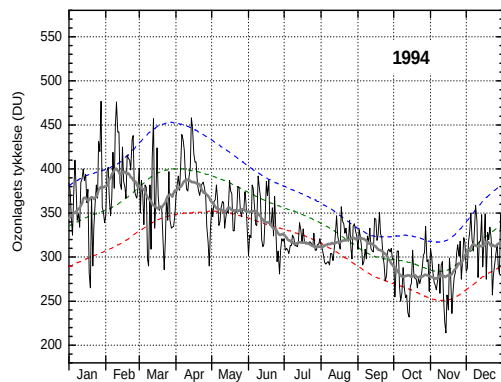
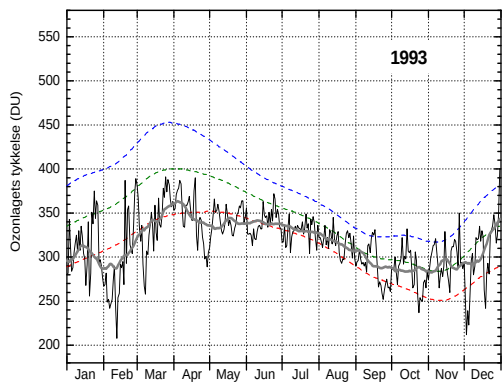
Ozone layer thickness over Denmark, 1979–2024. Daily measurements (thin black line) are from NASA's TOMS instrument on the Nimbus-7 satellite for the period 1979–June 1992. From June 1992 onwards, the data are from DMI's daily measurements in Copenhagen.

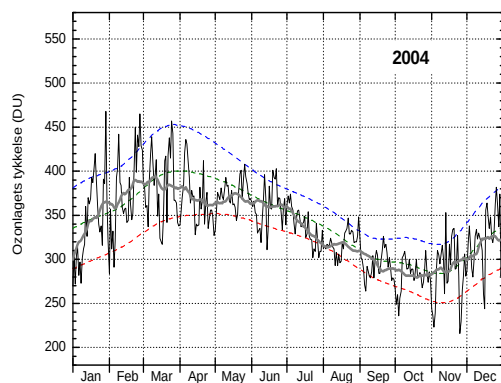
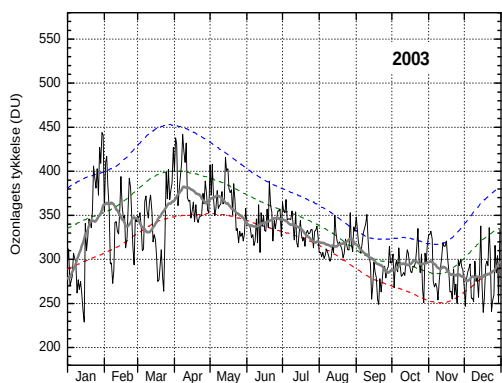
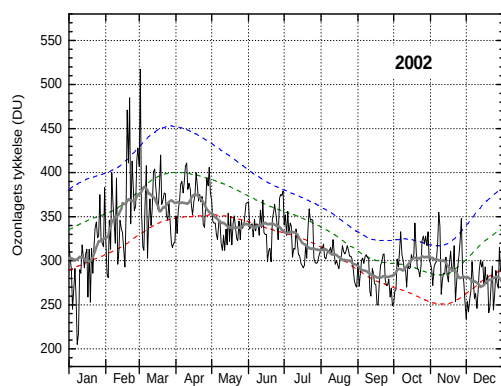
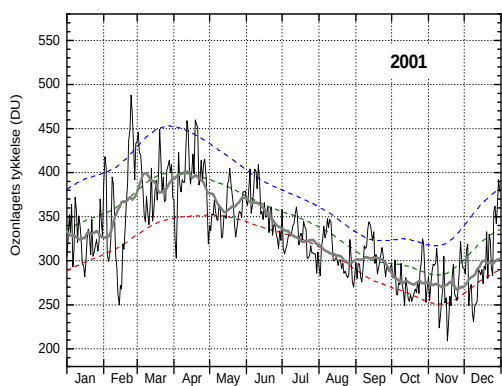
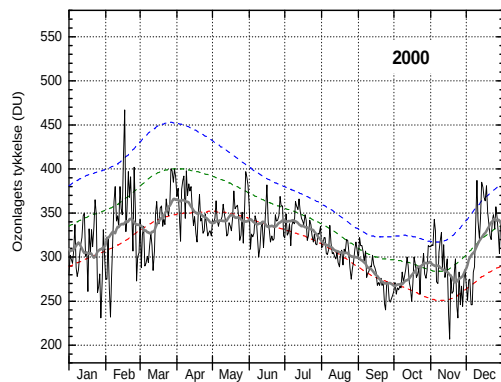
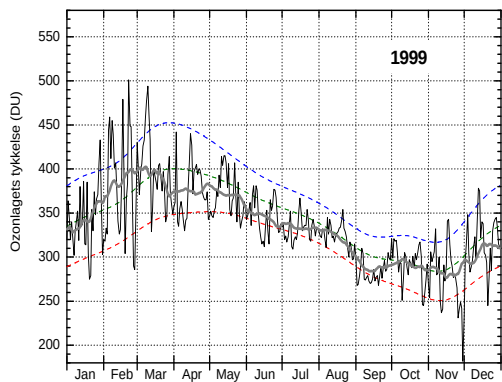
The green dashed line indicates the mean of the daily measurements for the 10-year period 1979–1988, while the blue and red dashed lines indicate the mean plus (blue) or minus (red) one standard deviation from the mean. This means that approximately two-thirds of all measurements in the period 1979–1988 fall between the blue and red lines. The thick grey line represents a 31-day running mean of the daily measurements.

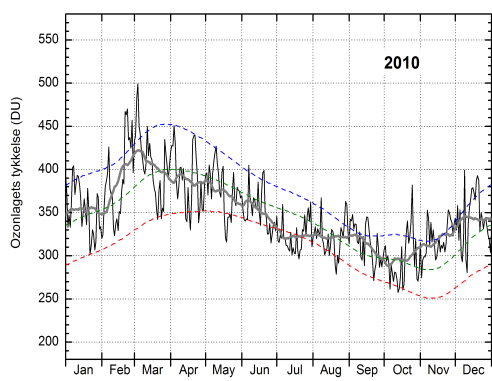
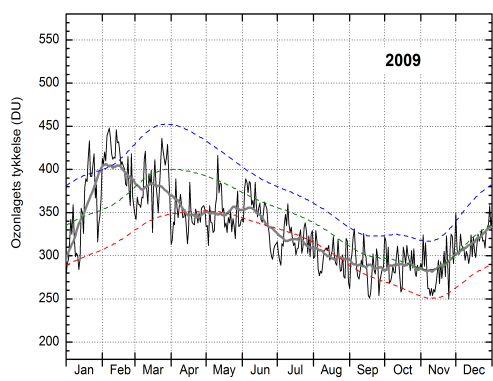
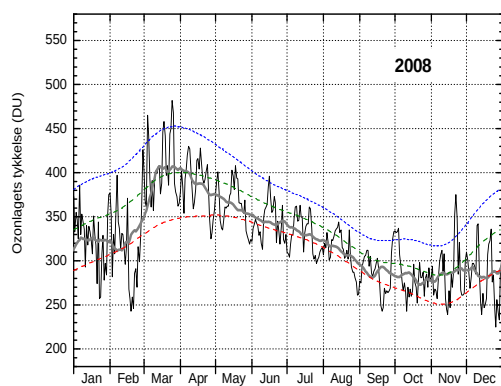
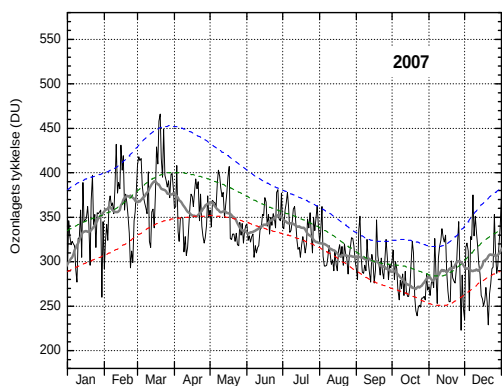
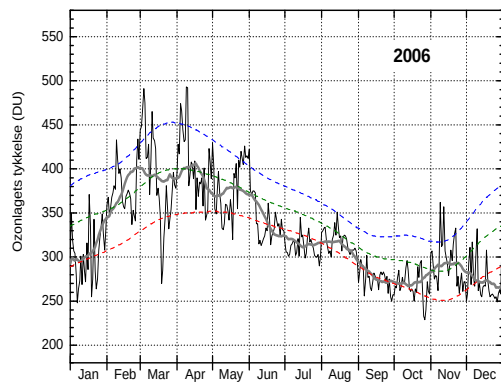
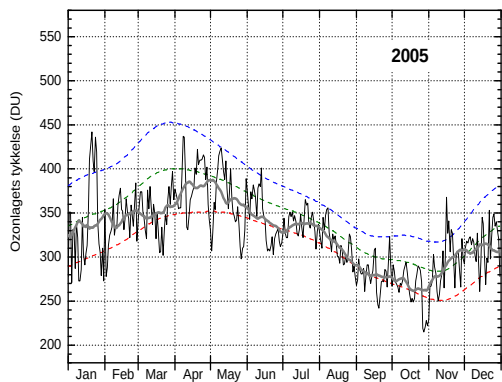


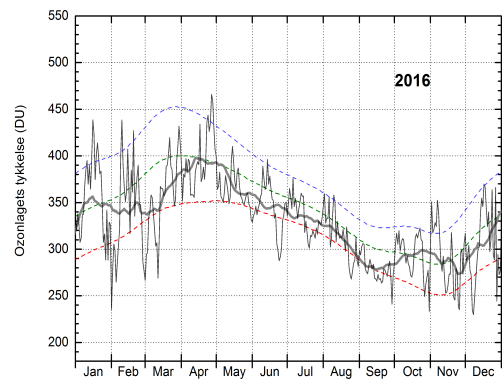
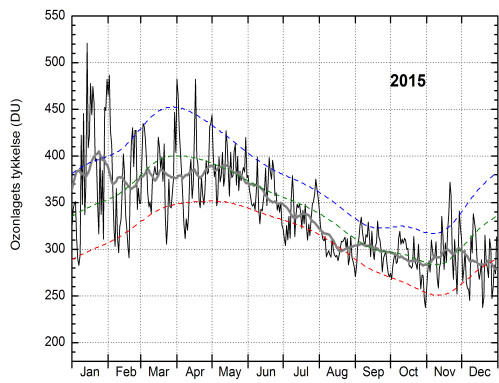
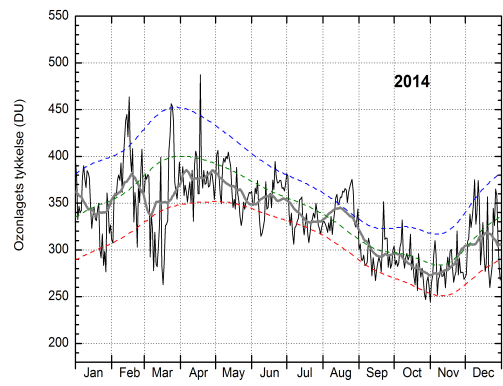
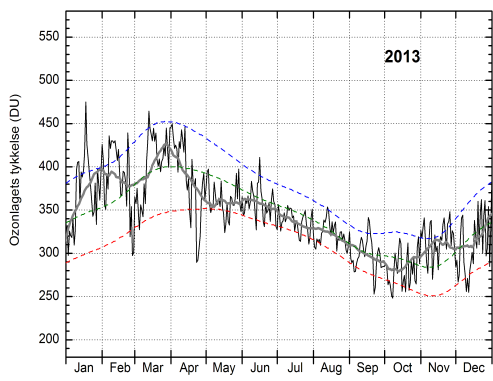
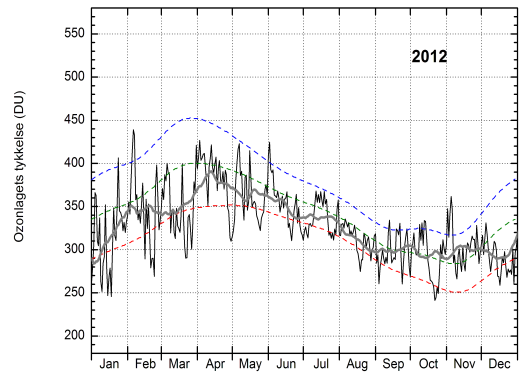
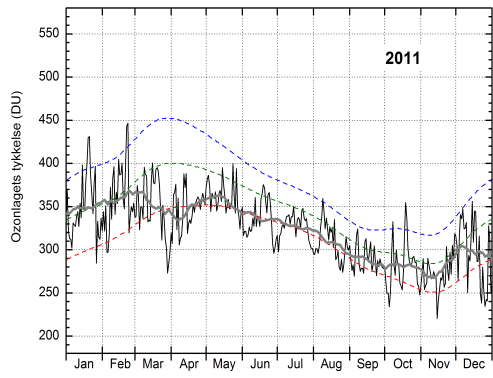


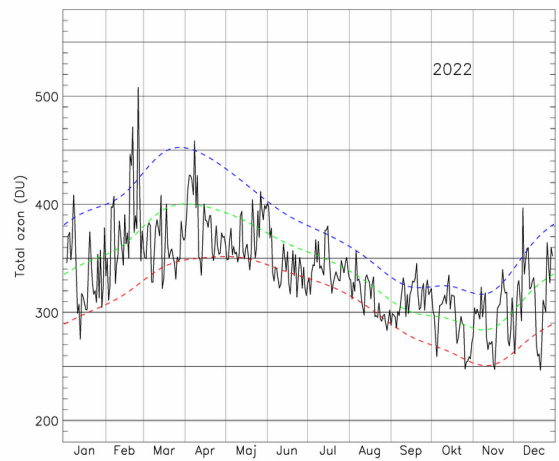
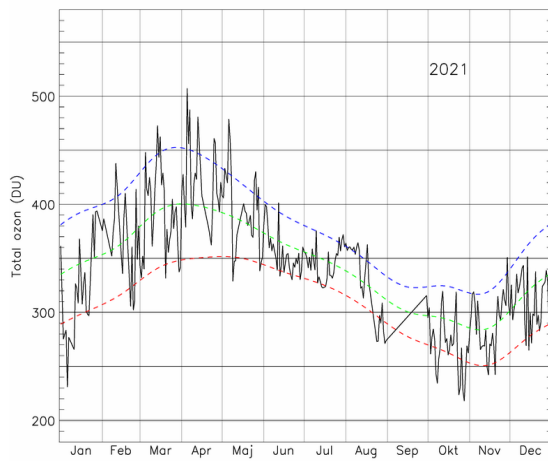
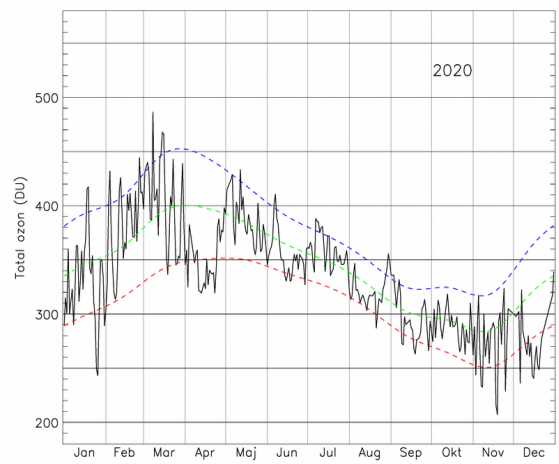
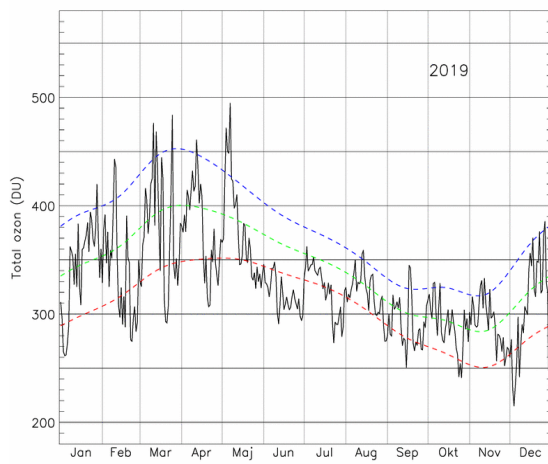
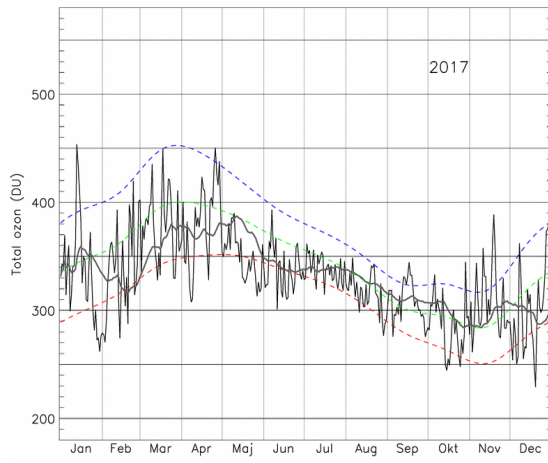


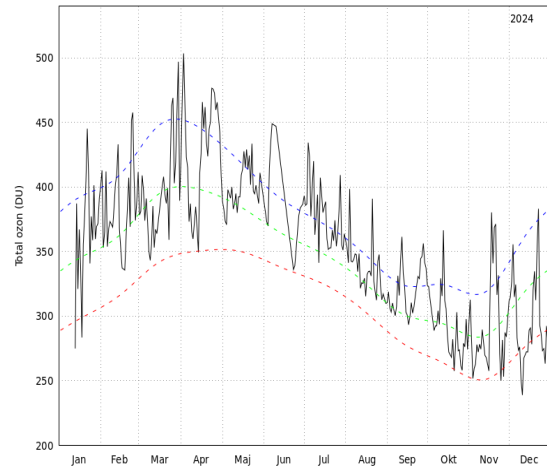
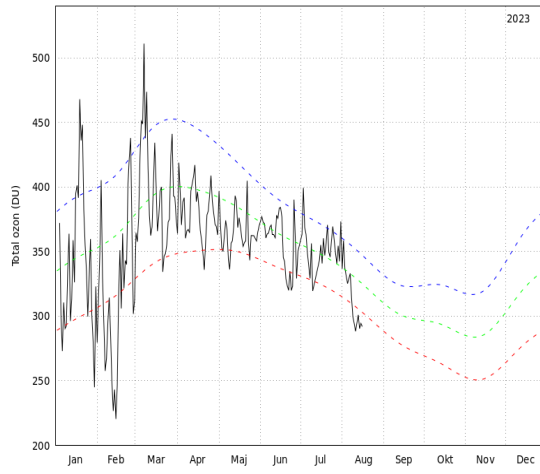










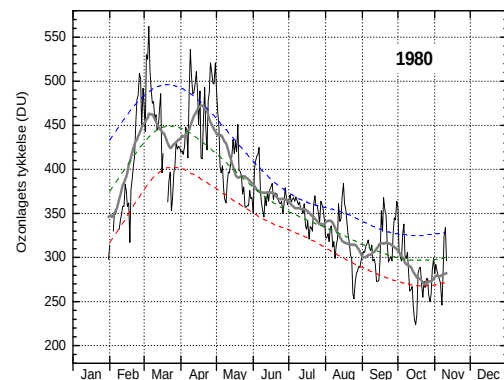
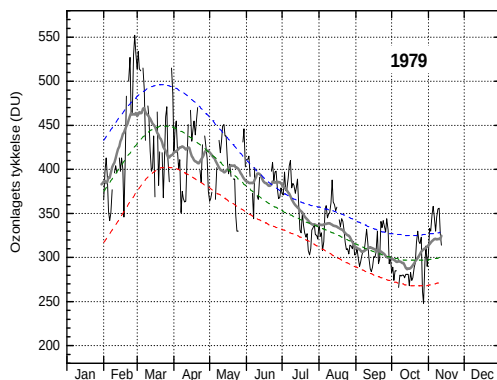


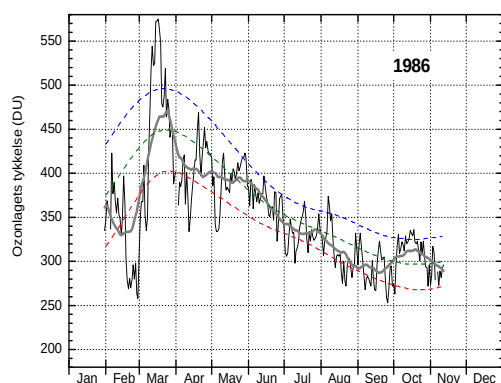
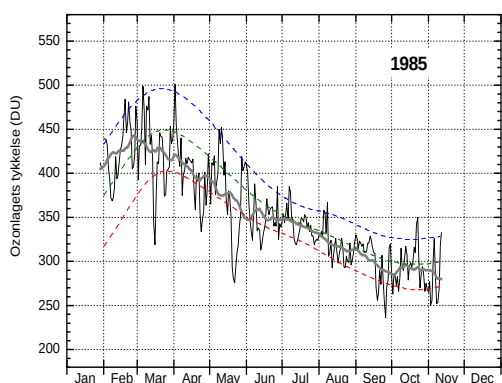
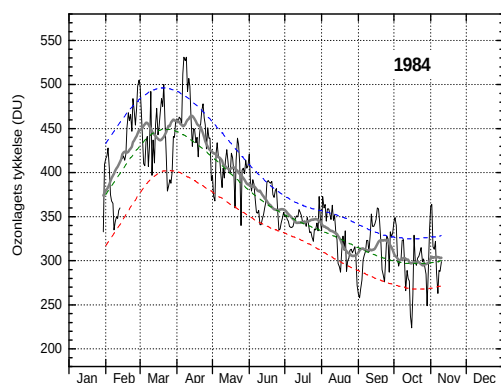
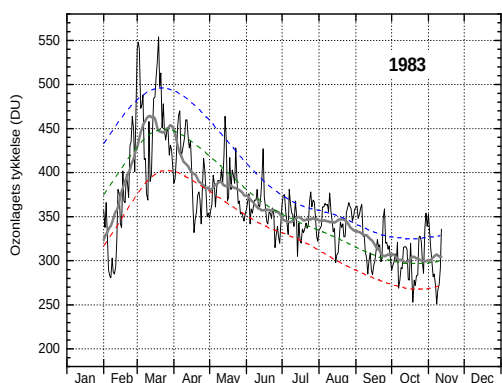
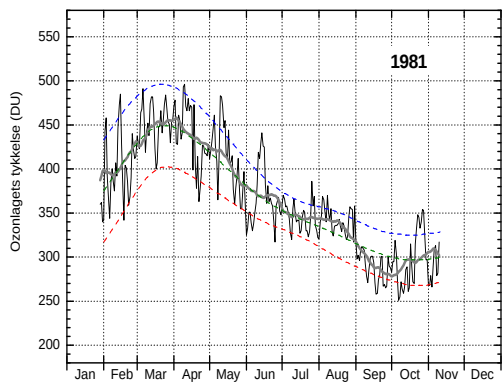
## Appendix B

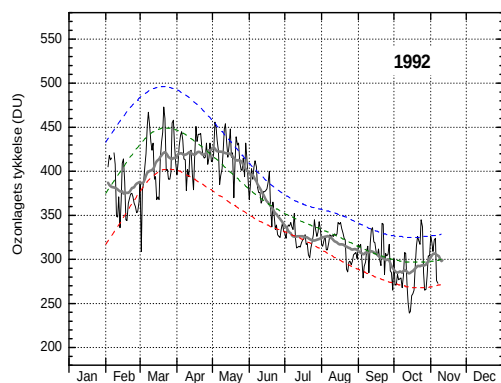
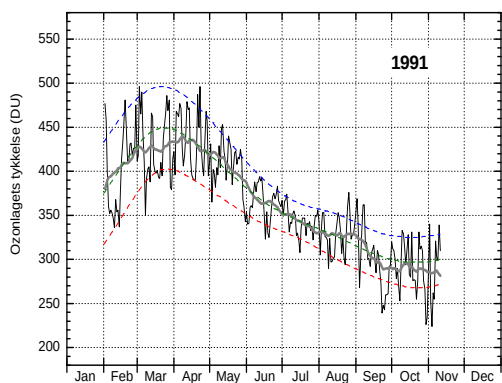
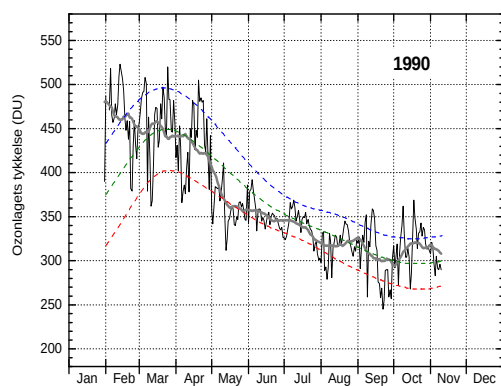
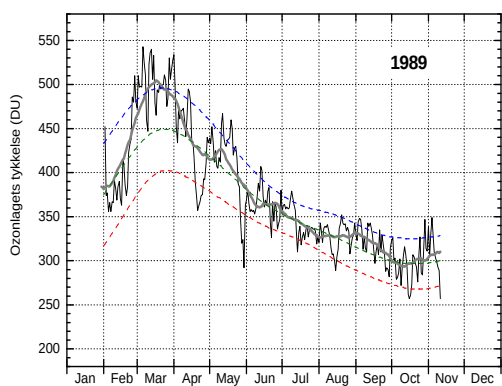
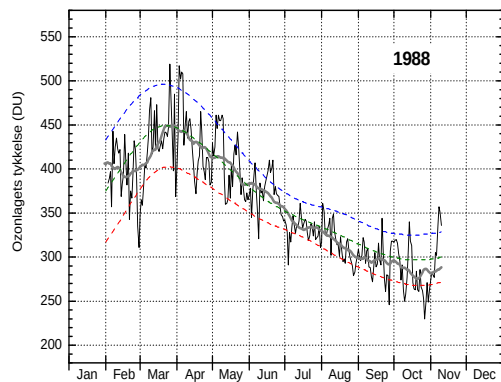
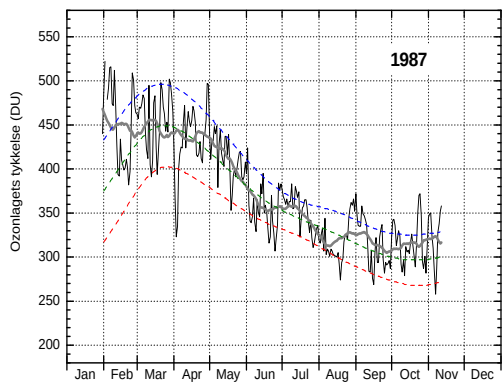
# Daily Measurements of the Ozone Layer over Kangerlussuaq

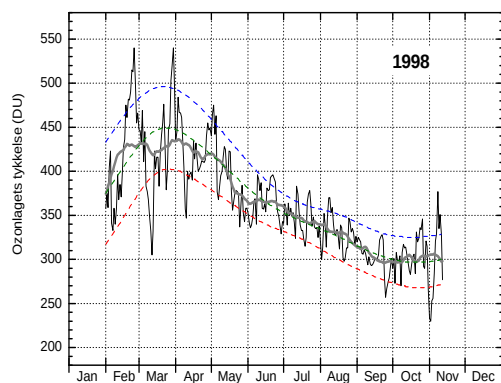
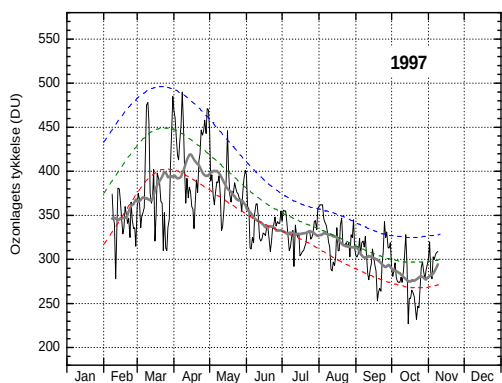
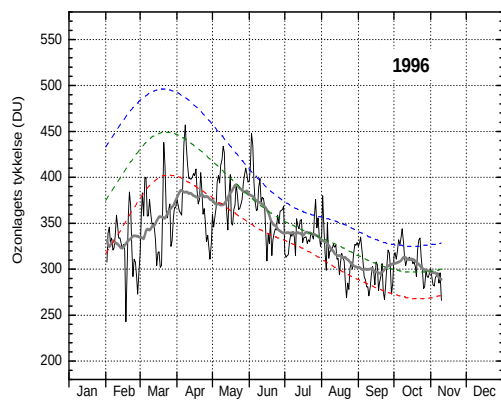
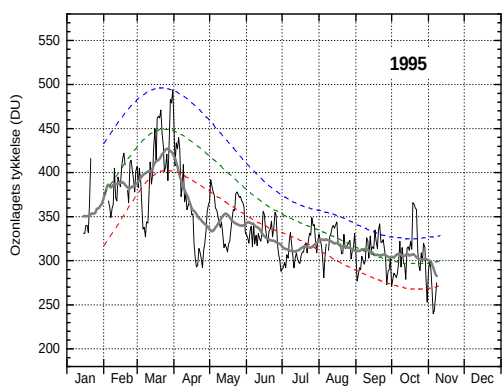
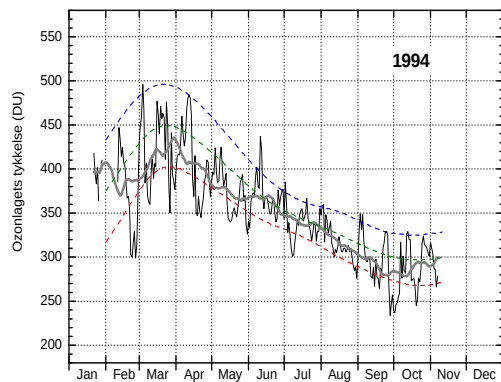
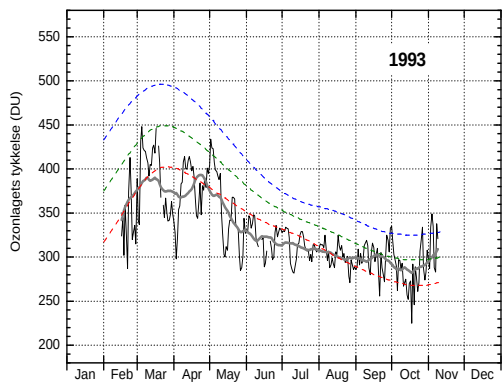
Ozone layer thickness over Kangerlussuaq, 1979–2024. Daily measurements (thin black line) are from NASA's TOMS instrument on the Nimbus-7 satellite up to 1991, and from 1991 onwards from DMI's measurements in Kangerlussuaq.

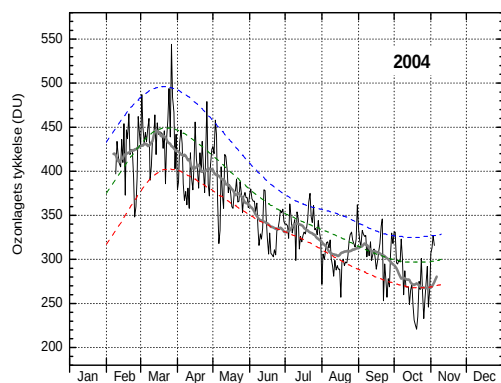
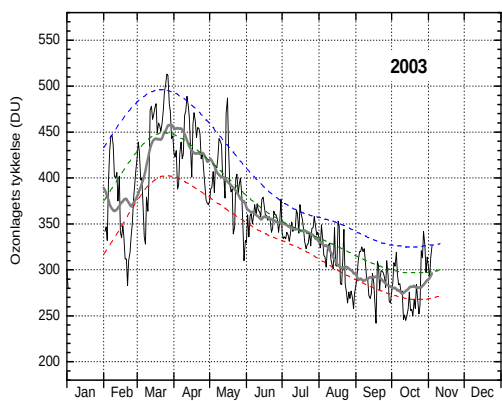
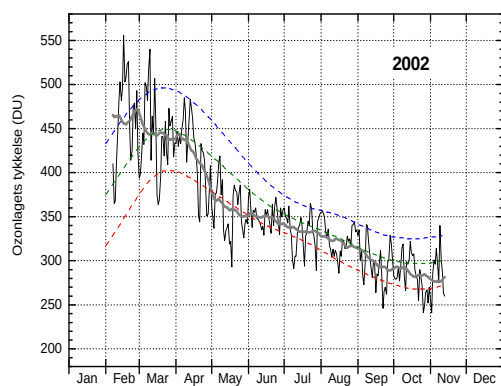
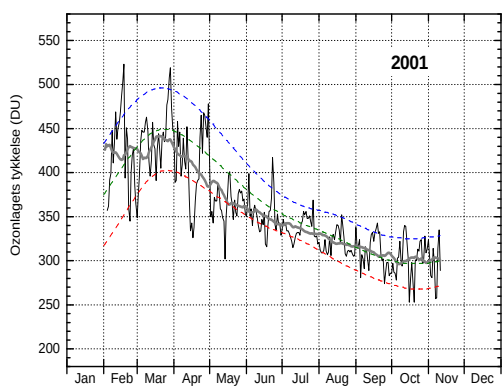
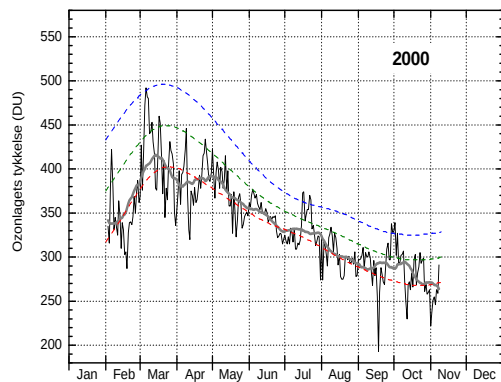
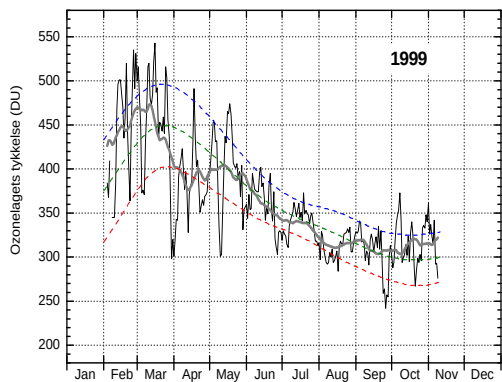
The green dashed line indicates the mean of the daily measurements for the 10-year period 1979–1988, while the blue and red dashed lines indicate the mean plus (blue) or minus (red) one standard deviation from the mean. This means that approximately two-thirds of all measurements in the period 1979–1988 fall between the blue and red lines. The thick grey line represents a 31-day running mean of the daily measurements.

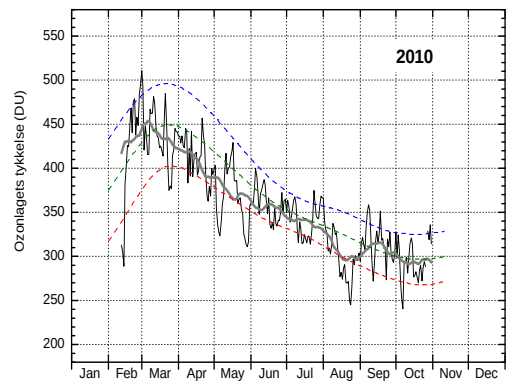
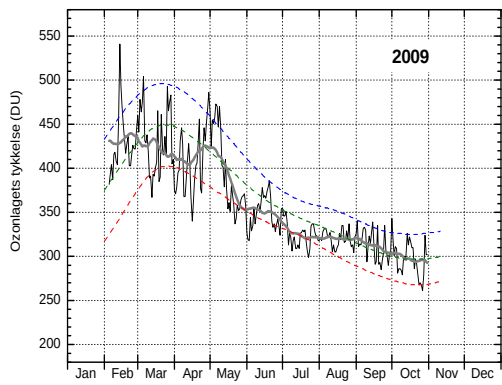
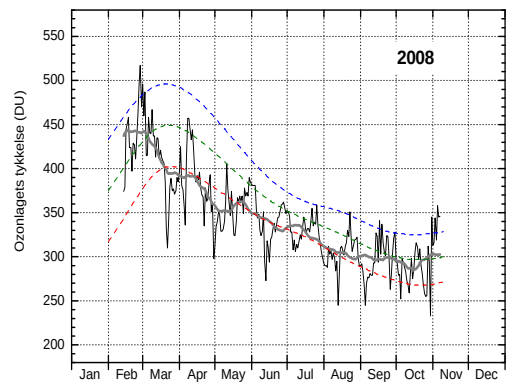
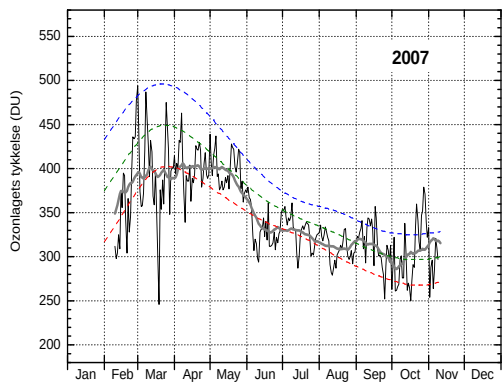
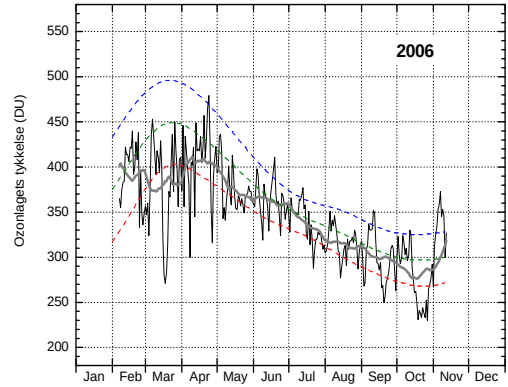
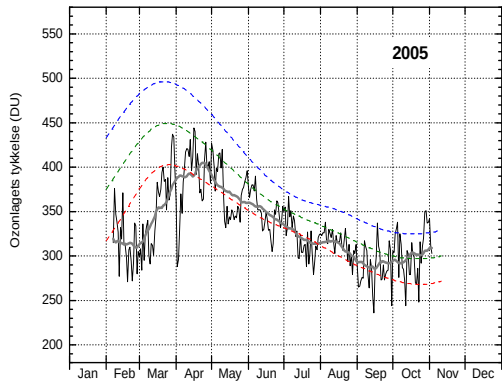


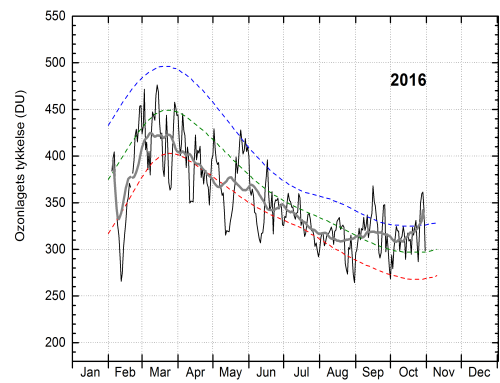
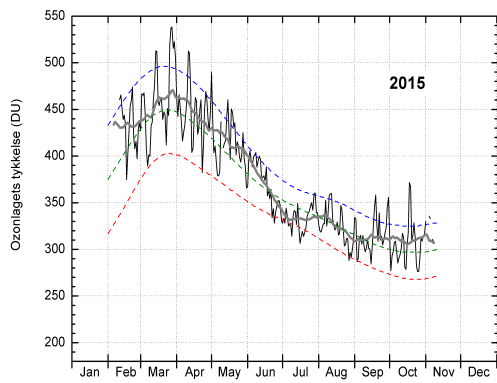
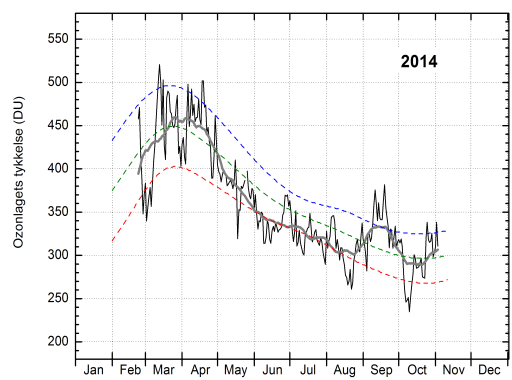
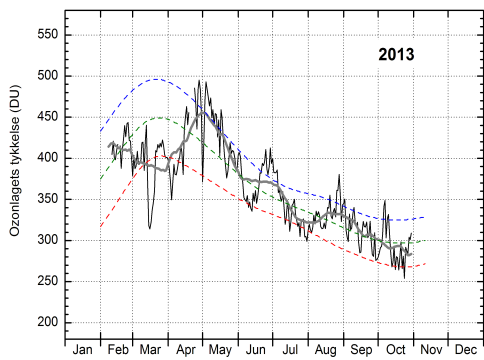
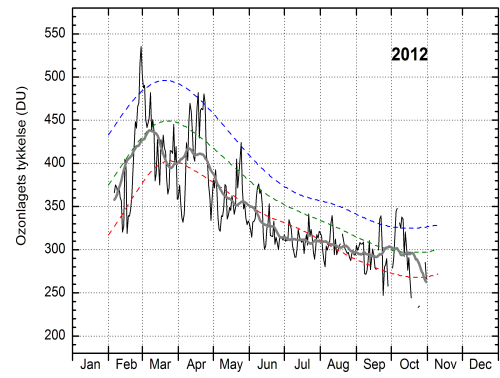
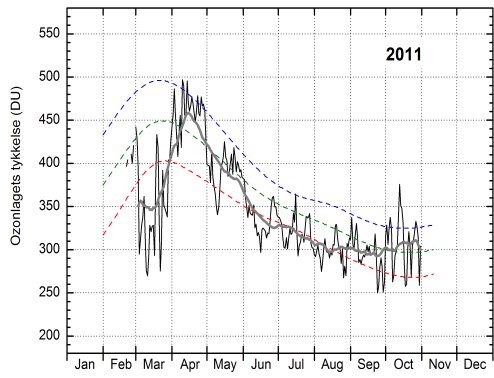


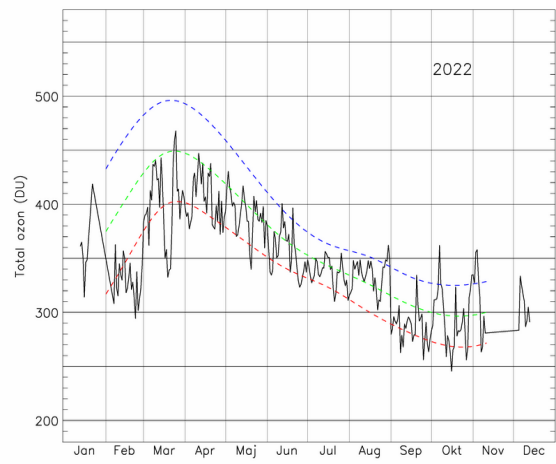
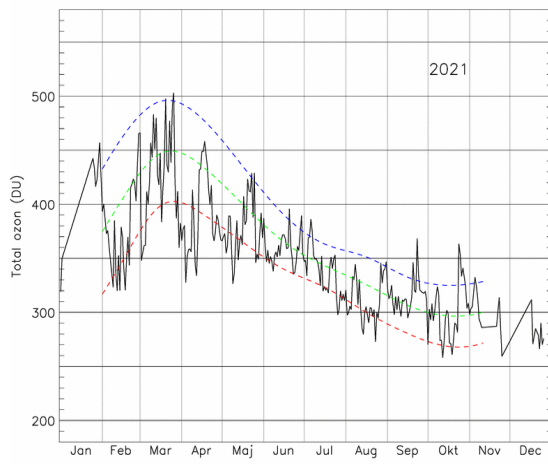
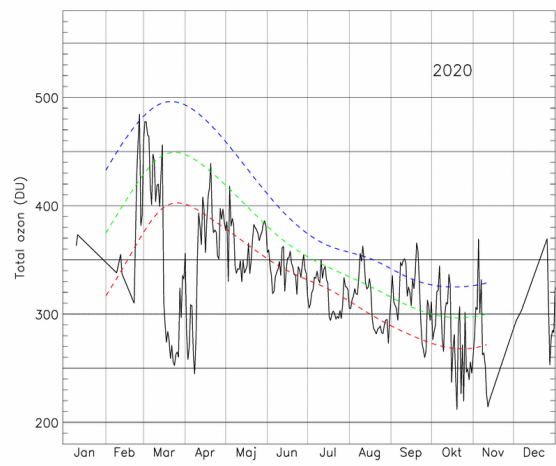
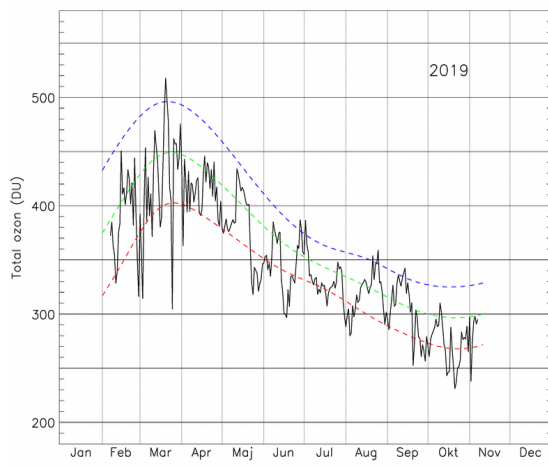
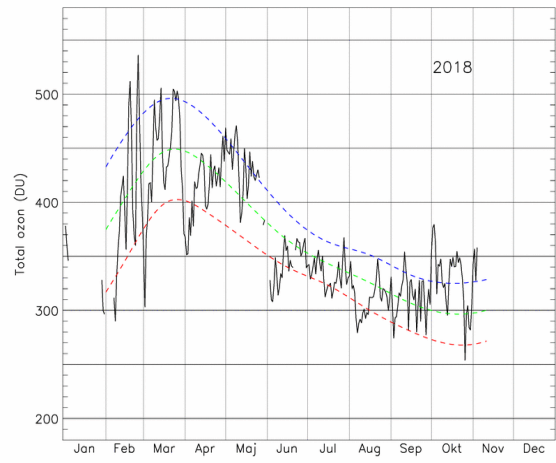


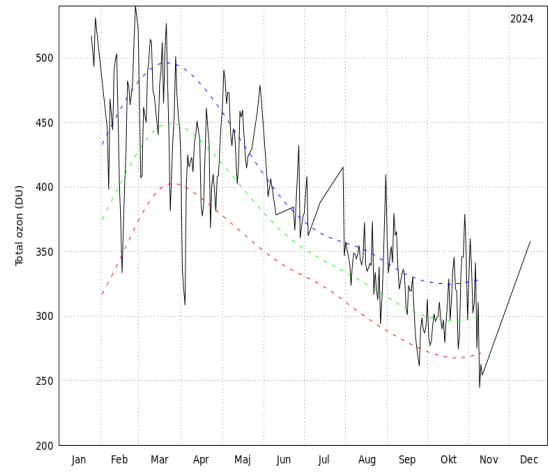
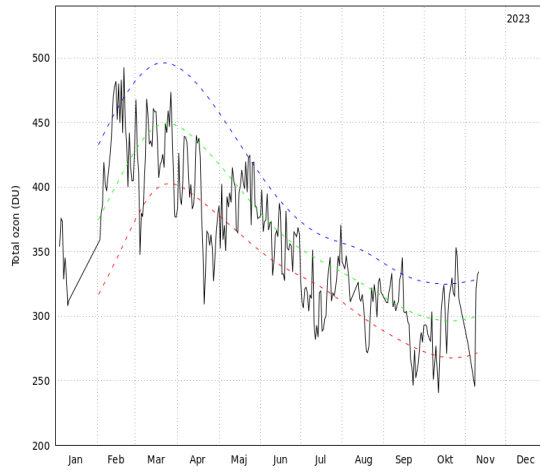










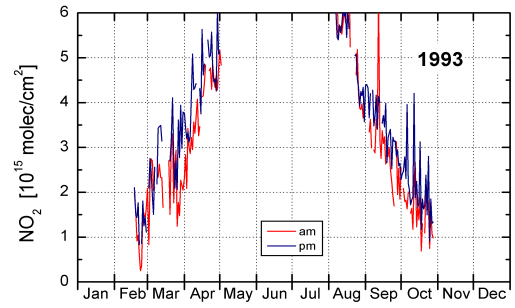
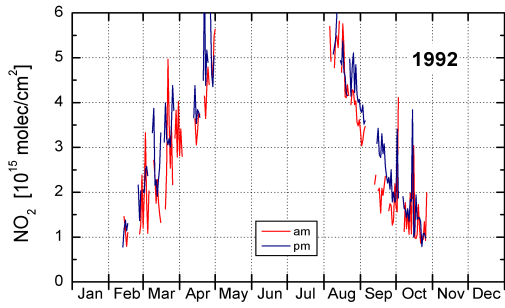
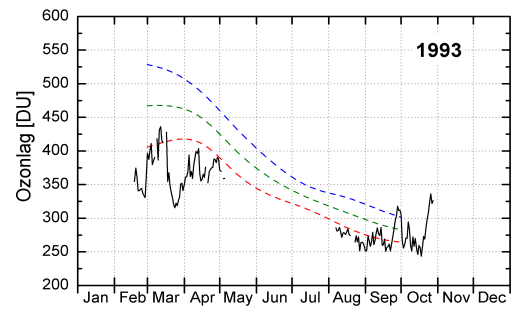
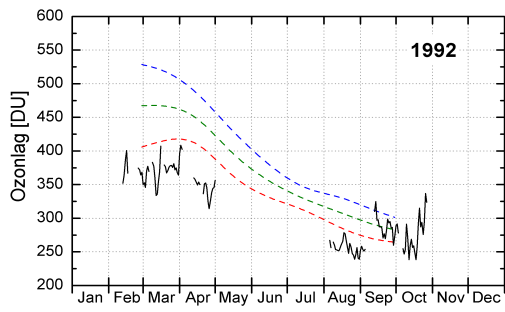
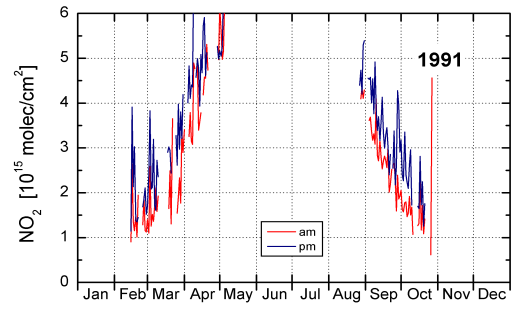
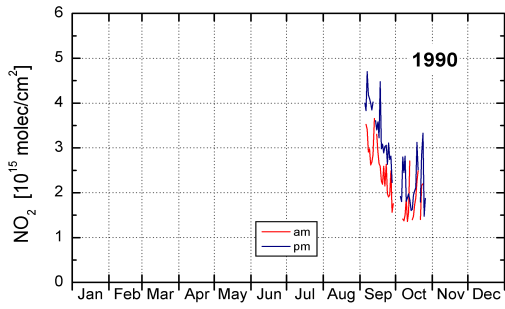
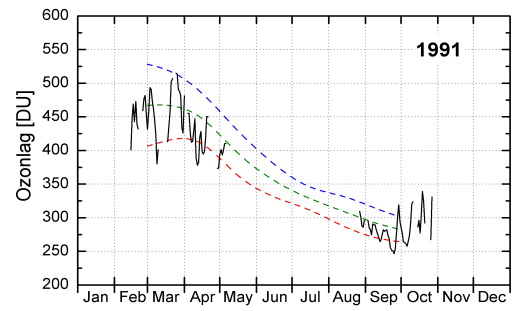
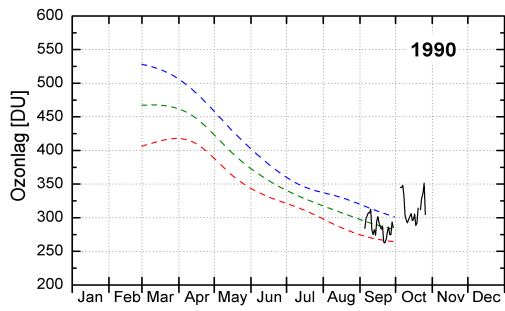


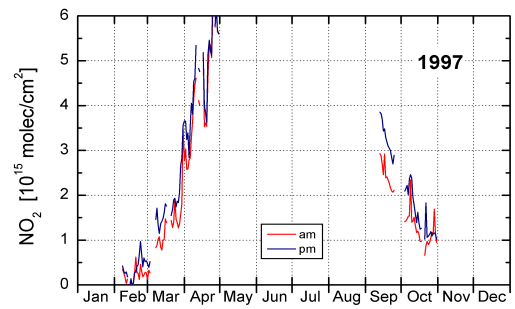
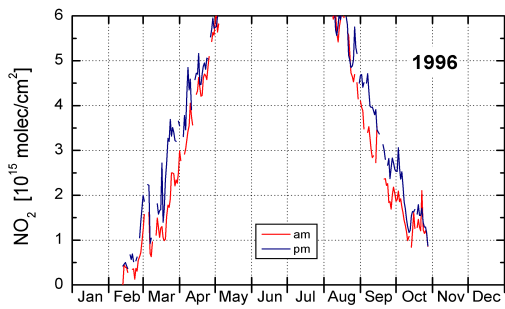
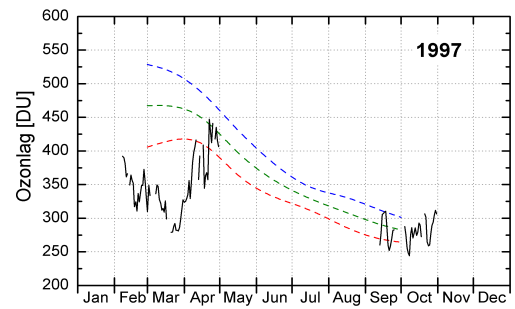
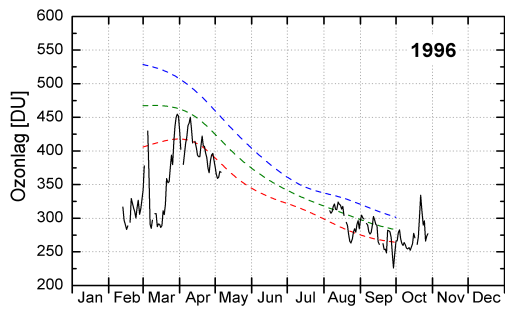
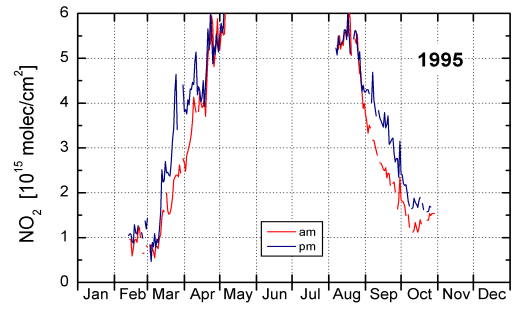
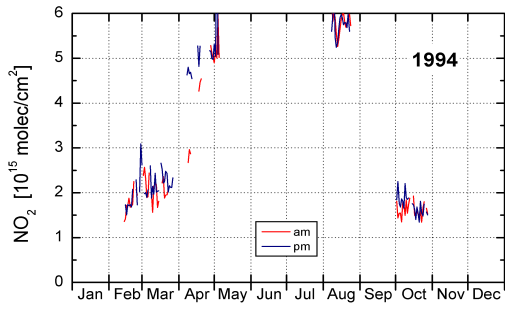
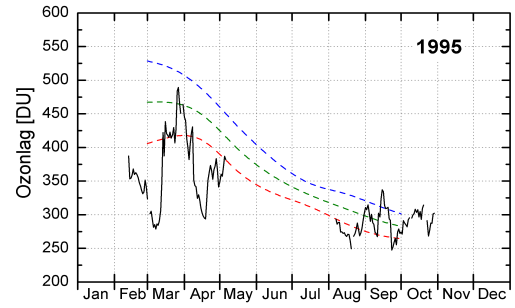
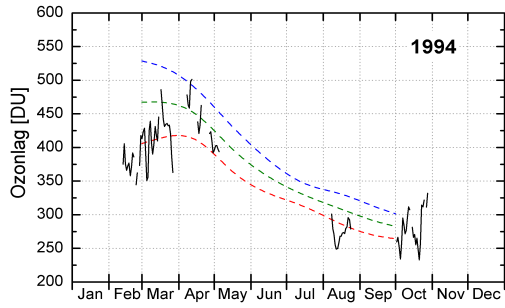
## Appendix C

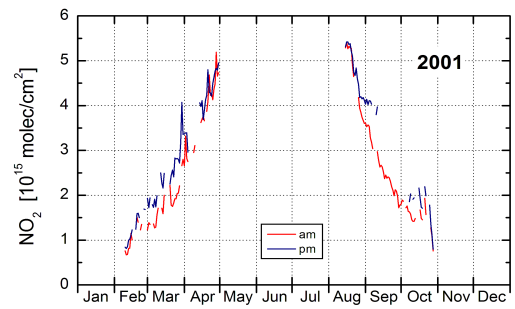
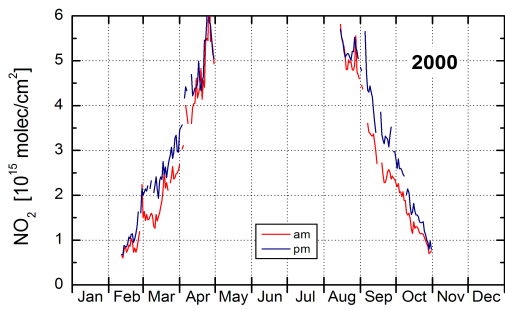
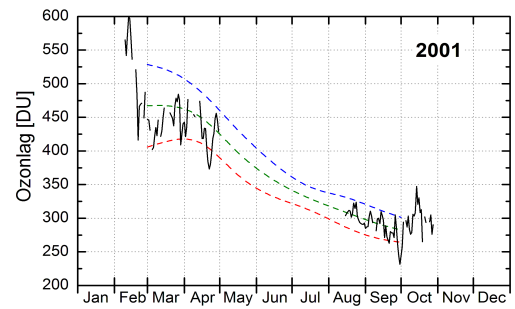
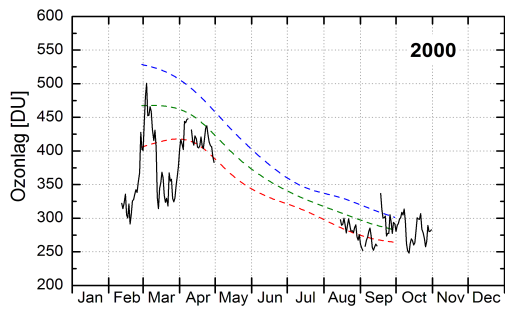
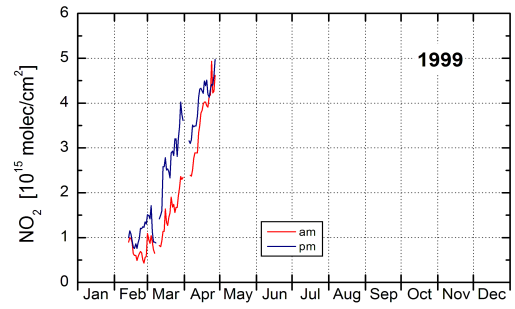
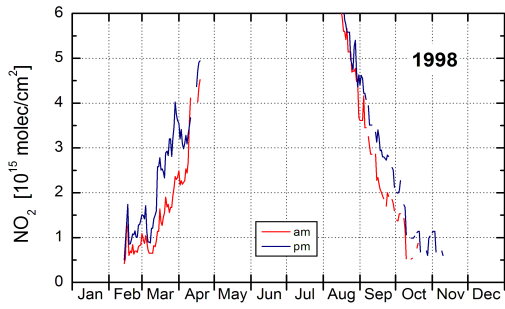
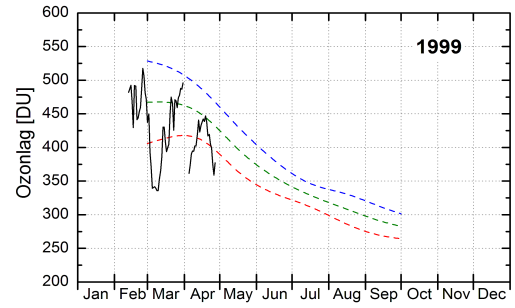
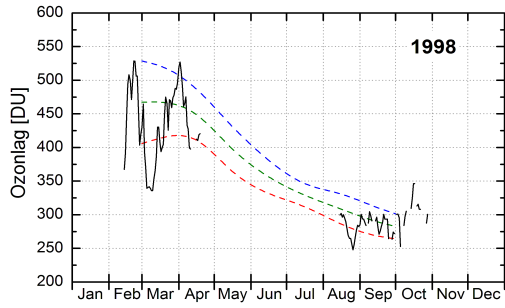
# Daily Measurements of the Ozone Layer over Pituffik

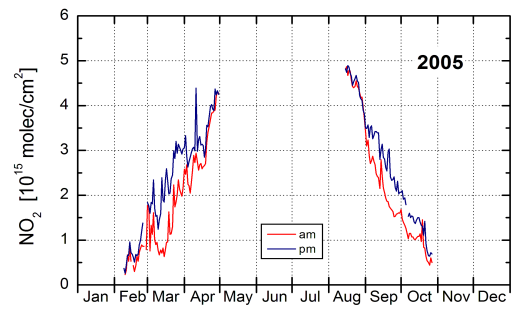
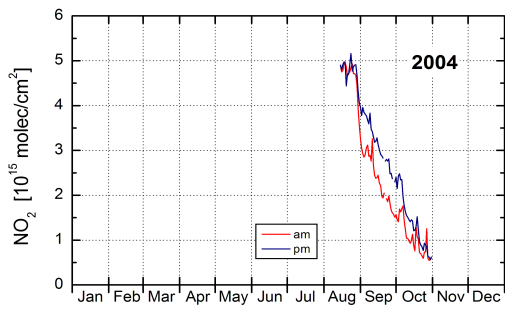
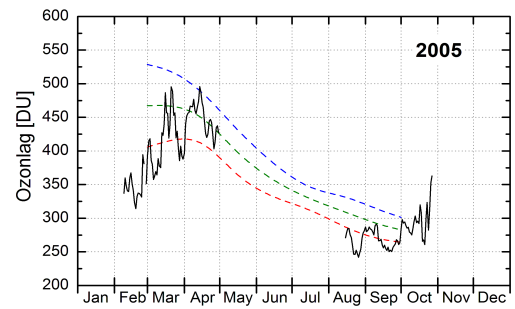
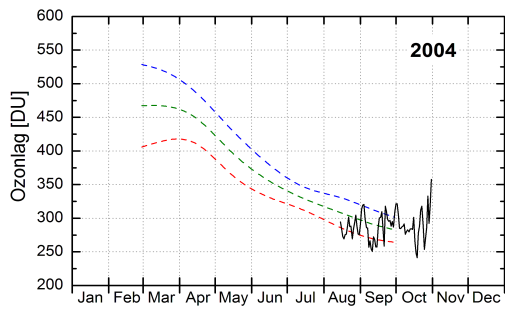
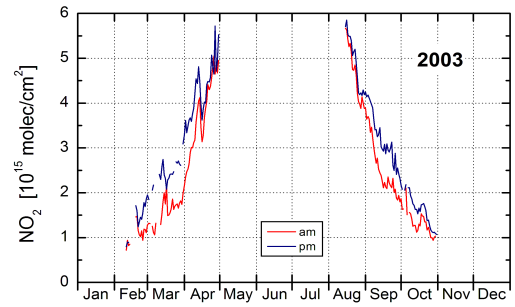
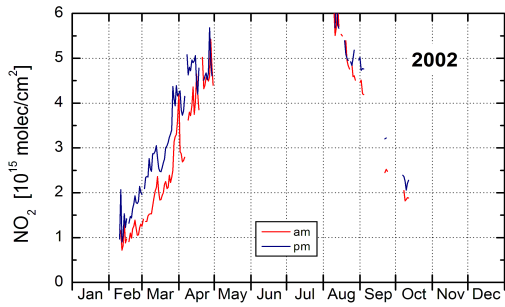
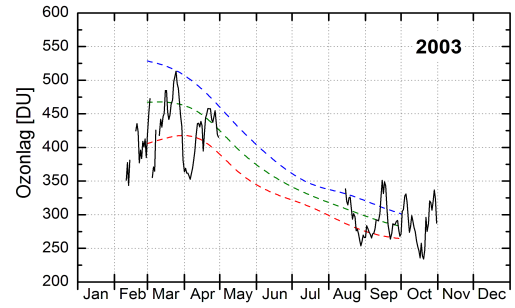
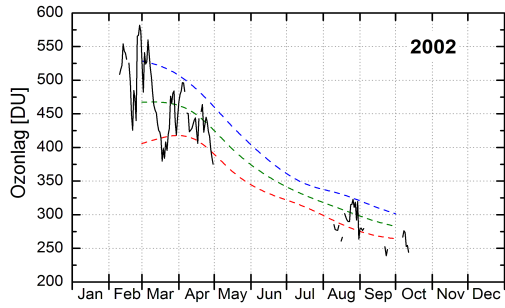
Daily measurements of ozone layer thickness and stratospheric NO<sub>2</sub> (SAOZ spectrometer) over Pituffik, 1990–2016. For the ozone layer, the green line represents the mean of daily measurements during the ten-year period 1979–1988, obtained with the TOMS instrument on the Nimbus-7 satellite. The blue and red dashed lines indicate, respectively, plus one and minus one standard deviation from this mean. This means that approximately two-thirds of all measurements in the period 1979–1988 fall between the blue and red lines.

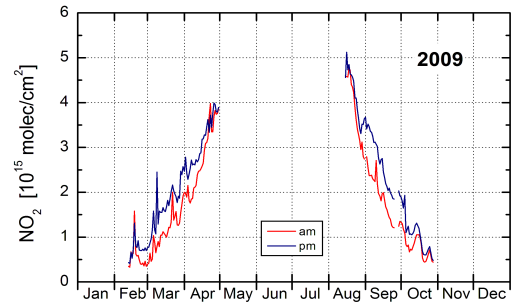
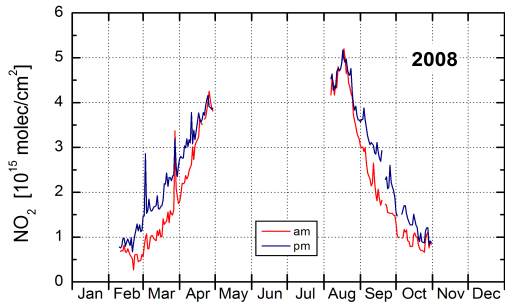
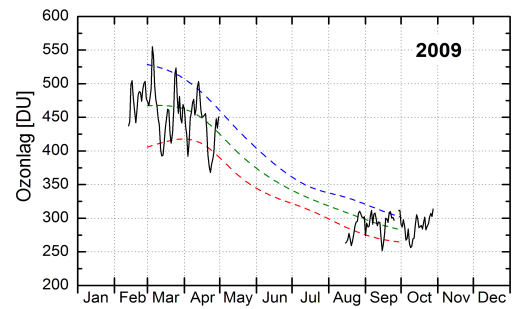
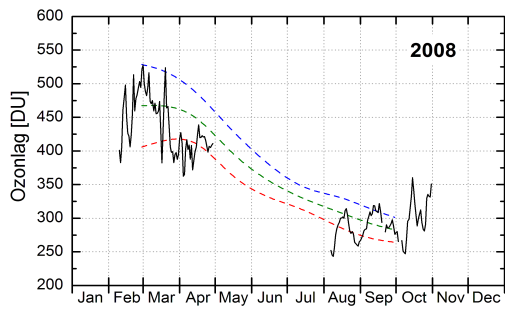
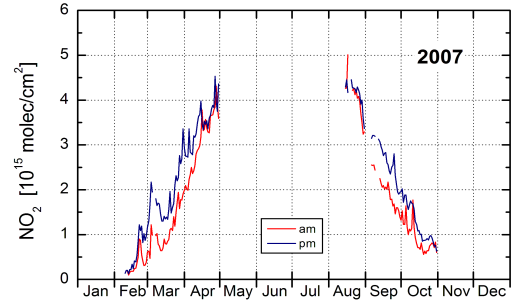
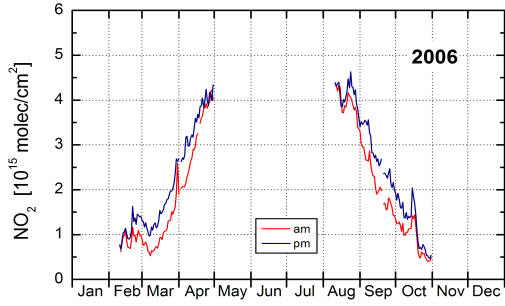
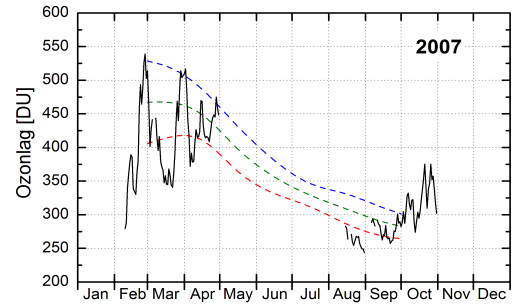
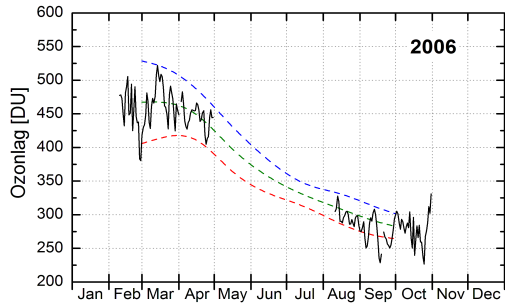
The NO<sub>2</sub> measurements represent morning values (sunrise – am) and evening values (sunset – pm). The measurements were discontinued at the end of 2016, and the SAOZ instrument was relocated to Kangerlussuaq.

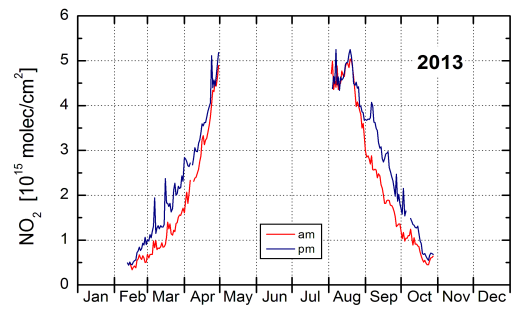
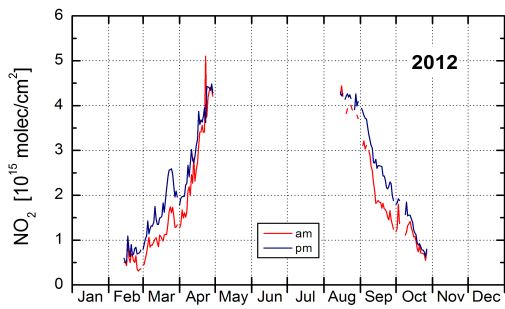
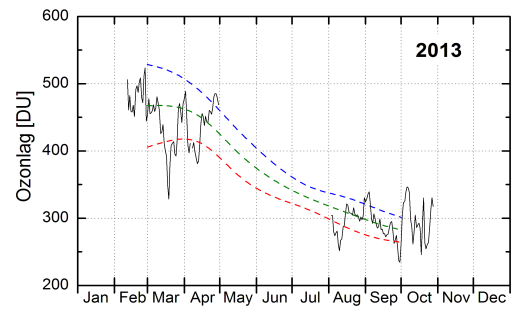
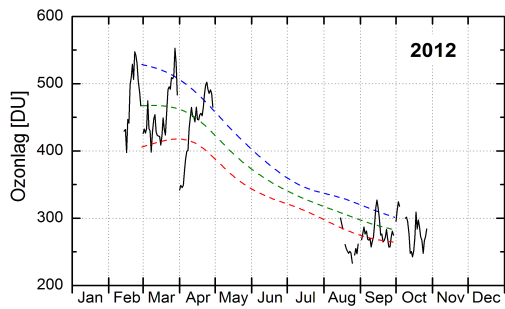
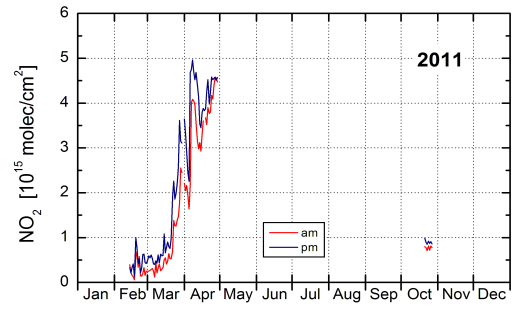
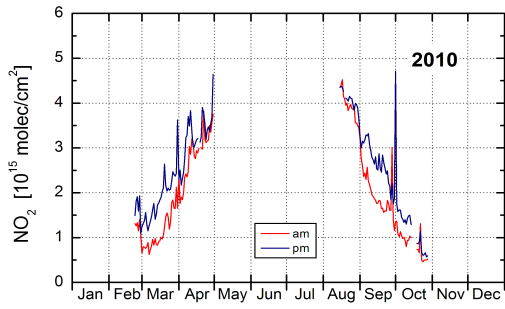
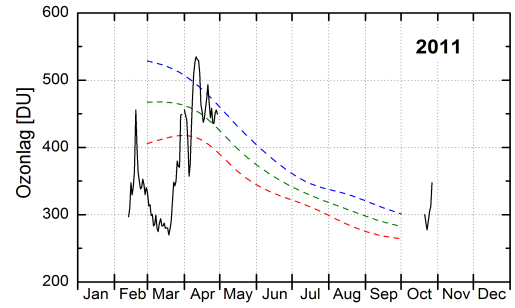
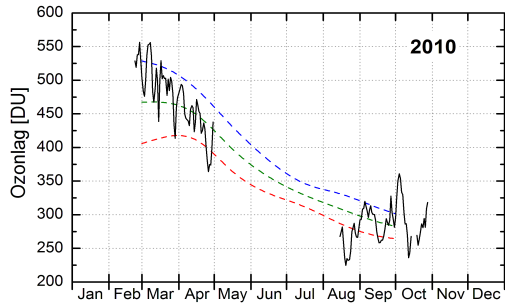


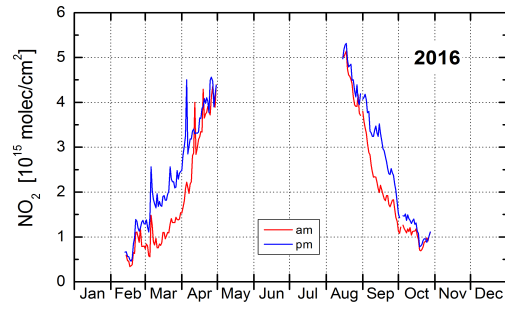
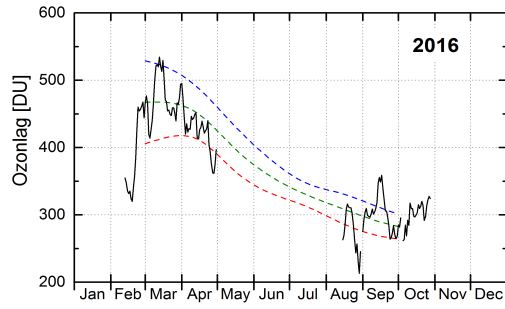
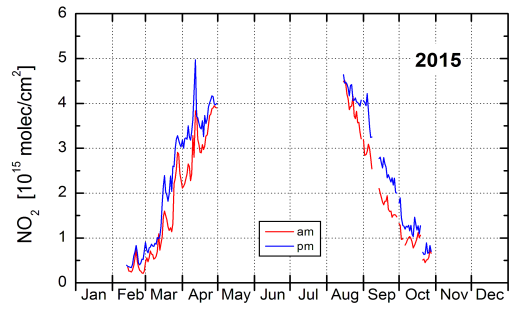
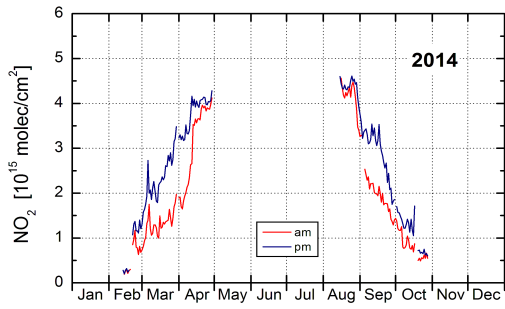
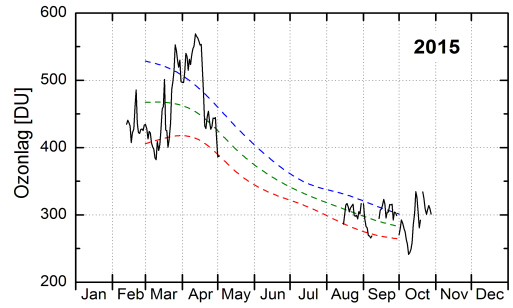
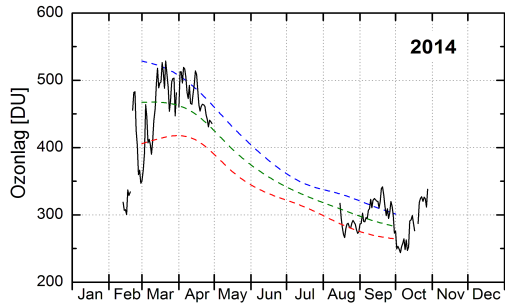












## Appendix D

# PSC area over the Northern Hemisphere

The following figures show the area of the Northern Hemisphere covered by PSCs (Polar Stratospheric Clouds) in the potential temperature range 350–675 K (Y-axis), corresponding to approximately 14–26 km in altitude. The figures indicate ozone depletion, which typically begins around day 30 from 1994–2025. Each winter is named after the year in which it ends. For example, “winter 1995” refers to the period from 1 November 1994 to 31 March 1995. In the figures, 1 November is indicated as day –60, 1 January as day 0, and 31 March as day 90, marking the end of the PSC area calculations.

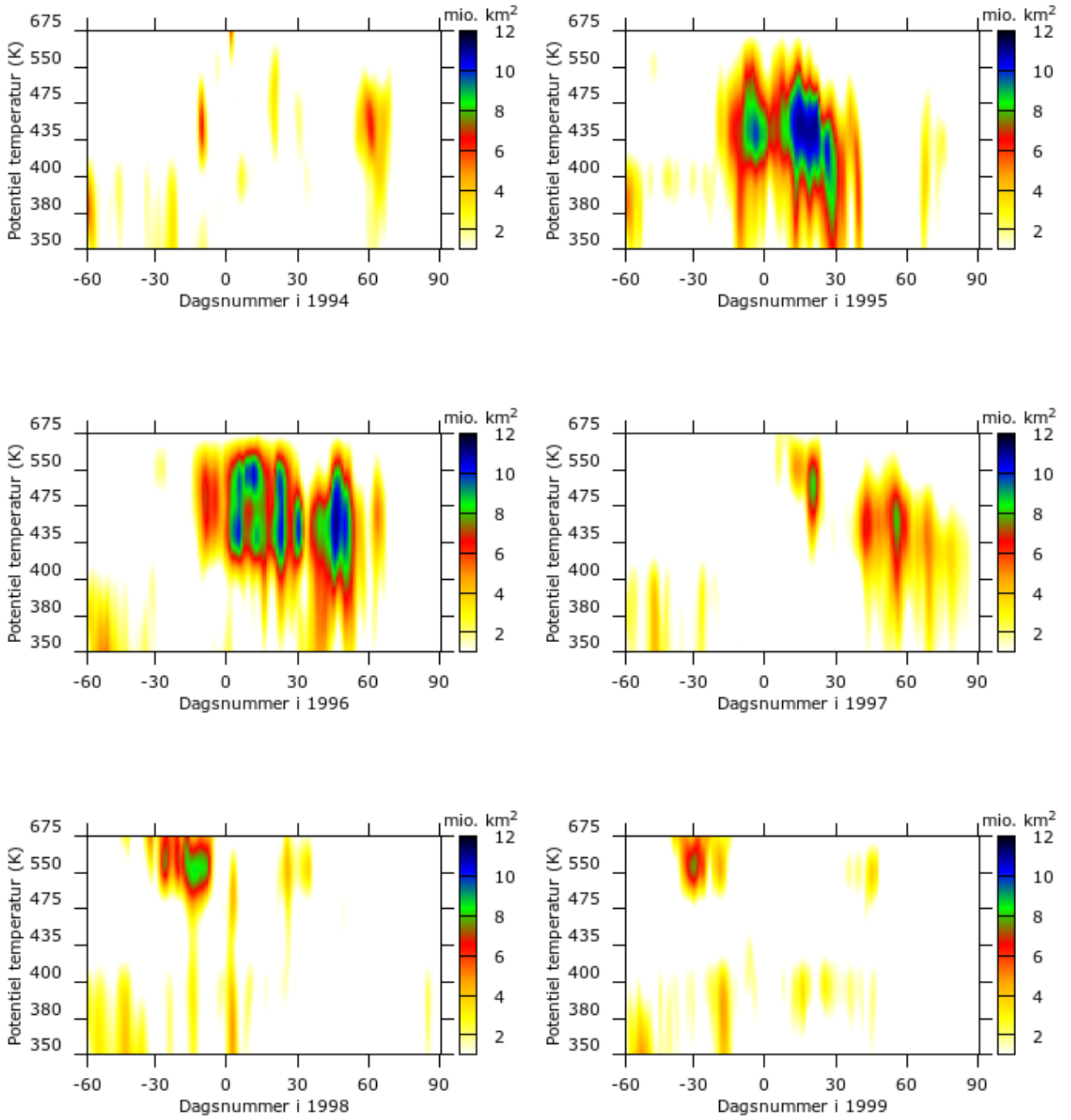


Figure D.1: PSCs in the years 1994–1999. Y-axis: Potential temperature (K). X-axis: day number for each year.

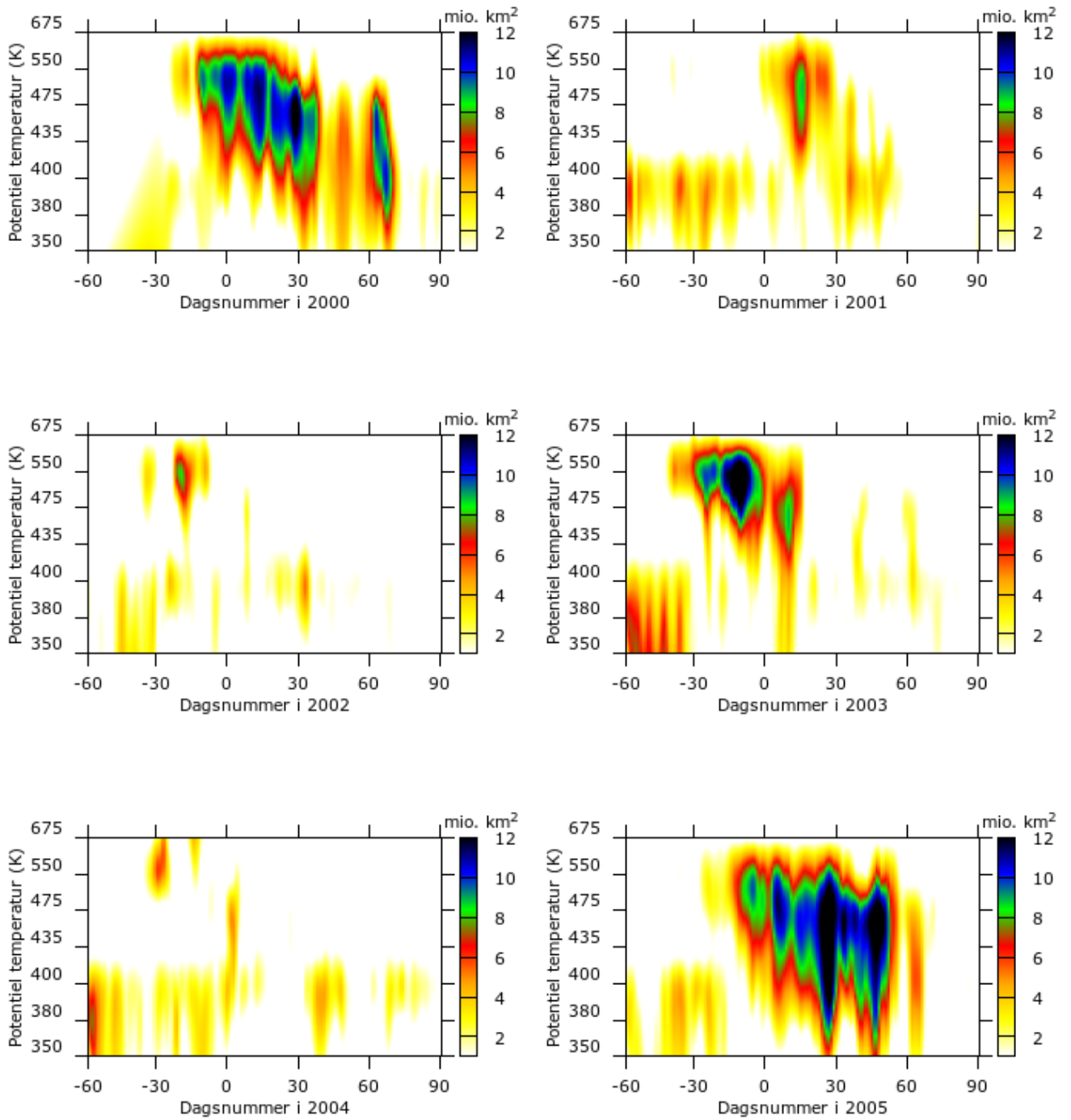


Figure D.2: PSCs in the years 2000–2005. During this period, there was some depletion in 2000 and significant depletion in 2005.

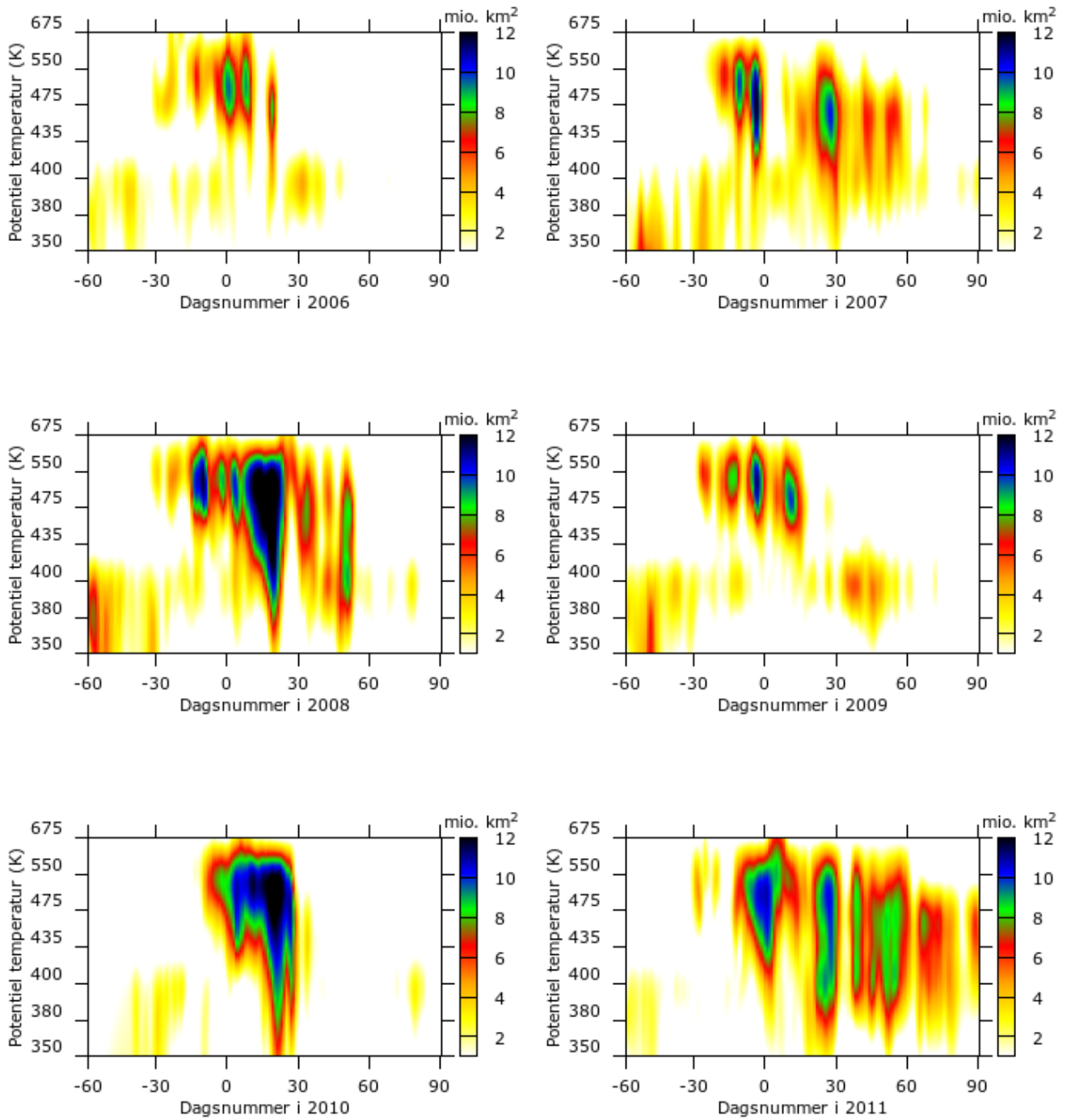


Figure D.3: PSCs in the years 2006–2011. During this period only limited depletion occurred, except in 2011 when significant depletion was observed, leading to the formation of the first Arctic ozone hole.

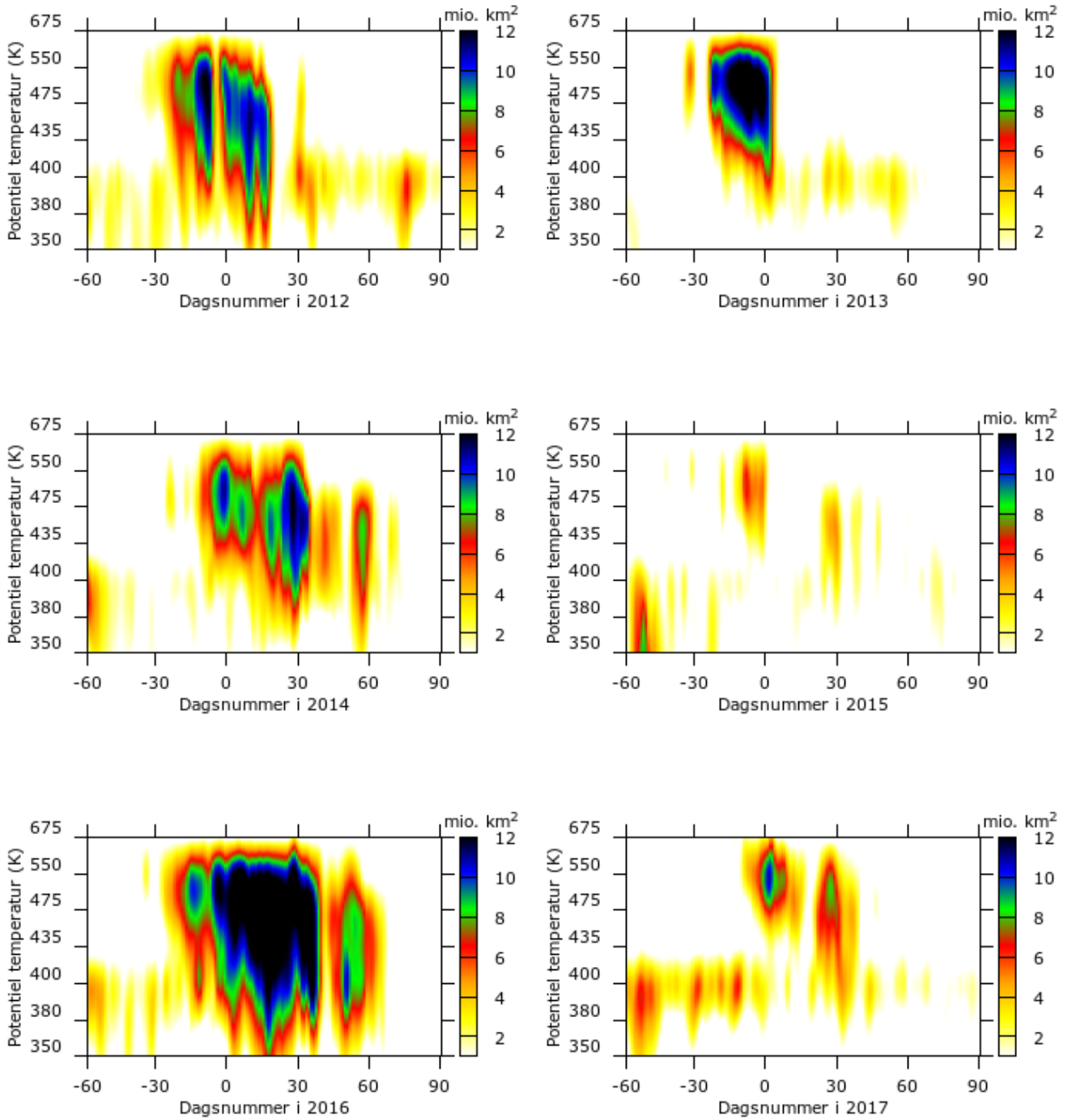


Figure D.4: PSCs in the years 2012–2017. During this period minor depletion occurred in 2014, with more pronounced depletion observed in 2016.

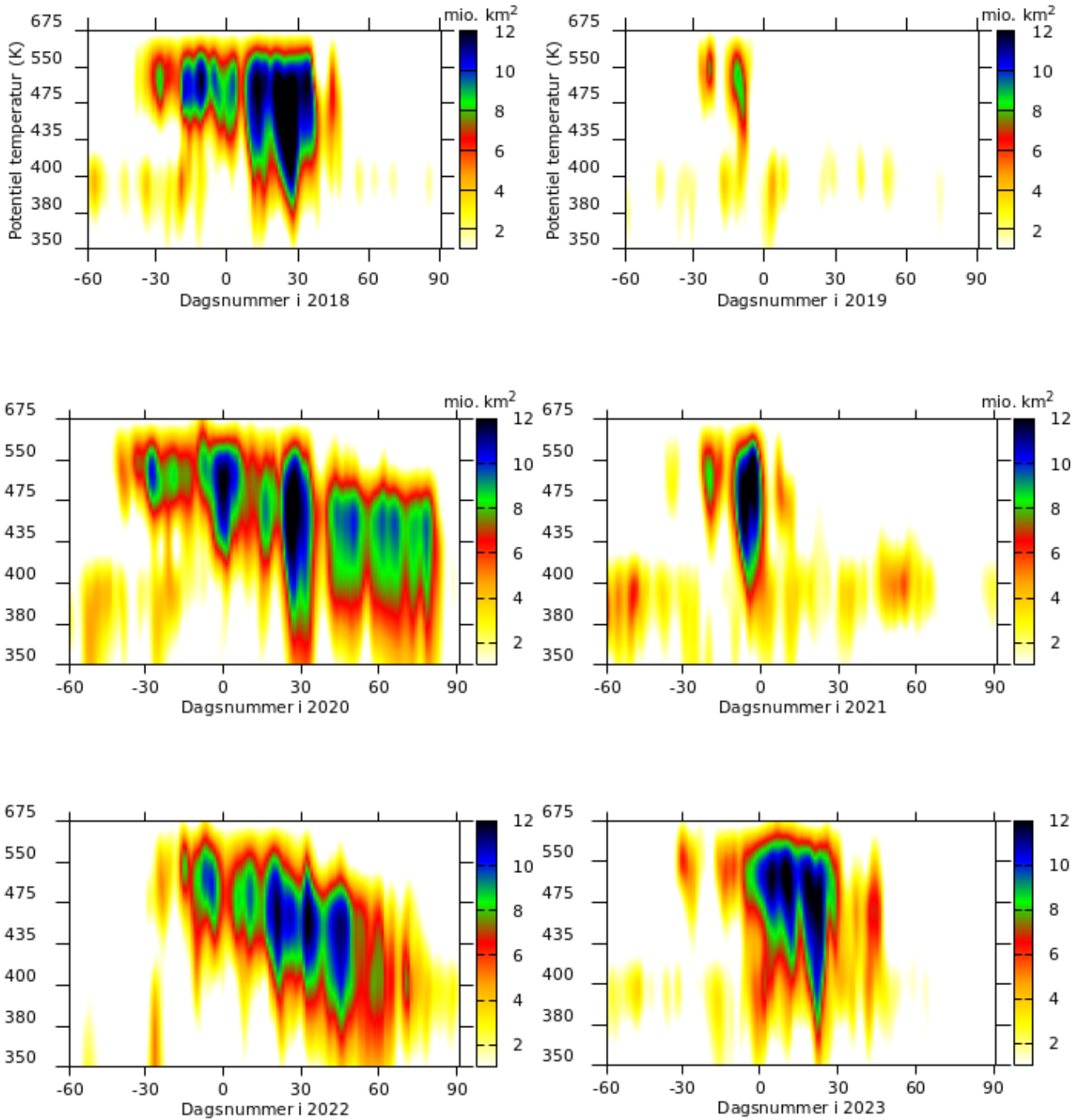


Figure D.5: Area of PSCs in 2018–2022. During the winter of 2018–19, PSC formation was limited, with maximum coverage reached by the end of December. A sudden stratospheric warming then disrupted the Arctic vortex, followed by a cold outbreak over the US east coast a few weeks later. The winter of 2019–20 saw an extended PSC period, lasting until April, when the calculation of PSC area was concluded (see Appendix I). In 2020–21, the PSC area remained very small throughout the period of potential ozone depletion. The winter of 2021–22 featured the largest PSC area during February since 2005. In 2022–23, the PSC area was very large in January but declined rapidly in February.

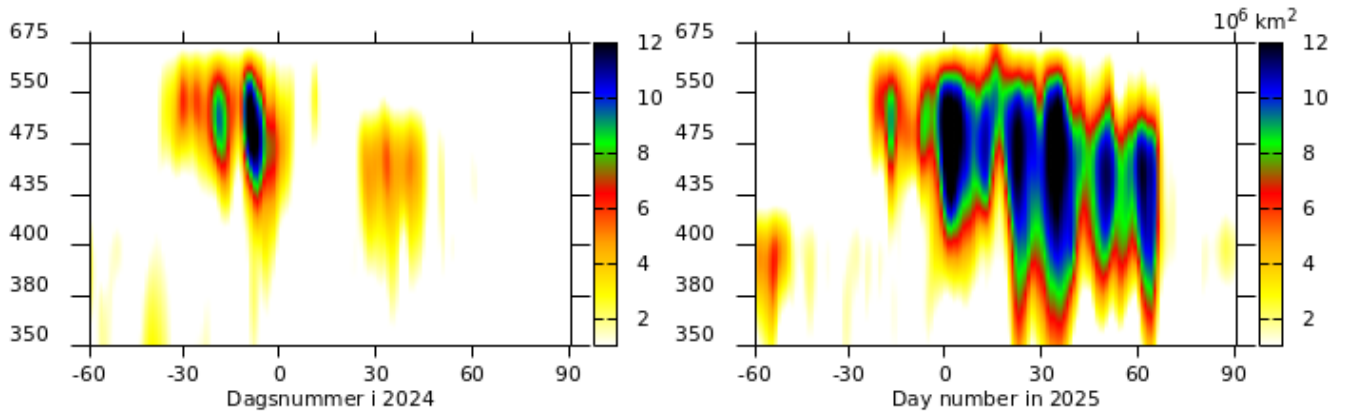


Figure D.6: Area of PSCs in 2024–25. In December 2023, PSC coverage was large, but a stratospheric warming in January prevented significant PSC formation, leaving only a small area in early February 2024. In contrast, the vortex and PSC area in 2025 were large and stable until early March, resulting in substantially greater ozone depletion than the previous year.

## Appendix E

# UV Dose measured in Copenhagen

Figures [E.1–E.9](#) show the measured total daily (left panel) and monthly (right panel) doses of harmful UV radiation in Copenhagen. In the right panel, the blue marks indicate the mean, minimum, and maximum values for the preceding years since 2000. Monthly doses were not calculated if more than three days of measurements were missing.

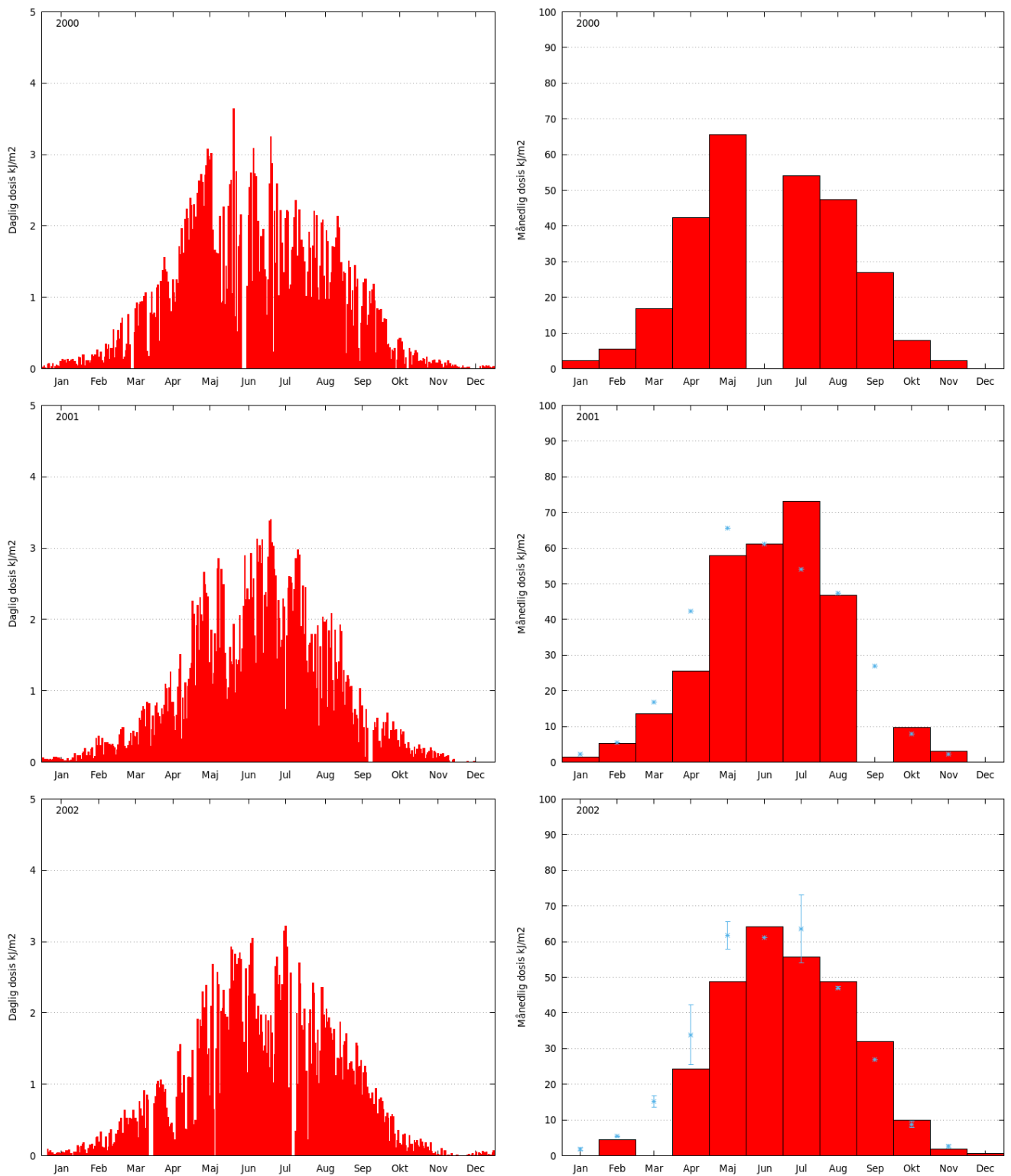


Figure E.1: Measured UV radiation in Copenhagen for 2000–2002.

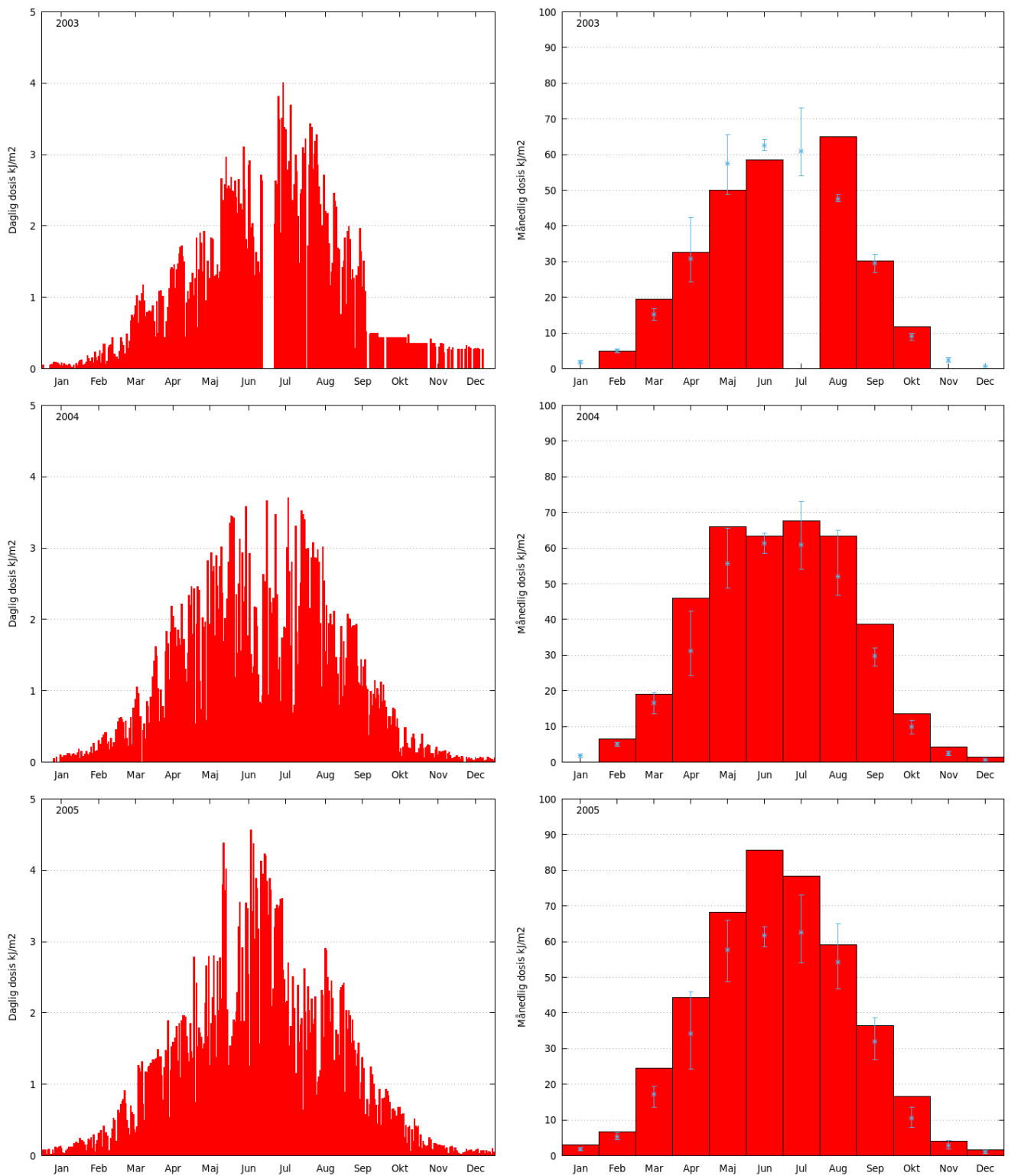


Figure E.2: Measured UV radiation in Copenhagen for 2003–2005. 2005 was exceptionally sunny from January to July, setting an annual UV record.

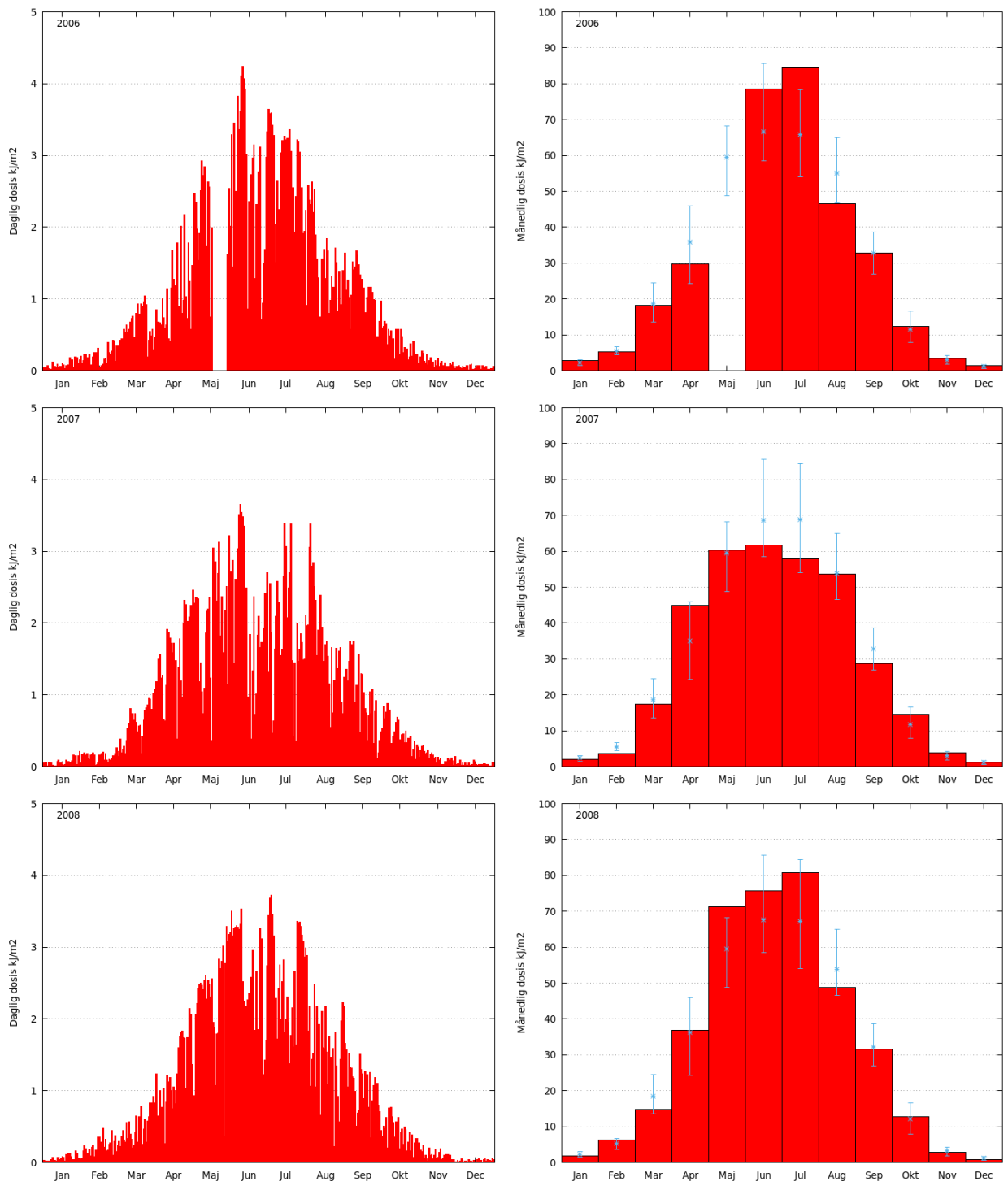


Figure E.3: Measured UV radiation in Copenhagen for 2006–2008.

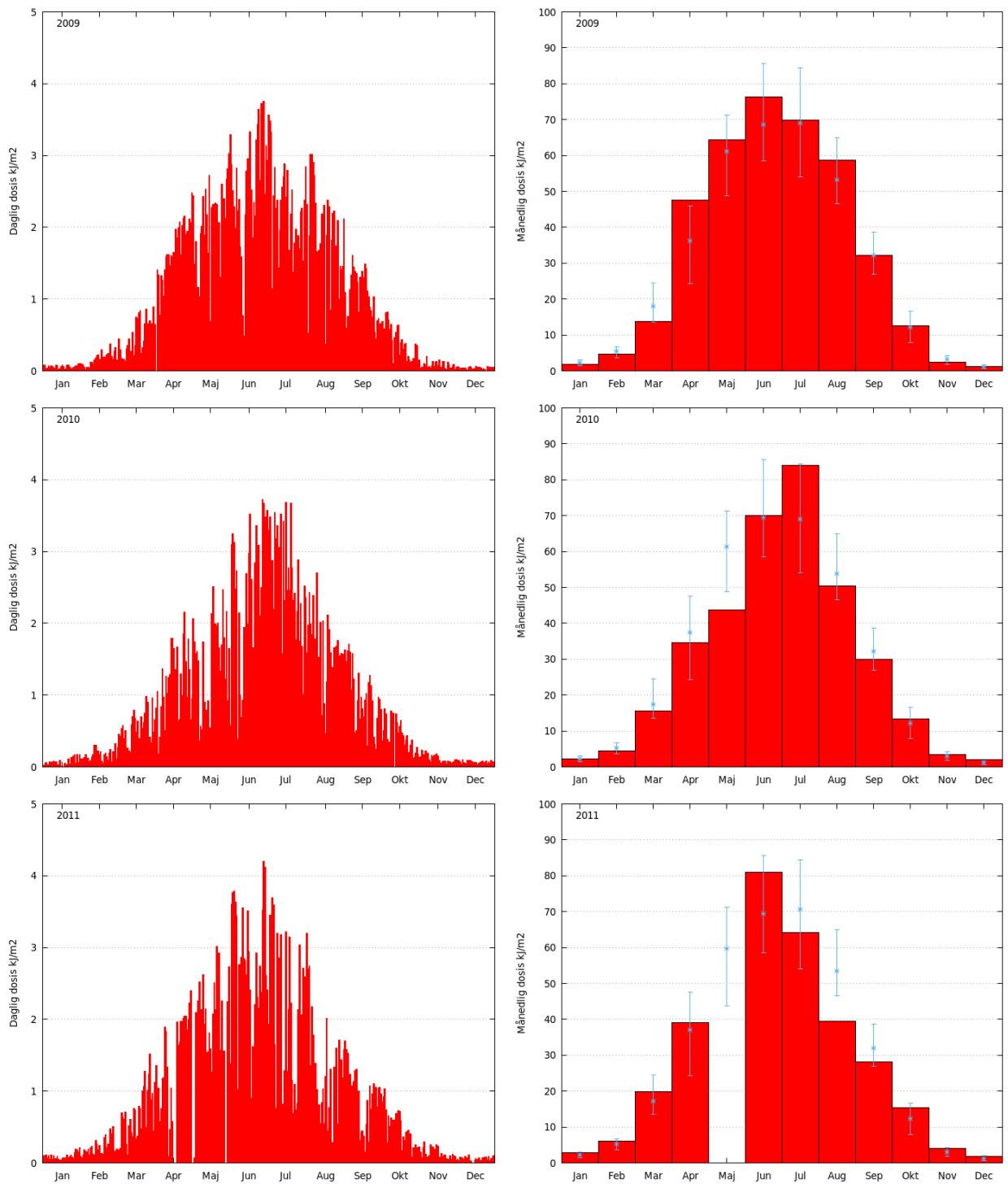


Figure E.4: Measured UV radiation in Copenhagen for 2009–2011.

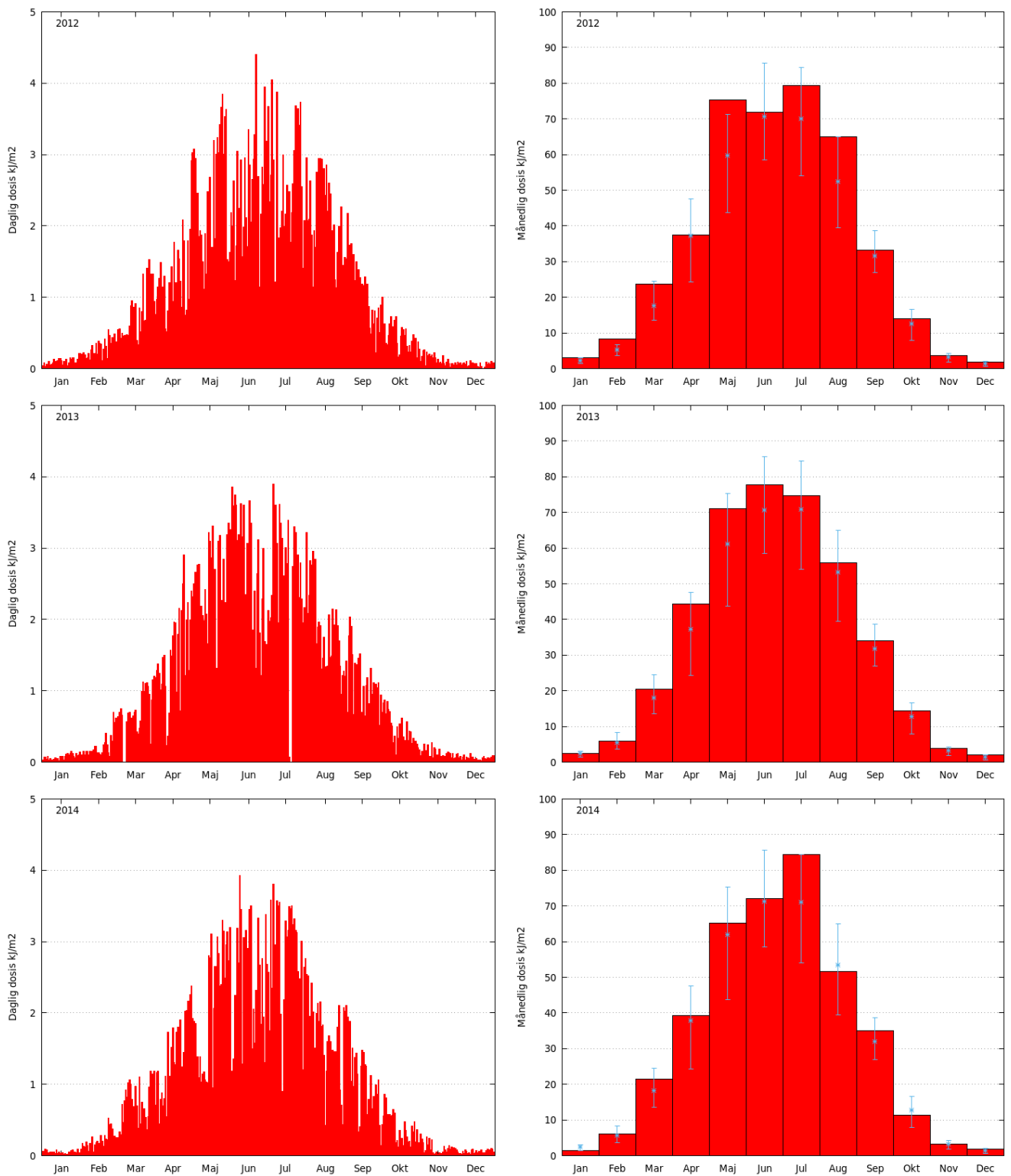


Figure E.5: Measured UV radiation in Copenhagen for 2012–2014.

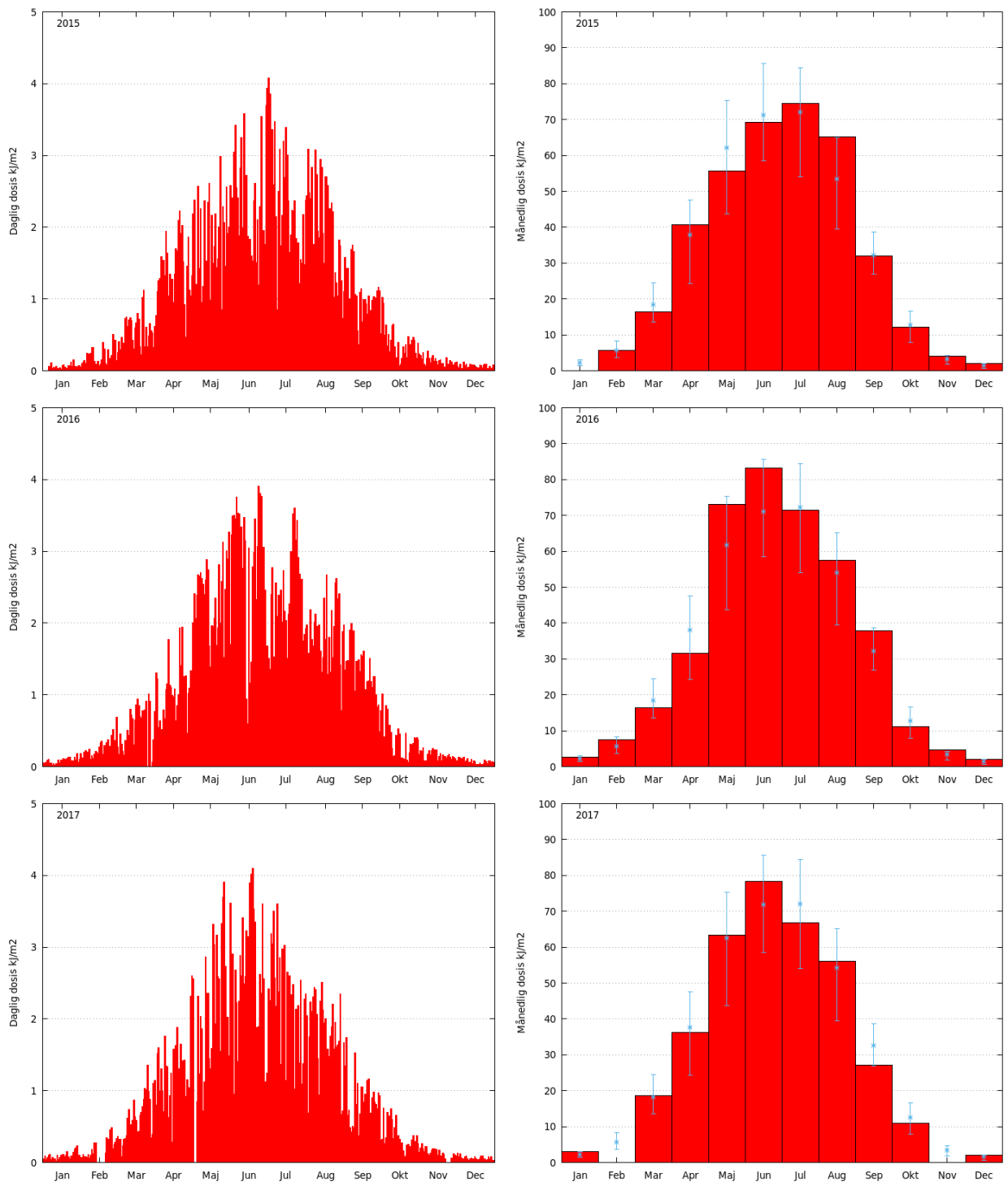


Figure E.6: Measured UV radiation in Copenhagen for 2015–2017.

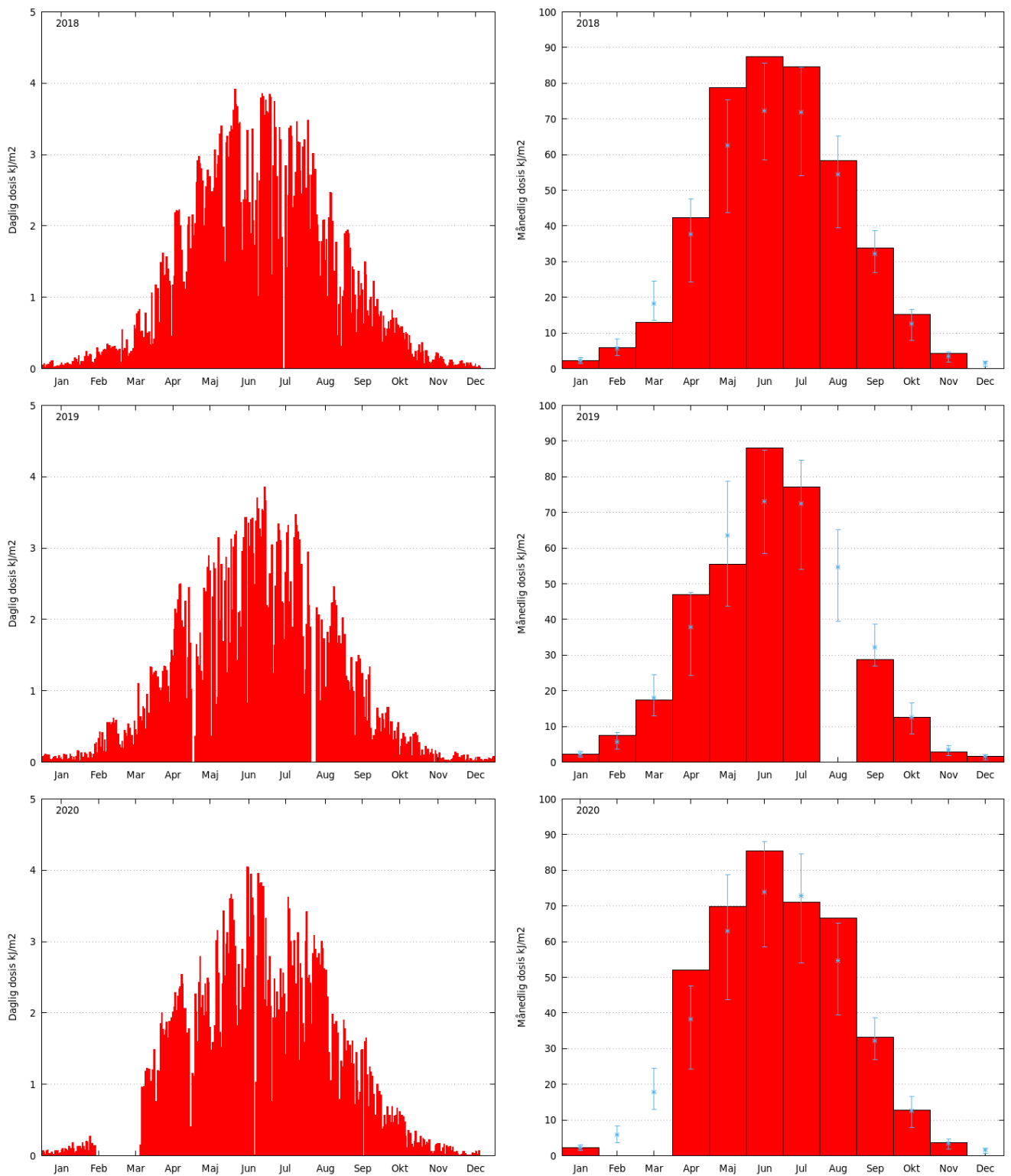


Figure E.7: Measured UV radiation in Copenhagen for 2018–2020. 2018 started low in March but set new maxima in May–July, surpassing the previous annual record from 2005. 2019 was average, and in 2020 the total April dose exceeded previous years due to a combination of high Arctic ozone depletion and sunny weather.

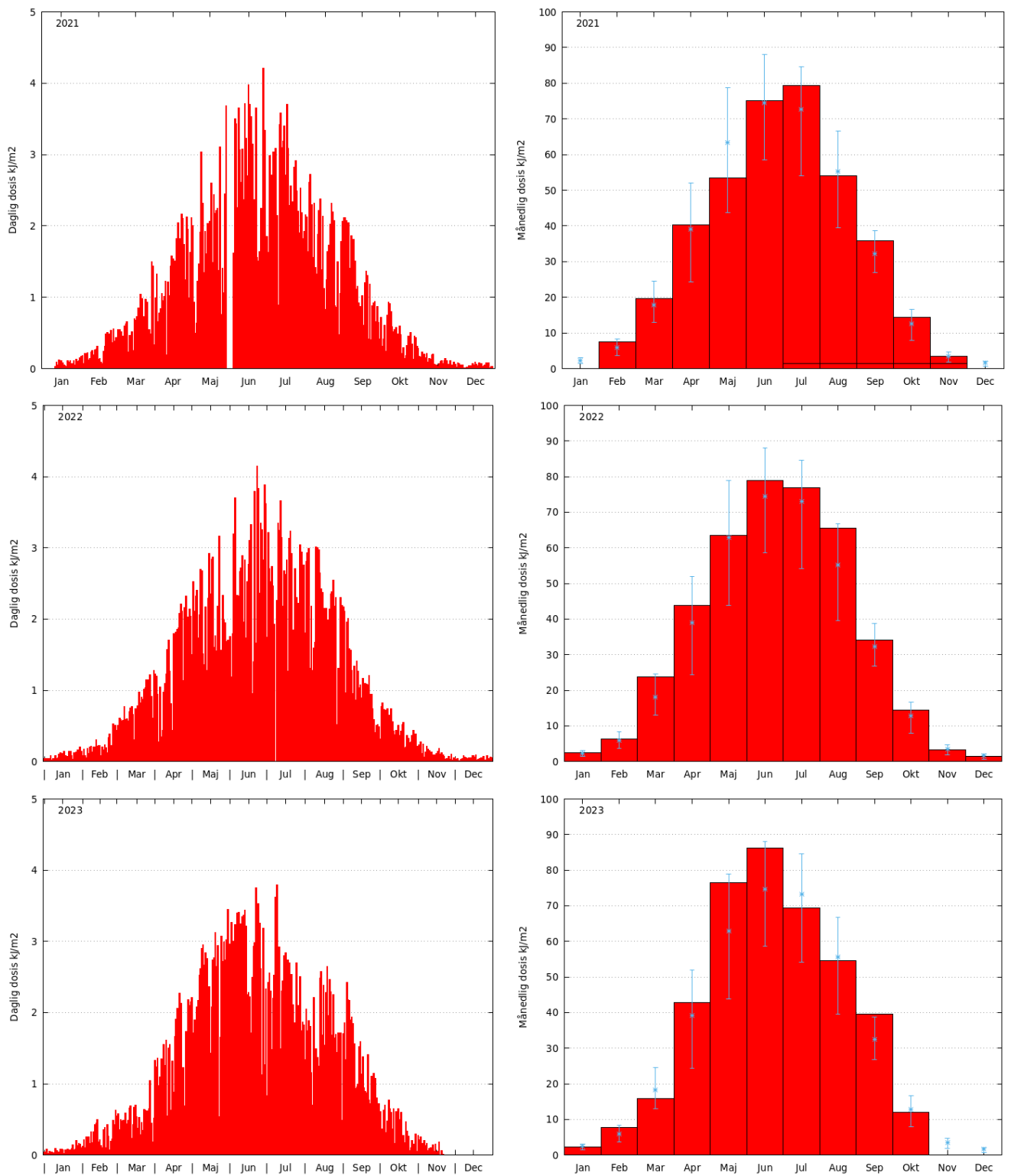


Figure E.8: Measured UV radiation in Copenhagen for 2021–2023. In 2022, March and August doses were high, leading to an annual total 8% above normal. September 2023 set a new UV dose record.

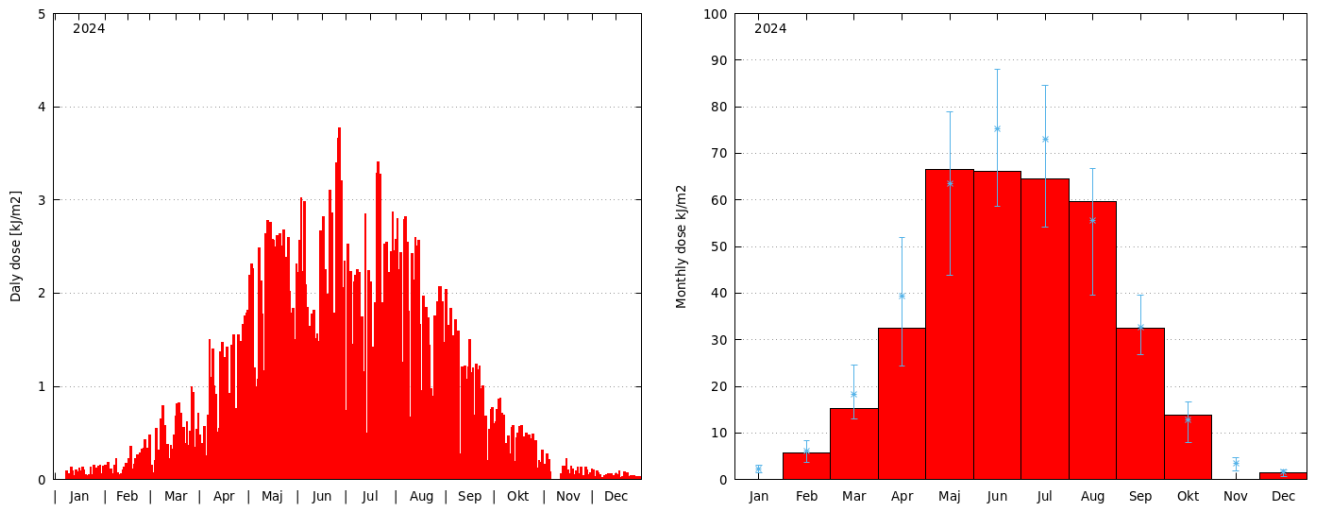


Figure E.9: Measured UV radiation in Copenhagen for 2024. The UV doses were lower than the average for most months, especially June with the lowest dose observed since 2007.

## Appendix F

# The Ozone Layer

Ozone ( $O_3$ ) is a molecule consisting of three oxygen atoms. Ozone plays a crucial role in many atmospheric processes and is vital for life on Earth. Most of the ozone is located high above the Earth's surface, in the stratosphere from about 10 km to 50 km altitude. At these altitudes, ozone has a significant beneficial effect, as it shields the Earth's surface from harmful ultraviolet (UV) radiation from the Sun.

Ozone also occurs at ground level as part of air pollution, particularly over and around most large cities. Ground-level ozone is harmful, as it can cause irritation of the mucous membranes, respiratory problems, and can negatively affect vegetation. Over the last century, the amount of ground-level ozone has doubled over large parts of the Northern Hemisphere, due to air polluted by human activity.

The ozone layer concept refers to the highest concentrations in the atmosphere, which is found between 15 and 35 km altitude. It is quantified as the total number of ozone molecules in a vertical column of air from the surface to the top of the atmosphere. Practically, the top can be set around 50 km because ozone above this altitude contributes very little. The amount of ozone can be expressed in several ways: molecules per cubic meter of air, grams per cubic meter of air, or the Dobson Unit (DU). DU is the most commonly used and it refers to the thickness in millimeters that the ozone column would have if compressed to standard pressure at the surface. Typical values are 200–500 DU. The unit is named after Gordon Dobson, an early ozone researcher.

## Vertical Ozone Distribution in the Earth's Atmosphere

Figure F.1 shows a typical ozone profile from Ittoqqortoormiit, Greenland. The ozone concentration is measured with an ozonesonde carried aloft by a balloon recording ozone concentration during ascent. The measurement terminates at about 36 km altitude, when the balloon bursts. The concentration is expressed as DU per kilometer (Figure F.1a) and as the portion of the total air pressure that is exerted by ozone molecules alone in milliPascal (mPa) (Figure F.1b). The solid blue curve shows the ozone concentration as a function of altitude. Up to about 11 km, the ozone concentration remains low, but above this level it increases sharply, reaching its maximum near 21 km altitude, before gradually declining with increasing height. Other types of measurements confirm that above 36 km the concentration continues to decrease with altitude. The red curve shows the temperature profile measured simultaneously with ozone concentration. Temperature decreases with altitude in the troposphere up to the tropopause (approximately 11 km), then it increases with altitude in the stratosphere.

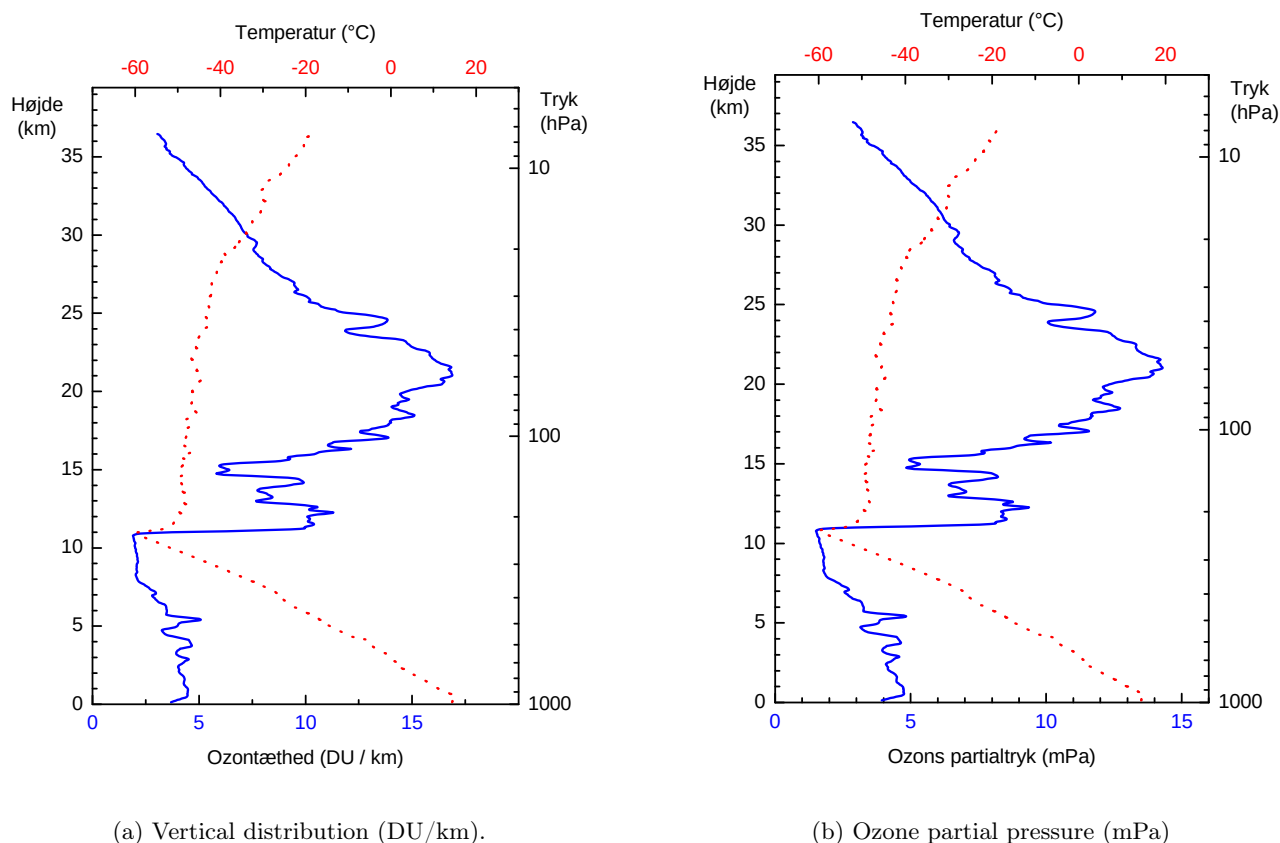


Figure F.1: Ozone and temperature profile from Ittoqqortoormiit, measured with an ozonesonde on 13 July 1994. Ozone concentration is shown by the solid blue curve, while temperature is shown by the dashed red curve. The scale for ozone is given at the bottom, and for temperature at the top. Right y-axis: Air pressure in hPa (hectoPascal, equivalent to millibar). Left y-axis: altitude above ground level (km).

Figure F.2 shows ozone concentration expressed as a mixing ratio, indicating how many ozone molecules are present per million molecules of the surrounding air. This is given in parts per million by volume (ppmv). When the ozone profile is expressed as a mixing ratio (ppmv), the maximum occurs at about 33–35 km altitude, whereas the maximum ozone concentration occurs around 21 km altitude (Figure F.1a) when expressed as number of molecules per cubic meter, in DU/km, or as partial pressure.

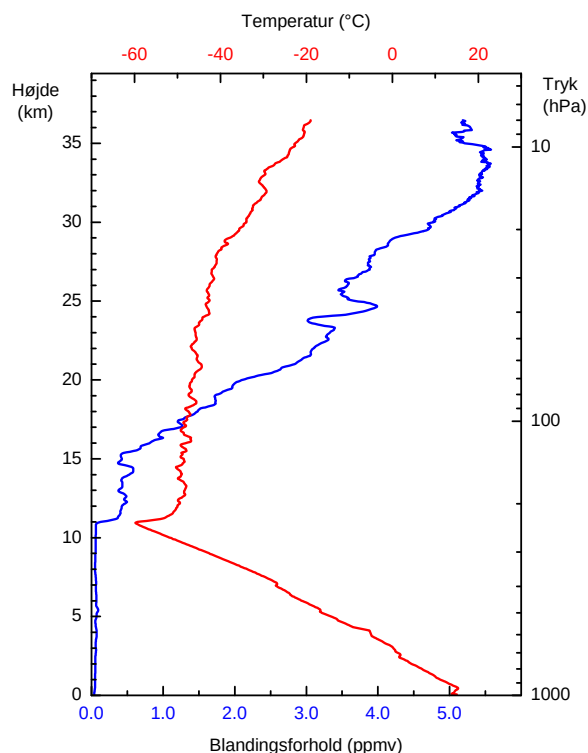


Figure F.2: Same profile as in Figure F.1 with ozone molecules concentration in the air expressed as parts per million per volume (ppmv). The scale for ozone is given at the bottom, and for temperature at the top.

## Spatial Ozone Distribution, and Seasonal Variation

High-energy UV radiation from the Sun continuously produces ozone in the atmosphere. Most ozone formation occurs at altitudes of 30 to 50 km, especially over the equator where the Sun is high in the sky and UV radiation is most intense. At the same time, UV radiation also destroys ozone, which means that ozone in this altitude range has a relatively short lifetime.

Air circulation in the upper stratosphere transports the ozone formed at the equator towards the poles. As it moves poleward, the ozone sinks to lower altitudes, where UV radiation is weaker and its lifetime becomes much longer. This leads to an accumulation of ozone around 20 km altitude, where it can persist for several months.

The tropopause at about 10 km altitude prevents ozone from being transported further down into the troposphere. Poleward transport is strongest towards the Northern Hemisphere during winter and early spring (November to March). As a result, the ozone column there increases from its seasonal minimum in October–November to a maximum in March–April, before declining again towards the next minimum. A similar annual cycle is observed in the Southern Hemisphere, but offset by six months. Examples of this seasonal variability are shown in Figure F.3.

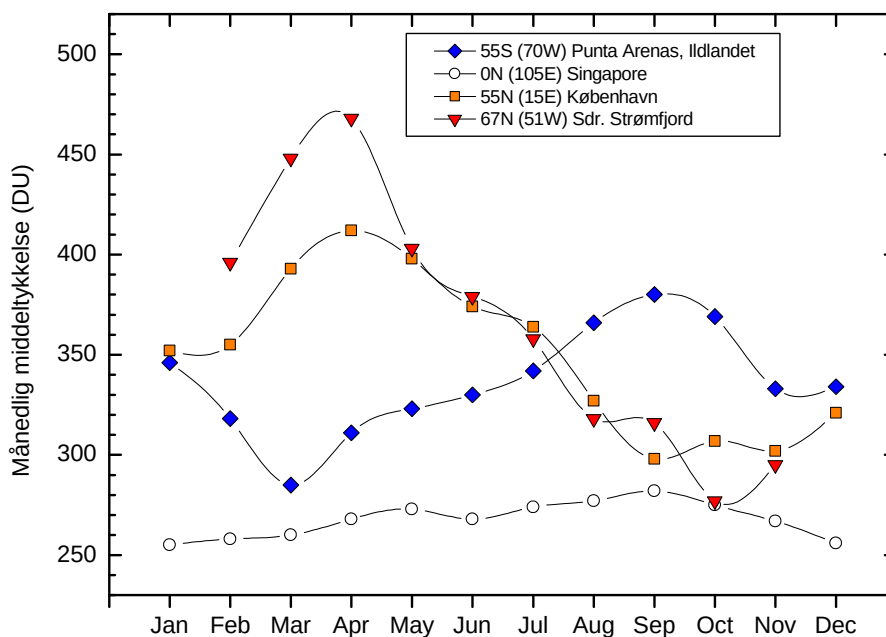


Figure F.3: The annual variation of the ozone layer for four different geographic locations: Punta Arenas, Chile at 55° S latitude, Singapore at the equator, Copenhagen at 55° N latitude, and Kangerlussuaq (Søndre Strømfjord) at 67° N latitude. The measurements are satellite observations from 1980 made by the TOMS instrument on NASA's Nimbus satellite. The gap of measurements in Kangerlussuaq is because the satellite instrument requires sunlight to take measurements, and at the same time, the sun must be more than 5–10 degrees above the horizon at local noon, which does not happen in Kangerlussuaq during January and December.

As shown in Figure F.3, total column ozone exhibits little seasonal variation at the equator (Singapore), whereas at mid- and high latitudes a pronounced annual cycle is evident, with a maximum in spring and a minimum in autumn. The amplitude of this cycle increases with distance from the equator. Superimposed on the seasonal cycle are short-term fluctuations on daily timescales, primarily linked to dynamical variability in the troposphere. Under anticyclonic (high-pressure) conditions the ozone column is typically lower than average, while cyclonic (low-pressure) conditions are associated with higher values. Day-to-day changes of up to 50 DU are common. Examples of these short-term variations are provided in Appendices A–C.

## Measurements of Total Column Ozone

The thickness of the ozone layer, usually expressed as total column ozone, is measured using a range of techniques. Several optical methods exploit ozone's strong absorption of ultraviolet (UV) radiation. These include ground-based observations with Dobson and Brewer spectrophotometers, vertical profile measurements with LIDAR (Light Detection and Ranging), and satellite-based instruments. Additional methods use ozone absorption in the visible or infrared spectral regions. Ground-based measurements are particularly important because they provide continuity with records that began in the 1930s at a few sites, offering a long-term perspective on ozone variability. They are also essential for validating satellite observations.

Satellite measurements complement these ground-based records by providing near-daily global coverage of total column ozone. A notable example is the TOMS (Total Ozone Mapping Spectrometer) instrument onboard the Nimbus-7 satellite, launched by NASA in 1978. Although designed for a five-year mission, TOMS operated until 1993, delivering 15 years of consistent data during a critical period of rapid ozone decline. Successor TOMS instruments were flown on

later satellites but typically had shorter lifetimes. Other key satellite instruments include SBUV (Solar Backscatter UV), TOVS (Total Ozone Vertical Sounder, based on infrared absorption), GOME (Global Ozone Monitoring Experiment) on ESA's ERS-2 satellite, SCIAMACHY on ESA's ENVISAT, OMI (Ozone Monitoring Instrument) on NASA's Aura satellite, and GOME-2 on EUMETSAT's MetOp series. Instruments that measure multiple trace gases, in addition to ozone, are particularly valuable for linking ozone variability to chemical processes in the atmosphere.

Figure F.4 shows an example of a global ozone distribution derived from the GOME-2 instrument onboard EUMETSAT's MetOp-A satellite on 12 June 2012.

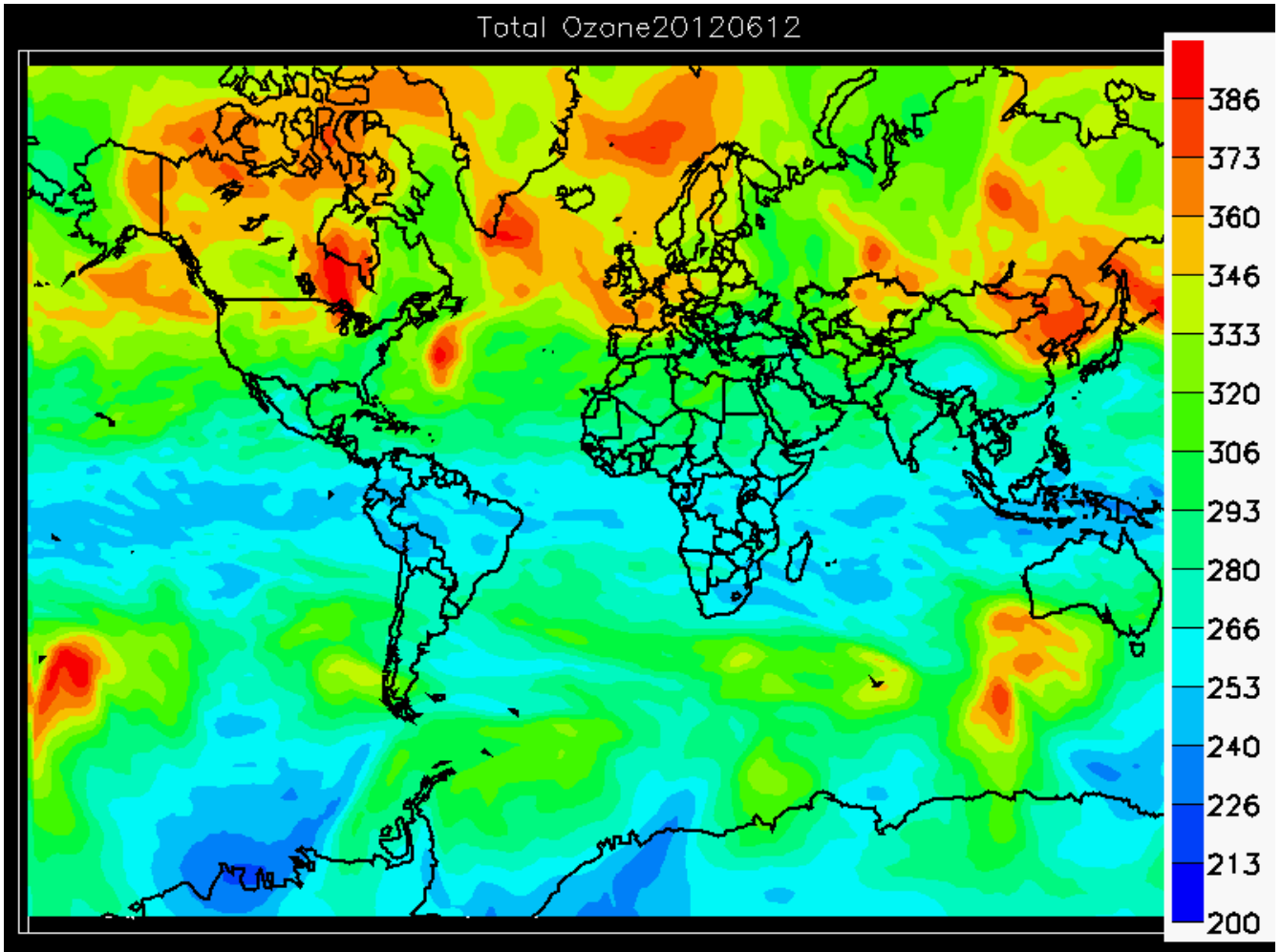


Figure F.4: Ozone layer on 12 June 2012 measured with the GOME-2 instrument onboard EUMETSAT's MetOp-A satellite. Colors indicate ozone thickness in DU. At this time of year, the ozone layer is still relatively thick over the Northern Hemisphere (summer) and it is thinner over Antarctica (winter) although before the ozone hole develops in September. Note also the broad equatorial belt where the ozone layer is relatively thin.

## Ozone Depletion and the Ozone Hole

The most severe destruction of the ozone layer occurs over Antarctica, where a so-called "ozone hole" forms every year in October. The concept of ozone hole means that the depletion is substantial compared to normal fluctuations in thickness. In practice, this means that the ozone layer is reduced to less than half of its typical value. The depletion is not uniform across altitudes but is strongest between 15 and 20 km, where nearly all ozone disappears during the Antarctic ozone hole event. The Antarctic ozone hole usually starts in August and it continues developing until December. Figure F.5 shows the ozone layer thickness on October 7, 2011, over the Southern Hemisphere. Balloon measurements from

Antarctica revealed that nearly all ozone between 14 and 20 km altitude had vanished—precisely the region where ozone concentrations are normally highest.

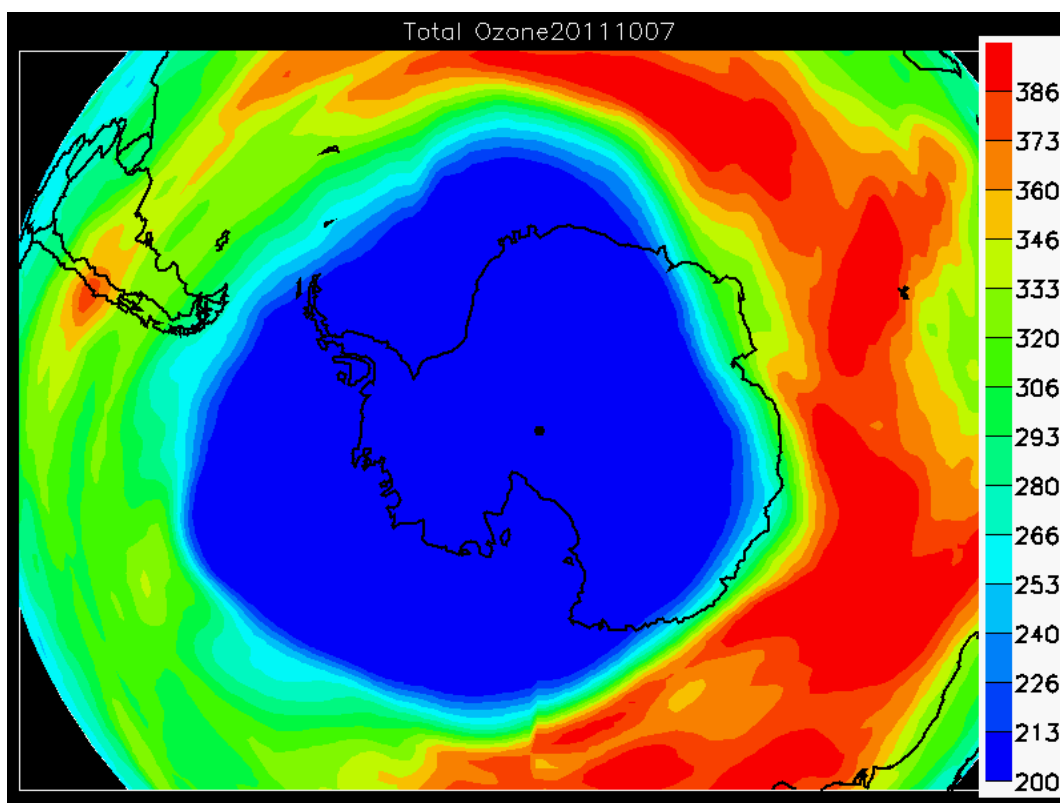


Figure F.5: Ozone hole over Antarctica on 7 October 2011. Data from EUMETSAT’s GOME-2 instrument on the MetOp-A satellite. Red colors indicate a thick ozone layer, blue colors a thin layer. Colours indicate ozone thickness in Dobson Units (DU). The central blue region represents the ozone hole where ozone thickness is less than 220 DU.

The depletion is driven by chlorine (Cl) and bromine (Br), which naturally occur only in trace amounts in the atmosphere. Over the past 30–60 years, however, large amounts have been added through emissions of CFCs (chlorofluorocarbons) and halons. CFCs are compounds containing chlorine, fluorine, and carbon, while halons are similar compounds containing bromine. CFCs were widely used due to their chemical stability—for example, as propellants in spray cans and as foaming agents in refrigerator insulation. Halons were primarily used in fire extinguishers. Their stability also allows them to drift upward through the atmosphere without breaking down. Once in the stratosphere, solar UV radiation can split them, releasing reactive chlorine and bromine.

For much of the year, chlorine in the stratosphere is bound in inactive chemical compounds. But during the polar winter, when temperatures fall below  $-80\text{ }^{\circ}\text{C}$ , ice clouds called polar stratospheric clouds (PSCs) form. These clouds consist of ice crystals containing nitric acid, which condenses from reactive nitrogen in the atmosphere. On the surface of these crystals, chlorine compounds are converted into chemically active forms capable of destroying ozone. As the particles sink due to gravity, they remove nitrogen compounds from the stratosphere—a process known as denitrification. With less reactive nitrogen present, active chlorine persists longer, allowing for more extensive ozone destruction.

In late autumn and winter, a strong polar vortex develops—a powerful westerly wind circulation above approximately 12 km altitude that effectively isolates the air over Antarctica. This prevents mixing with ozone-rich air from lower latitudes. While it remains dark during the polar night and the vortex persists, chlorine compounds remain inactive. But when sunlight returns in September, the chlorine becomes activated, rapidly destroying ozone. Because the vortex still prevents mixing with outside air, ozone levels within the vortex drop drastically, forming the ozone hole. This process typically ends in November–December, when warming breaks down the vortex and ozone-poor air mixes with ozone-rich air from lower latitudes.

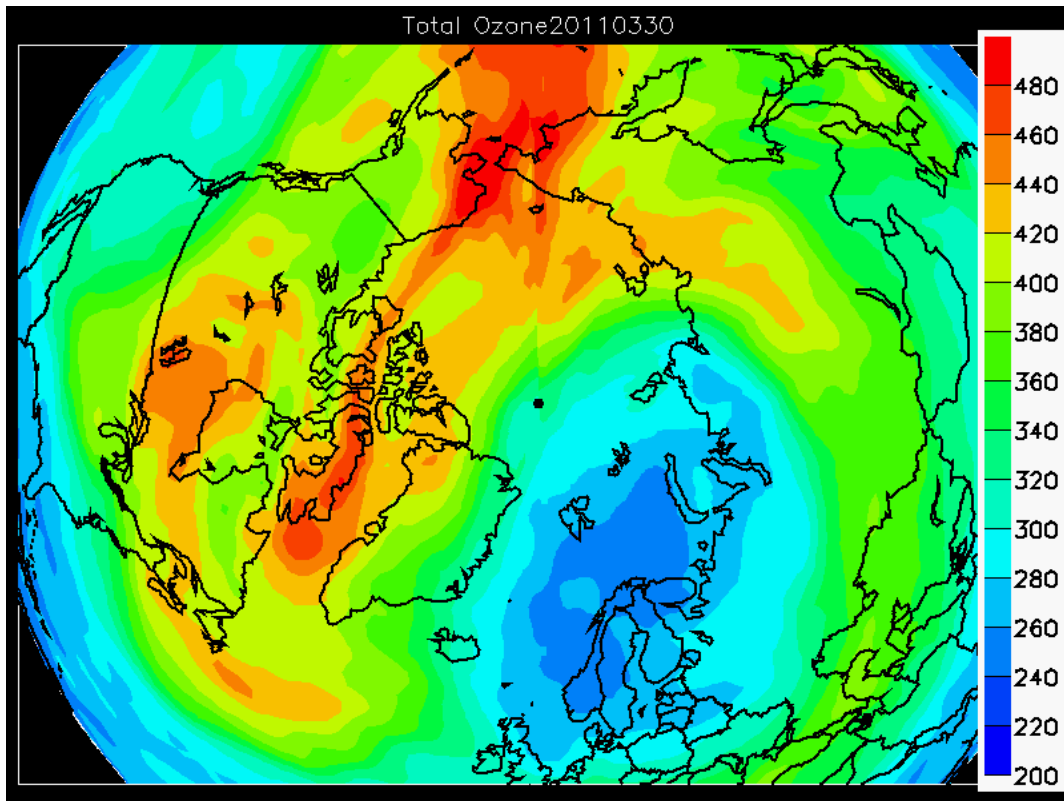


Figure F.6: Ozone thickness (in DU) over the Northern Hemisphere on 30 March 2011. Observed by the GOME-2 instrument on EUMETSAT's MetOp satellite. The polar vortex extended over Scandinavia, where ozone thickness dropped to around 250 DU.

Although an ozone hole has also developed in recent year over the Arctic it is not comparable in size or depth. This is mainly because winter temperatures at 15–25 km altitude are not as cold as over Antarctica, meaning fewer PSCs form.

In early 2011 (January–March), ozone sounding from balloon launches indicated that up to 80% of the ozone between 13 and 20 km disappeared. Figure F.6 shows a satellite image of ozone thickness on March 30, 2011, over the Northern Hemisphere, highlighting regions of very thin ozone over Scandinavia, caused by this strong Arctic ozone depletion.

## The Arctic Ozone Hole in Spring 2020

In the spring of 2020 severe ozone depletion occurred in the Arctic stratosphere leading to an ozone hole for the first time over the Arctic. Measurements from Ittoqqortoormiit (Figure F.7) show that large depletion occurred in spring 2020. Compared with October 2019 typical levels, profiles from February and April reveal losses of 80–90% at 17–18 km, caused by chemical destruction once sunlight returned to the polar vortex.

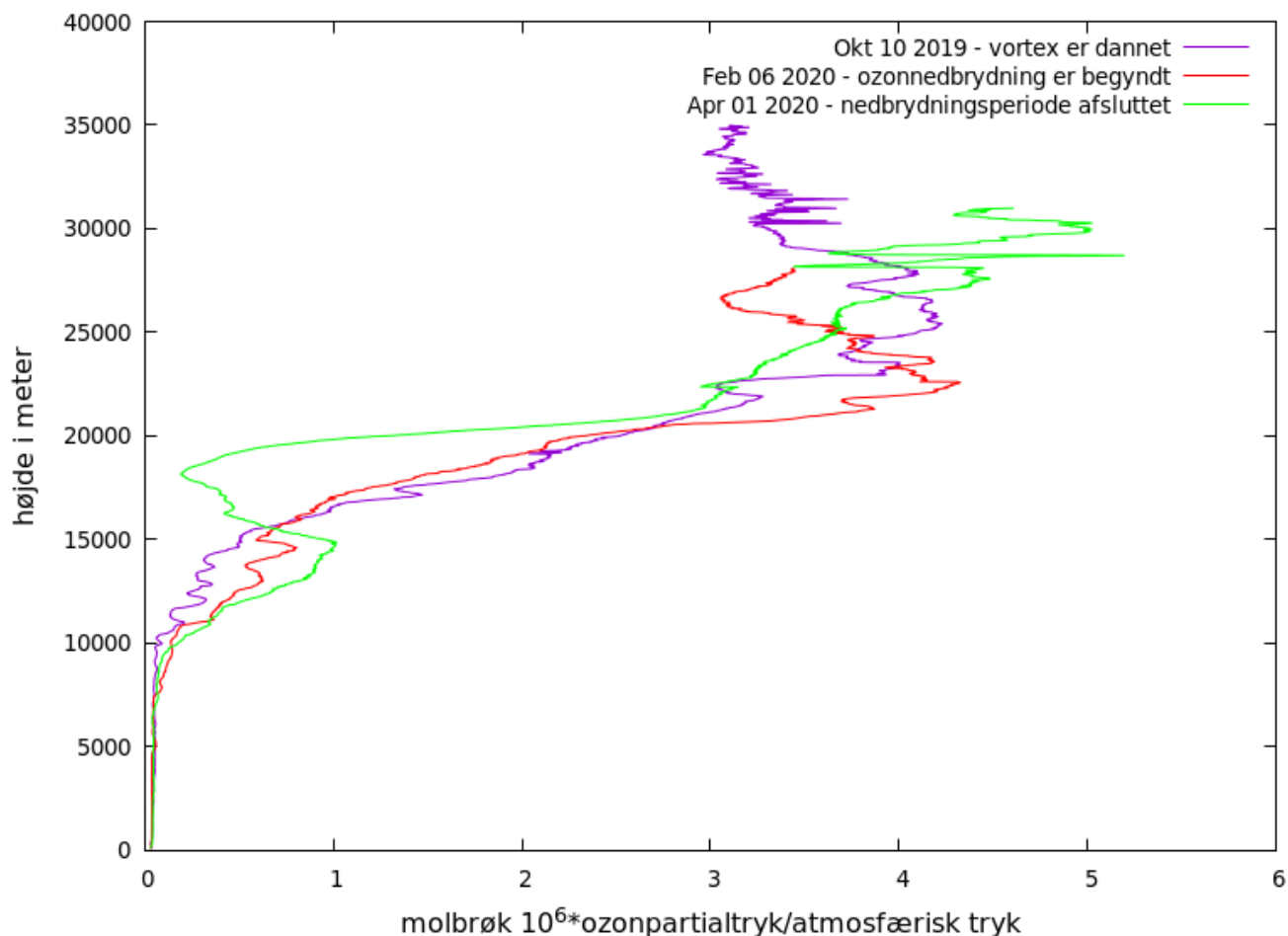


Figure F.7: Vertical ozone profiles measured at Ittoqqortoormiit during the Arctic winter 2019/2020. The purple curve (10 October 2019) shows typical ozone levels at the onset of the polar vortex. The red curve (6 February 2020) indicates the beginning of chemical ozone depletion. The green curve (1 April 2020) shows the end of the depletion period, with up to 80–90% ozone loss around 17–18 km altitude. X-axis: Mixing ratio ( $10^6 \times$  ozone partial pressure / atmospheric pressure)

Figure F.8 illustrates that in March and April 2020, Arctic ozone levels dropped to record lows for the past 11 years, falling below 220 DU — the threshold used to define an “ozone hole.” While this phenomenon has been observed annually over Antarctica since 1980, it had not previously been recorded over the Arctic.

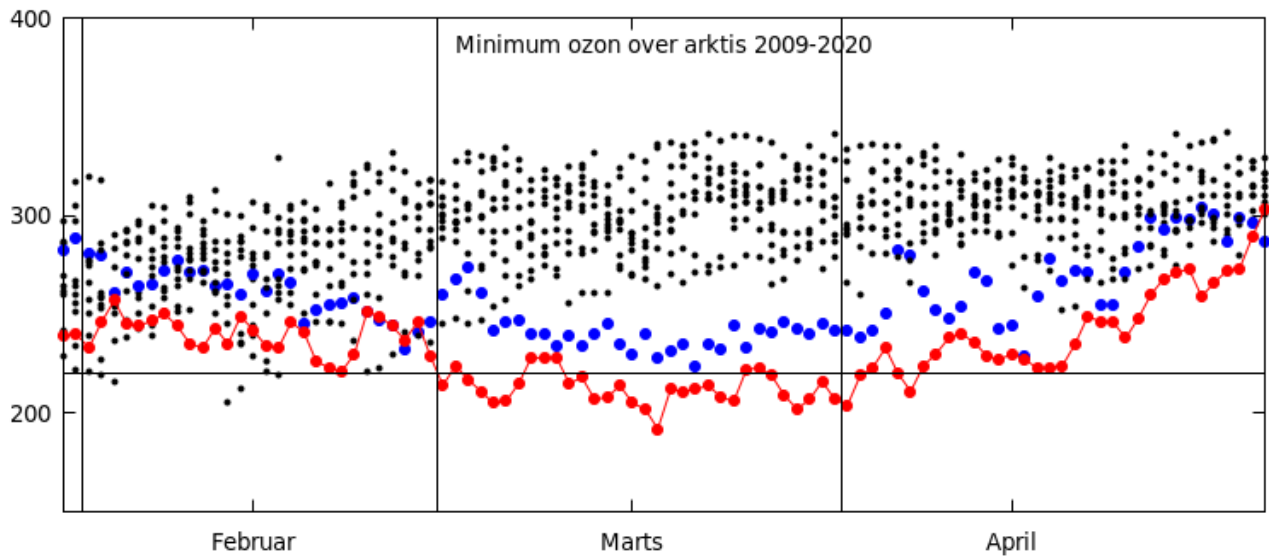


Figure F.8: Minimum ozone layer thickness over the Arctic from February to April during 2009–2020. The previous record low, observed in 2011, is marked in blue. In 2020, values (red) reached record lows from early March to late April, dropping below 220 DU (horizontal line) in March.

Figure F.9 shows ozone measurements from 9 stations in the SAOZ-network in the Arctic. Ozone had reached 37% depletion by March 2020 in all stations.

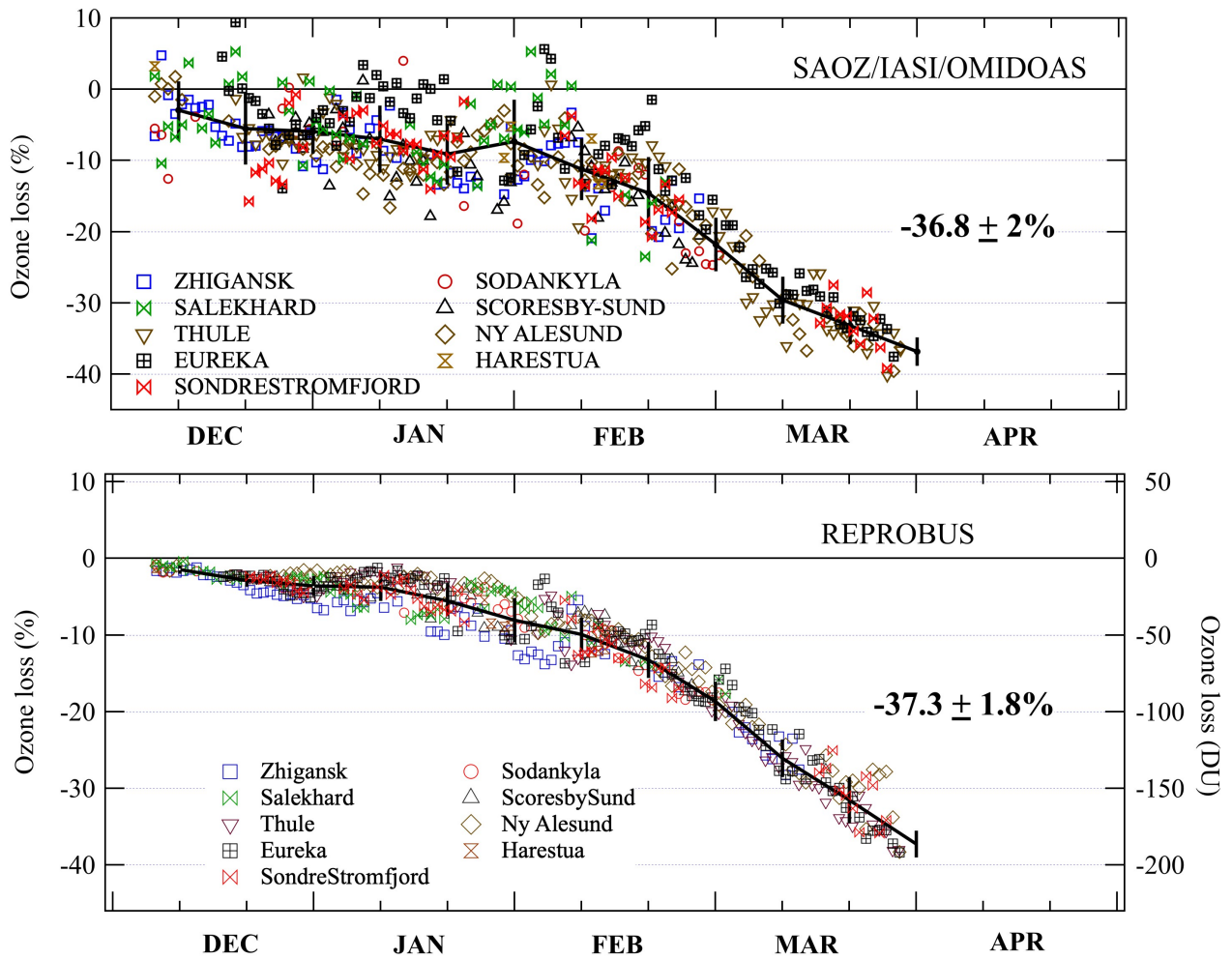


Figure F.9: Ozone depletion in the Arctic measured December 2019 to March 2020 by the SAOZ network.

As mentioned this was the first Arctic ozone hole, but total ozone depletion did not exceed the 2011 record, due to the vertical extent of the PSC region during solar illumination. Figure F.10 shows total ozone depletion plotted against the average PSC volume for February–March in the 475–675 K potential temperature range ( $\approx 20$ – $27$  km), revealing a clear correlation between ozone depletion and PSC volume in this layer. While the average PSC volume through the whole extent of the stratosphere during winter 2019–2020 was about 10% larger than in the 2010–2011 winter (see 2.13), the situation differs when only the upper layers are considered during the period of solar illumination.

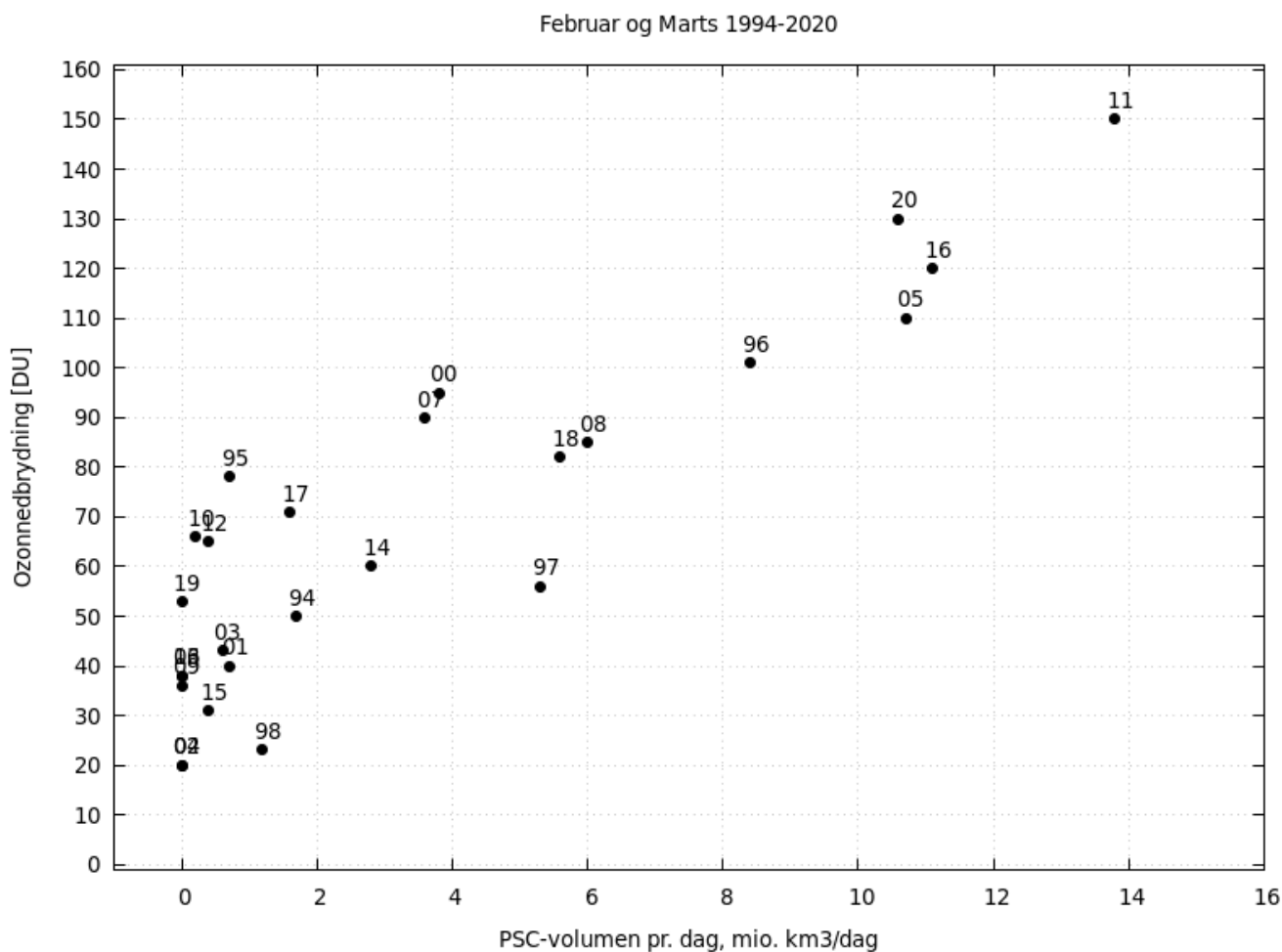


Figure F.10: Total ozone depletion in the Arctic during December–March for the years 1994–2020, derived from SAOZ network measurements, plotted against the average daily PSC volume (million km<sup>3</sup>/day) in the 475–675 K potential temperature range for February–March.

In Figure F.11, ozone measurements are shown for three locations in Greenland as well as Copenhagen. Pituffik, being the northernmost station, was affected by the thin ozone layer within the polar vortex from the beginning of 2020 until the end of April. On several occasions in March, total ozone column values as low as 220 DU were measured over Pituffik. From mid-March, the vortex—and thereby the region of very low ozone—shifted southwards from northern Greenland and shortly afterwards eastwards, which can be seen in the measurements from Kangerlussuaq and Ittoqqortoormiit. From the beginning of April, the region also extended over Scandinavia (Copenhagen), where satellite measurements on 6 April showed 280 DU over Copenhagen.

## The Ozone Layer in the Future

Thanks to international agreements (the Montreal Protocol and its amendments), emissions of many ozone-depleting substances (ODS) have been reduced (Figure F.14). As a result, the ozone layer is expected to gradually recover. However, this process will be slow, since many of the emitted substances remain in the atmosphere for a very long time.

Climate change may influence ozone recovery. A colder stratosphere could produce more polar stratospheric clouds, delaying recovery in polar regions. Simultaneously, stronger Brewer–Dobson circulation driven by greenhouse gas increase may transport additional ozone to mid-latitudes, potentially causing ozone levels there to temporarily exceed pre-depletion baselines [Butchart, 2014].

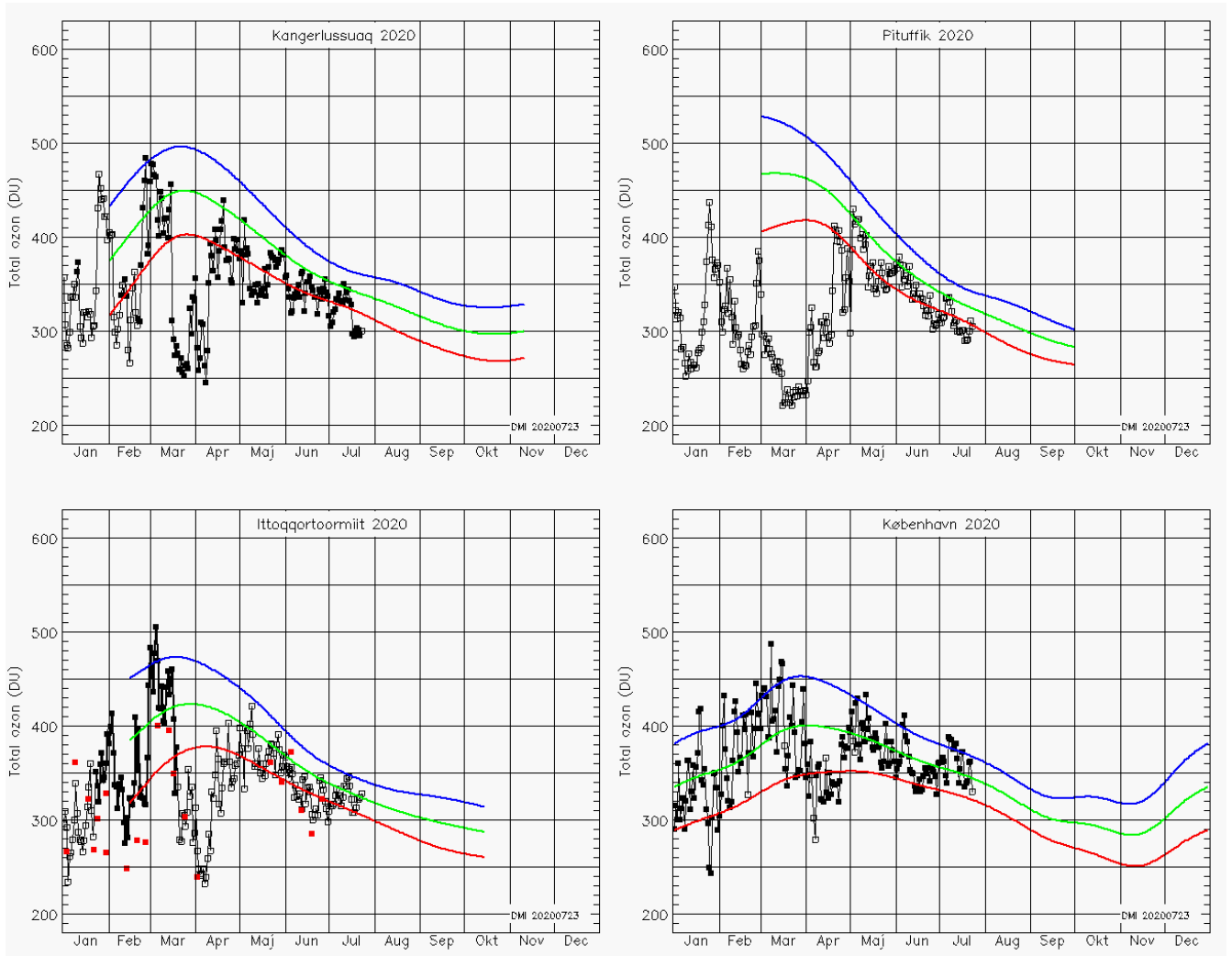


Figure F.11: Ozone measurements at four locations. Black squares represent Brewer measurements, open squares are GOME-2 satellite measurements, and red squares are ozonesonde soundings. Green curve: satellite average measurements 1979-1988. Blue and red curves: average plus/minus one standard deviation respectively.

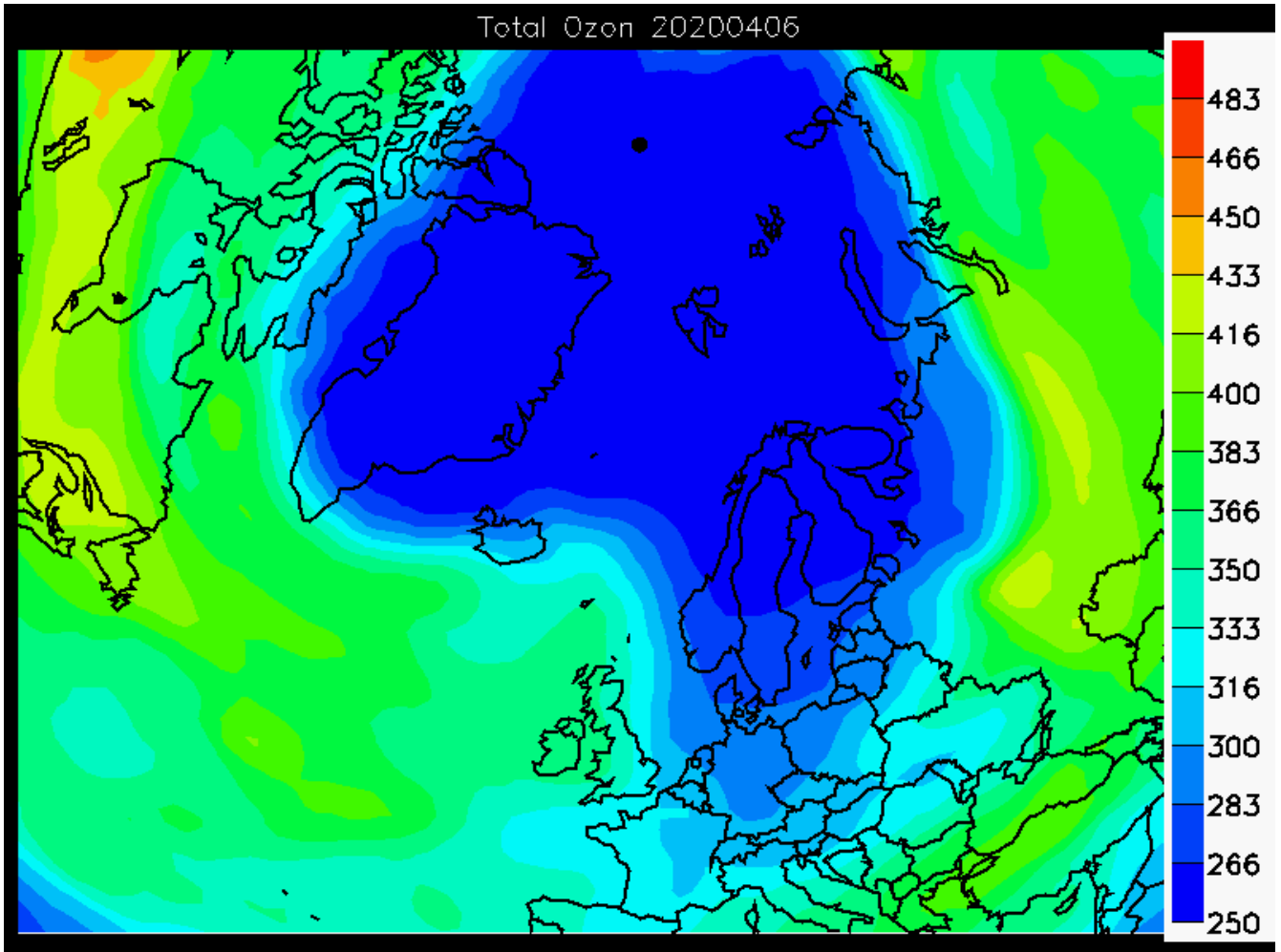


Figure F.12: Ozone layer thickness on 6 April 2020, measured in DU by GOME-2 onboard the MetOp-B satellite.



Figure F.13: Position of the polar vortex on 6 April 2020 at an altitude of approximately 23 km.

The next challenge is to determine whether the reductions in ozone-depleting substances are indeed having a measurable positive effect on the ozone layer's thickness. This is a complex task, as the ozone layer naturally undergoes large variations.

Figure F.14a shows the development of ODS in the troposphere. As a result of the Montreal Protocol (see Appendix G), concentrations are expected to return to 1980 levels around the middle of this century. Figure F.14b shows the projected increase in CO<sub>2</sub> concentrations, which also affect the stratosphere and thus the ozone layer. The shaded area indicates the natural annual variability under a scenario that includes changes in ODS. Figure F.14c illustrates the development of the Antarctic ozone hole, measured as the mean thickness in October. The ozone hole is the most visible manifestation of ODS effects, and the Antarctic ozone layer is not expected to be fully restored until the end of the 21st century. CO<sub>2</sub> (F.14b), as well as nitrous oxide (N<sub>2</sub>O) and methane (CH<sub>4</sub>). Figure F.14d shows the annual mean ozone layer thickness at 30–60°N. Natural variability makes it difficult to pinpoint exactly when pre-1980 levels will be restored, but this is expected to happen before the middle of this century—i.e. before ODS concentrations in the stratosphere have fully declined to 1980 levels and before recovery over Antarctica. The faster recovery at northern mid-latitudes is partly due to cooling of the stratosphere, which slows down ozone depletion here (in contrast to the polar regions). By the end of the century, the ozone layer at northern mid-latitudes is expected to exceed the 1980 level. Figure F.14e shows the development of UV radiation under cloud-free conditions at northern mid-latitudes. While clouds, aerosols, and air pollution also have a strong influence on actual UV levels, these factors are not included in the calculations. Due to the over-recovery of the ozone layer (Figure F.14d), UV levels are expected to be lower than before 1980 towards the end of the century.

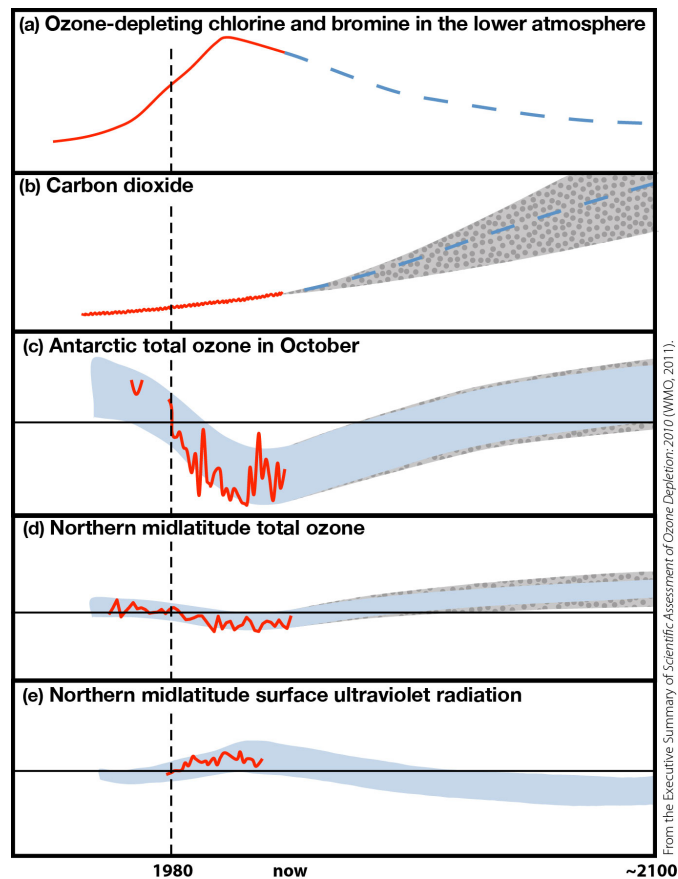


Figure F.14: Schematic development of the ozone layer. Red curves show observations up to the present, while blue dashed curves represent a widely accepted future scenario. Shaded areas indicate annual variability and uncertainties in measurements and simulations. The vertical dashed line at 1980 marks the year when ozone depletion first became evident. The CO<sub>2</sub> curve is included because rising concentrations affect stratospheric temperatures and winds, both of which influence the ozone layer [WMO, 2011].

## Appendix G

# The Vienna Convention and the Montreal Protocol

In response to growing concern over ozone layer depletion in the early 1980s, the international community took coordinated political action. Under the United Nations Environment Programme (UNEP), two major agreements were adopted: the Vienna Convention for the Protection of the Ozone Layer and the Montreal Protocol, including its subsequent amendments, which regulate the use and emissions of chlorine- and bromine-containing substances.

The Vienna Convention of 22 March 1985 on the Protection of the Ozone Layer was ratified by Denmark on 23 September 1988. The announcement of the Vienna Convention was issued by the Ministry of Foreign Affairs on 9 August 1990. The Convention is administered by the Ministry of the Environment.

The Vienna Convention entails the establishment of a Conference of the Parties (to the Convention). For scientific support of the conference, the Ministry of Foreign Affairs receives invitations to participate in preparatory meetings called the Meetings of the Ozone Research Managers of the Parties to the Vienna Convention. Meetings are held every 3 years under the auspices of the United Nations' World Meteorological Organization (WMO) in Vienna. Through the Environmental Protection Agency, DMI has been invited to participate as Denmark's representative at all past meetings.

The meetings result in a series of recommendations regarding, among other things, the necessity of continued monitoring of the state of the ozone layer and ultraviolet radiation, particularly in the Arctic regions, as well as research into the relationship between ozone layer recovery and climate change, including the quantification of chemical and dynamic processes. At the subsequent ministerial meeting of the Parties to the Vienna Convention (COP 11) in Montreal, Canada, it was, among other things, decided to encourage the Parties to continue monitoring the ozone layer and its interaction with climate change.

Danish obligations under the Vienna Convention include participating in international research and assessments through competent organisations. This is carried out via DMI's extensive ozone research, involvement in EU- and nationally funded projects, and contributions to scientific assessments on stratospheric ozone depletion coordinated by WMO, UNEP, and EU bodies. The latest comprehensive assessment of the ozone layer was published in 2022 [[WMO, 2022](#)].

Article 3.2 of the Vienna Convention encourages Parties to promote systematic ozone observations through international programmes. Denmark contributes to this through DMI's membership in the Network for the Detection of Atmospheric Composition Change (NDACC), supported by UNEP and the International Ozone Commission. DMI operates observation stations in Greenland (Kangerlussuaq and Ittoqqortoormiit) and Copenhagen, with data regularly reported to NDACC and the World Ozone and UV Data Center under WMO's Global Atmosphere Watch. Since 2007, DMI has collaborated with the Danish Environmental Protection Agency to monitor ozone and UV levels in Greenland, a project registered under the Arctic Monitoring and Assessment Programme (AMAP).

The Montreal Protocol, associated with the Vienna Convention, is a legally binding treaty for Parties to phase out ozone-depleting substances (ODS), including CFCs, HCFCs, and halons. Since its adoption in 1987, the Protocol has been amended several times. Denmark, via the EU, has introduced stricter measures than those required by the Protocol, including accelerated phase-outs of ODS.

The effectiveness of the Montreal Protocol is evident in the stabilisation and subsequent decline of atmospheric ODS concentrations (Figure [G.1](#)). Since many ODS are also potent greenhouse gases, the Protocol has prevented emissions equivalent to roughly five times the Kyoto reduction target, underscoring its central role in both protecting the ozone

layer and mitigating global warming. Nevertheless, because these compounds are long-lived, stratospheric chlorine and bromine levels will take many decades to return to their early-1980s values.

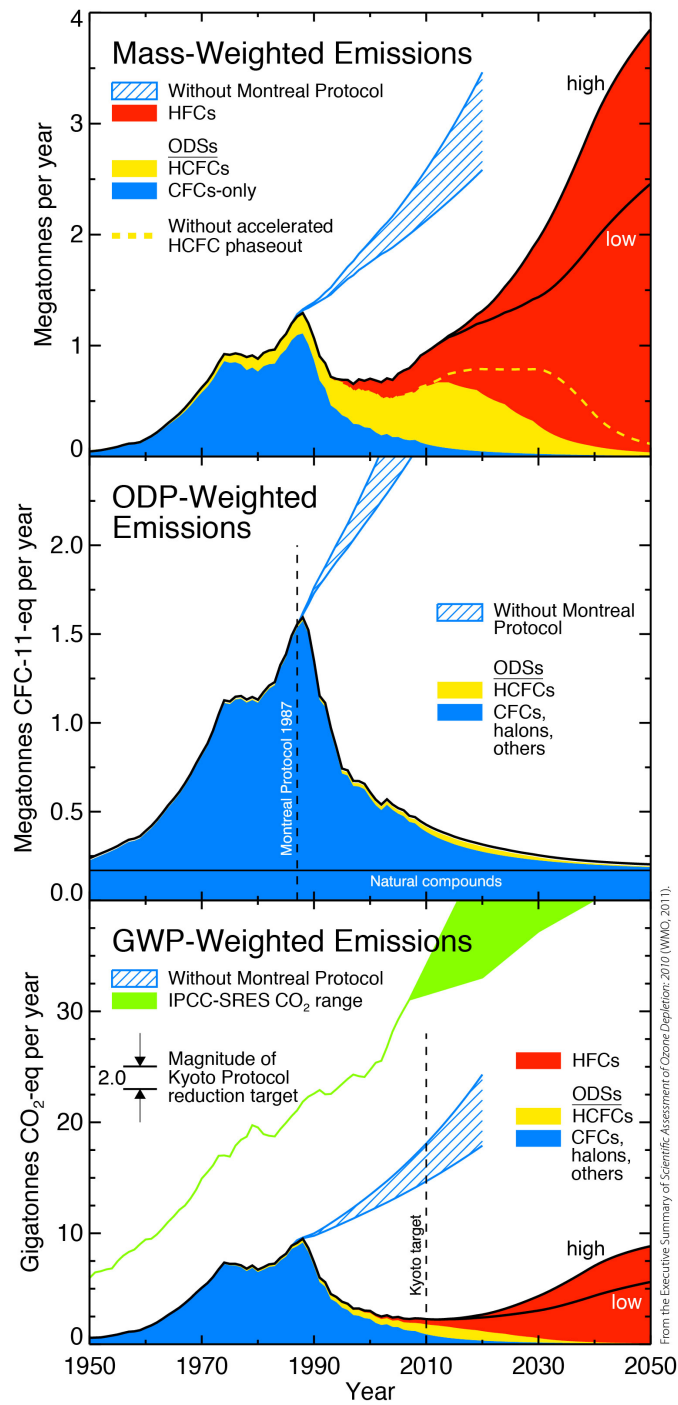


Figure G.1: Global emissions of ozone-depleting substances (ODS) and their replacement HFCs, 1950–2050. Shown are mass-weighted, ozone depletion potential (ODP)-weighted, and global warming potential (GWP)-weighted emissions. The Montreal Protocol (1987) and its later amendments, including the 2007 accelerated HCFC phaseout, prevented a sharp rise in emissions [WMO, 2011].

## Appendix H

# International Cooperation

DMI conducts stratospheric research with both Danish and international support. Since 1990, DMI has participated in 35 projects funded by the European Commission, and during the same period has also received support from Danish research foundations. Throughout the 1990s, DMI took part in all major European–American Arctic ozone research campaigns, including EASOE, SESAME, THESEO, THESEO-2000/SOLVE, Vintersol, and SCOUT-2/AMMA.

DMI's stratospheric observatories in Greenland serve as Arctic stations within NDACC, a global network of monitoring sites equipped with standardised, high-quality instrumentation for observing the state of the stratosphere and the processes that lead to chemical ozone depletion. DMI also participates in NDACC's steering committee.

In addition, DMI's research and monitoring activities are included as a priority area under the Arctic Monitoring and Assessment Programme (AMAP) of the Arctic Council. Furthermore, DMI contributes to the EUMETSAT Satellite Application Facility on Atmospheric Composition Monitoring (AC SAF), focusing on the development of operational UV index products based on satellite measurements of the ozone layer.

# Bibliography

Neal Butchart. Reviews of Geophysics The Brewer-Dobson circulation. *Rev. Geophys*, 52:157–184, 2014. ISSN 19449208. doi: 10.1002/2013RG000448.One.

Gloria L. Manney, Michelle L. Santee, Markus Rex, Nathaniel J. Livesey, Michael C. Pitts, Pepijn Veefkind, Eric R. Nash, Ingo Wohltmann, Ralph Lehmann, Lucien Froidevaux, Lamont R. Poole, Mark R. Schoeberl, David P. Haffner, Jonathan Davies, Valery Dorokhov, Hartwig Gernandt, Bryan Johnson, Rigel Kivi, Esko Kyrö, Niels Larsen, Pieternel F. Levelt, Alexander Makshtas, C. Thomas McElroy, Hideaki Nakajima, Maria Concepción Parrondo, David W. Tarasick, Peter Von Der Gathen, Kaley A. Walker, and Nikita S. Zinoviev. Unprecedented Arctic ozone loss in 2011. *Nature*, 478(7370):469–475, 2011. ISSN 00280836. doi: 10.1038/nature10556.

Regeringen. Danmarks Nationale Strategi for rummet for rummet, 2021. URL <https://bu.dk/bu-i-danmark/danmarks-nationale-strategi/>.

M. Rex, R. J. Salawitch, P. von der Gathen, N. R.P. Harris, M. P. Chipperfield, and B. Naujokat. Arctic ozone loss and climate change. *Geophysical Research Letters*, 31(4):94–97, 2004. ISSN 00948276. doi: 10.1029/2003GL018844.

M. Rigby, S. Park, T. Saito, L. M. Western, A. L. Redington, X. Fang, S. Henne, A. J. Manning, R. G. Prinn, G. S. Dutton, P. J. Fraser, A. L. Ganesan, B. D. Hall, C. M. Harth, J. Kim, K. R. Kim, P. B. Krummel, T. Lee, S. Li, Q. Liang, M. F. Lunt, S. A. Montzka, J. Mühle, S. O’Doherty, M. K. Park, S. Reimann, P. K. Salameh, P. Simmonds, R. L. Tunnicliffe, R. F. Weiss, Y. Yokouchi, and D. Young. Increase in CFC-11 emissions from eastern China based on atmospheric observations. *Nature*, 569(7757):546–550, 2019. ISSN 14764687. doi: 10.1038/s41586-019-1193-4.

W. Steinbrecht, U. Köhler, H. Claude, M. Weber, J. P. Burrows, and R. J. Van Der A. Very high ozone columns at northern mid-latitudes in 2010. *Geophysical Research Letters*, 38(6):2–5, 2011. ISSN 00948276. doi: 10.1029/2010GL046634.

S. M. Uppala, P. W. Kållberg, Adrian J. Simmons, U. Andrae, V. da Costa Bechtold, M. Fiorino, J. K. Gibson, J. Haseler, A. Hernandez, G. A. Kelly, X. Li, K. Onogi, S. Saarinen, N. Sokka, R. P. Allan, E. Andersson, K. Arpe, M. A. Balmaseda, A. C.M. Beljaars, L. van de Berg, J. Bidlot, N. Bormann, S. Caires, F. Chevallier, A. Dethof, M. Dragosavac, M. Fisher, M. Fuentes, S. Hagemann, E. Hólm, B. J. Hoskins, L. Isaksen, P. A.E.M. Janssen, R. Jenne, A. P. McNally, J. F. Mahfouf, J. J. Morcrette, N. A. Rayner, R. W. Saunders, P. Simon, A. Sterl, K. E. Trenberth, A. Untch, D. Vasiljevic, P. Viterbo, and J. Woollen. The ERA-40 re-analysis. *Quarterly Journal of the Royal Meteorological Society*, 131(612): 2961–3012, 2005. ISSN 00359009. doi: 10.1256/qj.04.176.

Ronja Vitt, Gudrun Laschewski, Alkiviadis F. Bais, Henri Diémoz, Ilias Fountoulakis, Anna Maria Siani, and Andreas Matzarakis. UV-index climatology for europe based on satellite data. *Atmosphere*, 11(7):1–26, 2020. ISSN 20734433. doi: 10.3390/atmos11070727.

WMO. Scientific Assessment of Ozone Depletion: 2002. Technical Report 47, 2003. URL [https://library.wmo.int/?lvl=notice\\_display&id=7318](https://library.wmo.int/?lvl=notice_display&id=7318).

WMO. Scientific Assessment of Ozone Depletion: 2006 - Report of the Montreal Protocol Scientific Assessment Panel. Technical report, 2007. URL <https://library.wmo.int/records/item/28326-scientific-assessment-of-ozone-depletion-2006-report-of-the-montreal-protocol-scientific-assessment-offset=3918>.

WMO. Scientific Assessment of Ozone Depletion: 2010, Global Ozone Research and Monitoring Project-Report. Technical Report 52, 2011.

WMO. Scientific Assessment of Ozone Depletion: 2022, GAW. Technical Report 278, 2022.

I. Wohltmann, P. von der Gathen, R. Lehmann, H. Deckelmann, G. L. Manney, J. Davies, D. Tarasick, N. Jepsen, R. Kivi, N. Lyall, and M. Rex. Chemical Evolution of the Exceptional Arctic Stratospheric Winter 2019/2020 Compared to Previous Arctic and Antarctic Winters. *Journal of Geophysical Research: Atmospheres*, 126(18), 2021. ISSN 21698996. doi: 10.1029/2020JD034356.